Grey Water Reclamation Utilising Solar Thermal Energy

by
Gerhard Rudolf Hartwig

Thesis presented in fulfilment of the requirements for the degree of Master of Science in Engineering (Mechatronic) in the Faculty of Engineering at Stellenbosch University

Supervisor: Adoniya Ben Sebitosi

December 2013

DECLARATION

By submitting this thesis electronically, I declare that the entirety of the work contained therein is my own, original work, that I am the sole author thereof (save to the extent explicitly otherwise stated), that reproduction and publication thereof by Stellenbosch University will not infringe any third party rights and that I have not previously in its entirety or in part submitted it for obtaining any qualification.

Date: .....

ABSTRACT

The objective of this research was to obtain clean drinkable water from treated sewage effluent by using a solar-powered distillation cycle. Technologies and concepts were borrowed from the solar desalination industry to propose a unique circular distillation cell design. From the design, a specific mathematical correlation was developed to predict the distillate mass flow rate by using only evaporation and condensation temperature as inputs.

This model was incorporated into a simulation model built using Transient System Simulation software. Long-term simulations were carried out to determine the operating capabilities of the design. A prototype was successfully constructed and operated. Experimental results indicated good agreement with the mass flow rate mathematical correlation. Water quality levels were tested against the South African National Standard 241 national drinking water quality standard. Four quality parameters are outside acceptable levels. Evidence suggested that acceptable quality levels could be reached.

The circular distillation cell design is a major contribution made by this research. Another contribution is the simulation model capable of predicting an output for different locations. Finally, the proposed prototype is potentially a very valuable device contributing towards the reduction of consumer demand in terms of water and energy as well as the household load on the wastewater treatment system.

OPSOMMING

Die doel van hierdie tesis is om te beskryf hoe behandelde rioolwater deur middel van ’n son aangedrewe distillasiesisteem gesuiwer kan word om drinkbare water as eindproduk te lewer. Die nodige tegnologieë en konsepte is oorgeneem uit kommersiële sonaangedrewe ontsoutingsisteme om met ’n unieke ontwerp voorendag te kom wat uit ’n sirkelvormige natuurlike konveksie distillasiesel bestaan. Met behulp van hierdie ontwerp is ’n wiskundige korrelasie ontwikkel om die gesuiwerde water se massavloei te bepaal. Slegs die verdampings- en kondensasietemperature word as insetwaardes gebruik om die massavloei te bereken.

’n Simulasiemodel is met behulp van die Transient System Simulation programmatuur gebou. Die wiskundige korrelasie is by die simulasiemodel geïnkorporeer om langtermynsimulasies te kan uitvoer. Voorts is ’n demonstrasiemodel suksesvol gebou en aangedryf. Eksperimentele resultate toon goeie ooreenstemming met die simulasieresultate. Die gesuiwerde water se gehalte is met die nationale SANS 241 drinkwaterstandaard as maatstaf getoets. Slegs vier gehalteparameters val buite die aanvaarbare vlakke, hoewel dit blyk dat hierdie elemente wel tot aanvaarbare vlakke verlaag kan word.

Hierdie navorsing se grootstet bydrae is die ontwerp van die unieke sirkelvormige distillasiesel. ’n Bykomende bydra is die aanpasbaarheid van die simulasiemodel sodat dit produksievermoë op verskillende plekke kan voorspel. Die demonstrasiemodel is ’n potensieel waardevolle ontwerp wat kan bydra tot die verlaging in verbruikersaanvraag na water en energie. ’n Ontwerp van hierdie aard kan die las wat huishoudings op suiweringaanlegte vir rioolwater plaas, verlig.

ACKNOWLEDGEMENTS

I would like to thank my supervisor, Professor AB Sebitosi, for all the time and effort that he contributed towards this thesis and especially for the timely feedback on every query.

Many thanks also to Nathi Hlwempu from STERG, Cobus Zietsman from Stellenbosch Mechanical Services, Bryce from the Sustainability Institute and my father for their contributions towards making this project a reality.

TABLE OF CONTENTS

LIST OF TABLES

LIST OF FIGURES

NOMENCLATURE

Latin symbols

A	Ampere
b	Constant
C	Constant
c	Specific heat capacity [J/kg_°C]
D	Diffusion coefficient [m^2/s]
d	Constant
e	Constant
Gr	Grashof number = $\frac{\beta g l^3 \rho^2 \Delta T}{\mu^2}$
g	Gravitational acceleration [m^2/s]
H	Height [m]
h	Convective transfer coefficient [W/m^2_°C]
K	Radius ratio
k	Thermal conductivity [W/m_°C]
Le	Lewis number = $\left(\frac{\alpha}{D_{AB}}\right)$
l	Characteristic length [m]
M	Molecular weight [kg/mol]
$\dot{m}$	Mass flow rate [kg/m^2_s]
Nu	Nusselt number = $\frac{h_{heat} l}{k}$
n	Constant
P	Pressure [Pa]
Pr	Prandtl number = $\frac{\mu c_p}{k}$
Q	Heat transfer [W]
$\dot{q}$	Heat flux [W/m^2]
R	Universal gas constant
Ra	Rayleigh number = $\frac{l^3 \rho g \beta}{\mu \alpha} \Delta T$
Sc	Schmidt number = $\frac{v}{D_{AB}}$
St	Stanton number = $\frac{h}{\rho V c_p}$
T	Temperature [°C]

u	Velocity component in y-direction [m/s]
V	Volts
v	Velocity component in x-direction [m/s]
W	Width [m]
x	Cartesian coordinate
y	Cartesian coordinate

Greek symbols

α	Thermal diffusivity [m^2/s]
β	Volumetric thermal expansion coefficient [1/K]
Δ	Differential
κ	Radius ratio
μ	Dynamic viscosity [N s/m^2]
ρ	Density [kg/m^3]

Superscripts

‘	Modification identifier
"	Modification identifier
b	Constant
n	Constant

Subscripts

1, 2	Effect identification
AB	Diffusion between phase A and B
a	Air
c	Condensation
coll	Solar collector
e	Evaporation
ew	Evaporation from water
f	Fluid
fg	Latent heat of vaporisation [kJ/kg]
heat	Relating to heat transfer
mass	Relating to mass transfer
p	Constant pressure
pv	Vapour pressure
pa	Air pressure
t	Total
v	Vapour
w	Water

1. INTRODUCTION

1.1 Background and Objectives

This research resulted from previous work done by the author on solar desalination systems (Hartwig & Sebitosi, 2010). It was found that solar desalination had several limitations, one of which is the fact that desalination systems are always required to be in close proximity to a saline water source. Consequently, an idea to make desalination systems more widely usable in South Africa by using grey water as a feed source emerged.

Grey water constitutes wastewater from households minus the sewage effluent flowing from toilets. The contamination levels of this grey water are believed to be low enough so that a desalination system would be able to produce fresh potable water from the grey water. A suitable case study was required to test the proposal, and the Lynedoch Eco-Village outside Stellenbosch provided the ideal location. After initial investigations into the Lynedoch wastewater system, it was revealed that the Lynedoch wastewater treatment facilities already produced treated sewage water. This treated sewage water is currently used as irrigation water and for the flushing of toilets.

The goal of the project is then to make use of this treated sewage water, henceforth also referred to as grey water, as a feed source for a solar desalination system. It would remove the need for refurbishments to the existing piping systems of most households, which currently do not separate the toilet wastewater from the other household effluent. This would further increase the applicability of the proposed system, allowing the system to slot into the existing wastewater treatment systems without any interference. Making use of an off-the-shelf solar collector for heating purposes increased the applicability of the proposed system as well as keep unknown costs limited to the distillation still.

Another aspect that emerged as a key attribute of the proposed system was energy savings. Since the produced fresh water of a desalination system is at an elevated temperature, potential savings in water heating are possible. Therefore, the proposal included investigation into the use of the produced fresh water as a feed source for household hot water cylinders.

Subsequently, the objectives of this study were as follows:

- Conducting a detailed literature review into small scale desalination systems and their application.
- Building a mathematical correlation to characterise the distillation process.

- Performing simulations of the system using suitable software capable of incorporating the developed mathematical correlation and using meteorological data from different locations as an input.
- Designing and constructing a prototype.
- Conducting experiments on the prototype to validate the chosen mathematical correlation, to determine the produced water quality as well as to validate the simulation of the system based on actual solar radiation data.

Although the proposal of distilling grey water has been mentioned in the literature (Hanson, 2004), no specific reference could be found for using treated sewage water as a feed source to a desalination system, producing heated water for use in household hot water cylinders. If successful, the proposed design would be an innovative tool in reducing consumer demand in both the water and energy sectors.

1.2 Implementation Environment

1.2.1 National Context

It is evident that South Africa finds itself in an energy supply crisis. Anybody watching television between six and eight at night can confirm the constant reminders that people need to switch off their non-essential appliances since the electricity supply is under pressure. South Africans are in a situation where their planning has let them down in terms of providing a constant energy supply to meet their growing demands. To complicate matters further, South Africa has an energy-intensive economy that requires high economic growth rates to stem unemployment and reduce poverty. Adding the fact that this is a water-scarce country, one can see that South Africa faces an uncertain future.

Unfortunately, both the energy and water supply reserves in South Africa have been taken for granted. For the past few years, the government has had to act rapidly to catch up in with the demand. South Africans are in a dire situation concerning electricity with Eskom again issuing warnings in early 2012 about tight supply margins due to required maintenance (Lazenby, 2012). Even worse is the fact that Eskom is keeping up with the demand by building more coal-fired power stations, a serious step in the wrong direction in an ever-increasing environmentally conscious world.

South Africa's water supply is in a similar situation as its electricity supply. Instead of rolling blackouts, various regions in the country have had rolling water restrictions. In some dire cases, the water supply has even dried up and water had to be transported in from other regions, as was the case in Beaufort Wes recently. By looking at the recent Blue Drop report by the Department of Water

Affairs (DWA, 2011a) one sees that the future might be dry as well as dark; yet water restrictions are less disruptive to people's daily lives than the total darkness experienced in electricity load shedding.

The 2011 Blue Drop Report provides a look at the state of the country's water supply and rates each region and municipality in terms of a percentage, with 100% reflecting a fully functioning water supply system. The national score came in at 72.90%, with Gauteng (95.10%) and the Western Cape (94.09%) receiving the highest scores. The lowest score was that of Mpumalanga at 56.50% (DWA, 2011a). Although progress has been made compared to the national average of 2010 (67.20%) and 2009 (51.40%), any score below 90% should be viewed as inadequate.

The Green Drop Report (DWA, 2011b) provides a similar account of wastewater treatment facilities in South Africa. The first Green Drop Report released in 2009 revealed the shocking state of these facilities. The average municipal score was well below 50%, falling in the 'very poor performance' category. Not only is an inadequate wastewater treatment system a health risk but it also affects downstream ecosystems. The updated Green Drop Report in 2011 paints an improving picture although the municipal average score is still only 45%, up from the previous 37% in 2009.

1.2.2 Local Context

Looking at the situation of Stellenbosch Municipality, one finds a glimmer of hope. The 2011 Blue Drop Report, relating to fresh water supply, presented Stellenbosch Municipality with a Blue Drop Award for the Stellenbosch area, indicating satisfactory water supply systems (DWA,2011a). However, the 2011 Green Drop Report, relating to wastewater treatment, shows the total opposite to how the fresh water supply systems are run (DWA, 2011b).

Although the Stellenbosch area received a 72.3% rating, the risk assessment rating stood at 91.3%, prompting the placement of the Stellenbosch Municipality wastewater treatment facilities under regulatory surveillance. Stellenbosch Municipality received the fourth worst rating in the entire Western Cape Province. The Green Drop Report furthermore states that the Stellenbosch wastewater treatment facilities are seen as being in a 'shocking state' and have been neglected for years. Additionally, several occupational health and safety contraventions are visible, and the risk of sludge run-off in the rainy seasons is very high (DWA, 2011b), indicating problem situations that need to be resolved urgently.

Fortunately, Stellenbosch Municipality has recently been politically more stable than in the past, resulting in a better supported municipal management structure.

This is reflected in the third Integrated Development Plan (Stellenbosch Municipality, 2012) released by the municipality. Although positive in its message and goal, the report nevertheless also highlights the immense challenges that lie ahead.

To start with, the housing backlog for Stellenbosch is estimated at 20 000 units. This backlog is due to Stellenbosch experiencing population growths of above 9% yearly for the past decade (Stellenbosch Municipality, 2012). All of these new housing units would expect to receive nothing less than adequate access to sanitation, electricity and water supply in line with current access levels of 95.9%, 97.9% and 98.6% respectively.

Regrettably, 38.6% of the water supply infrastructure is in a poor or very poor state with a capital expenditure backlog of over R324 million. The infrastructure is therefore also inadequate for future supply demands. Worst is the 43.4% of sanitation infrastructure that fall within the 'poor' to 'very poor' categories with a capital expenditure backlog of R283.4 million. Similarly, the Stellenbosch electricity network is also currently under pressure. The large Jan Marias substation requires an upgrade this year, and the main Stellenbosch substation requires replacement by 2014, together adding up to nearly R15 million in replacement costs (NETGroup, 2006).

Together these infrastructure costs have a significant impact on the municipal accounts. With 43% of the municipal revenue expected to come from electricity in the 2012/2013 financial year (Stellenbosch Municipality, 2012), it is imperative that the electricity grid be kept operating at acceptable levels. Over and above the financial impact of an inadequate electricity grid, is the damage that it can inflict on crucial services such as the ailing wastewater treatment facilities.

Stellenbosch is therefore in a critical situation in terms of current electricity and water supply capabilities as well as its ability to meet future demand. The wastewater treatment facilities are at a very high risk of polluting the areas surrounding them as well as the eco-system downstream of the facilities. Consequently, various opportunities exist in terms of electricity supply, water supply and water treatment options and meeting these challenges in the future.

Therefore, over and above meeting the objectives states in Section 1.1, this research also looked at how and where grey water reclamation using solar energy could contribute to solving both the current and future resource demands of Stellenbosch. Furthermore, the solution had to be capable of not only being utilised in Stellenbosch but also of showcasing Stellenbosch as a front-runner in developing innovative ideas for the challenges faced by modern society in terms of resources demands.

1.3 Methodology

1.3.1 Energy Hierarchy

Attempting to meet the objectives described in Section 1.1 was a complex task. In order to simplify the process, a suitable guide was identified to aid in confronting these problems. This guide is referred to as the 'Energy Hierarchy'. The Energy Hierarchy is a set of five steps put forward by the Institution of Engineering and Technology (IET, 2009) in the United Kingdom. These principles act as a general guide towards sustainability and are easily understood. The Energy Hierarchy is presented in Figure 1, with the first three steps being the desired guiding principles towards sustainability.

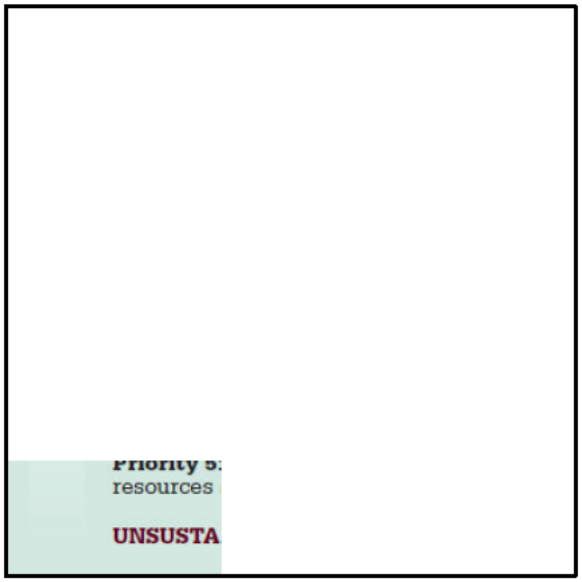

Figure 1: The Energy Hierarchy
(IET, 2009)

The first step in implementing the proposed grey water reclamation system in society was to find communities into which this proposal could be incorporated. This would allow the proposal to be showcased in a functional environment, adding credibility to the idea. The Energy Hierarchy served as a guideline to evaluate communities and identify potential aspects that would aid in implementing grey water reclamation. Various functions were looked at, such as renewable energy use, efficiency implementation, recycling programmes and wastewater treatment options. This investigation would provide insight into what

had already been done, where possible areas for improvement lay and how these improvements could be implemented in Stellenbosch together with the grey water reclamation.

1.3.2 Sustainable Communities

The first example of applying sustainable practices and reducing demand is the One Planet Living vision (BioRegional, 2012), a programme initiated by BioRegional, a British environmental organisation. The One Planet Living vision provides a framework for creating sustainable communities through focussing on 10 principal guidelines. These principles have been put into practice with four current communities living by these standards and another seven in development. The seven in development include Masdar in Qatar and Sibaya, in Durban, South Africa (One Planet Communities, 2012).

In the Western Cape, similar visions and principles are being implemented in existing communities. Examples of these are Goedgedacht (Goedgedacht, 2012) in the Malmesbury region and the Lynedoch Eco-Village (Sustainability Institute, 2012) in the Stellenbosch region. Both of these programmes aim at creating a sustainable society in all its forms. Most environmental movements tend to focus primarily on the energy footprint, but these communities strive to be sustainable in social and economic activities as well.

It is therefore evident that in order for Stellenbosch to solve its problems and face the challenges of the future, it needs to try to emulate these communities and developments and adapt the solutions that were found to its own needs. For this research project, the obvious choice for a case study community was the Lynedoch community. Not only does the Lynedoch community have various sustainable practices already in place, but it is also close to Stellenbosch and falls within the Stellenbosch Municipal area. Applying the practices of Lynedoch to the greater Stellenbosch area should therefore not be too arduous a task.

1.4 Structure of Thesis

The thesis is divided into nine chapters, including this one. Chapter 2 introduces the case study of the thesis, the Lynedoch Eco-Village, where the proposed system was implemented. The chapter focuses on the current water cycle, the various wastewater treatment operations as well as water usage patterns at Lynedoch. Chapter 3 looks into the different treatment options available for grey water. Comparisons between solar desalination methods and conventional treatment options are made to confirm the suitability of the solar desalination process.

Chapter 4 details the investigation into current small-scale solar desalination systems. A variety of different configurations and processes are compared and analysed, ensuring that these systems were capable of operating in a domestic situation. A new design was proposed, stemming from a combination of the investigated systems.

Chapter 5 details the building of a mathematical correlation for the proposed prototype design. The chapter starts with an investigation into the convective heat and mass transfer present in the proposed distillation system and continues with an investigation of current available mathematical correlations. After evaluating different correlations, a correlation is selected. Additions to the selected correlation are also proposed and described in the last sections of the chapter.

Chapter 6 details the design of the proposed demonstration model. A variety of variables governing the functionality and efficiency of the system are optimised to produce a design suitable for the situation at hand. The inclusion of a backup heating system into the design and the reasoning behind the inclusion is also detailed in the chapter.

In Chapter 7 the development of the simulation model is described. The choice of using the Transient System Simulation (TRNSYS) software with support from Excel is presented. Simulations are presented for solar- and auxiliary-driven situations with accompanying results presented in graphs.

The experimental results are presented in Chapter 8. Three areas of experimental investigation are described. These include validation of the mathematical correlation, determination of the quality of the water produced and validation of the simulation model for accurate modelling of the prototype. Results from each area are provided together with observations encountered in the experimental processes.

2. CASE STUDY: LYNEDOCH ECO VILLAGE

2.1 Lynedoch

Situated just outside of Stellenbosch, Lynedoch is a diverse community with people from different backgrounds all living, working, learning and enjoying life together. The community comprises a preschool, a primary school, the Sustainability Centre, housing various businesses as well as the Sustainability Institute's educational programmes, a guesthouse, 38 mixed-income houses, a wastewater treatment facility, renewable energy projects and a land reform programme (Sustainability Institute, 2012). All of these elements create a harmonious environment that makes Lynedoch a worthy example of a community striving towards sustainability.

The concept of the Lynedoch community was initiated by the Sustainability Institute. A partnership was formed by the Sustainability Institute Trust, Lynedoch Development, Spier Holdings and Stellenbosch Municipality. The Sustainability Institute is now housed in the renovated Sustainability Centre on the Lynedoch premises. Stellenbosch University also formed a partnership with the Sustainability Institute and has since developed master's and doctoral courses in sustainable development that are offered at the centre.

On the technical side, Lynedoch hosts a variety of sustainable living projects and systems. Houses are fitted with solar water heaters, low-energy lighting and gas-fired stoves. Solar-powered light-emitting diode (LED) lights provide street lighting. Recycling of household waste is required from each household. Waste is sorted into five different categories to be recycled as far as possible. Houses are constructed of various sustainable materials, and care is taken to minimise the impact on the environment during the construction phase.

In reference to the Energy Hierarchy and the potential of grey water reclamation, it was found that a culture of conservation already existed at Lynedoch. Implementation of grey water reclamation would therefore fit in perfectly with the sustainable vision of the Lynedoch community. However, more detail was needed on the current water supply and treatment facilities and implemented functions to determine where and how the grey water reclamation system could be applied.

2.2 Lynedoch Water Cycle

At Lynedoch, each household is provided with a dual water supply. Clean drinking water as well as recycled water used for toilet flushing and irrigation is supplied. Water-saving devices are also installed in households to further decrease water demand. An extensive wastewater recycling system is installed on the premises. This includes an artificial wetland and a Biolytix system. All of these systems create a setup with no need for bulk sanitation infrastructure.

The Biolytix system (Biolytix, 2008) is a system originating in Australia and has been used successfully at various sites, including campsites, hotels and resorts. The system works with a filter bed comprising three different filter layers. The first layer houses a wet-soil ecosystem. A variety of biological organisms, including worms and beetles, breaks up the organic material in this layer. This occurs while still allowing air to enter the system as well as ensuring adequate drainage to the second layer. The second layer performs the same function as the first, albeit on the smaller particles received from the first layer. The third layer is a filter that filters out all the organic particles still present. An in-ground Biolytix system is presented in Figure 2. Sewage enters at the top left corner, and treated water

exits at the top right corner. With a gravity feed system, as is the case at Lynedoch, the reclaimed water drains out at the bottom of the tank and no control systems or pumps are required.

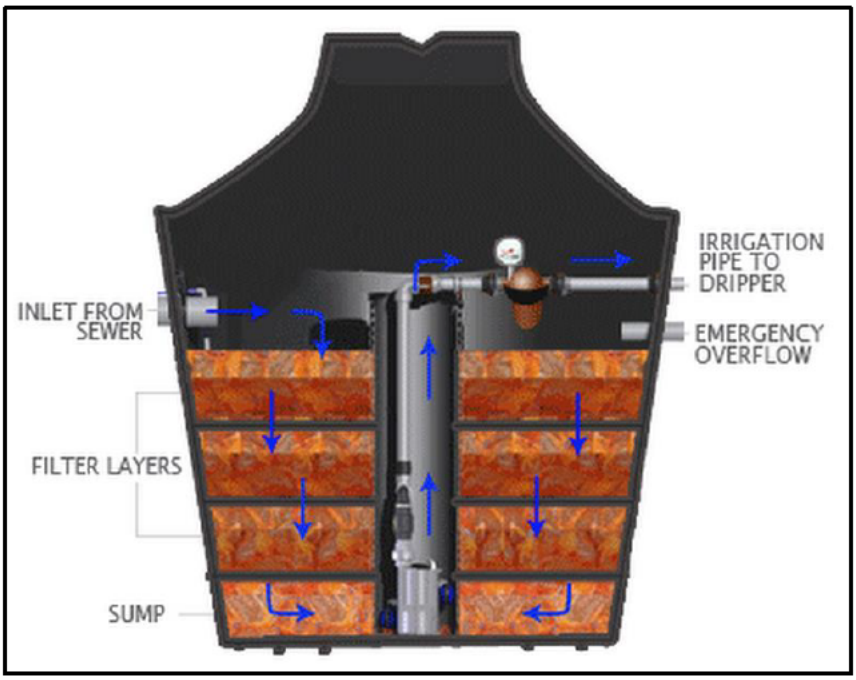

Figure 2: Biolytix Wastewater Treatment System

(Biolytix, 2008)

The artificial wetland is also made up of different layers. Within these layers microbial purification, chemical processes as well as plant physiological processes occur (Dowling, 2007). The chemical processes that take place entail that iron filings, which are added to the layers, converting into iron (III) phosphate. On the plant physiological side, plants such as arum lilies absorb the nitrogen in the system.

A graphical representation of the overall water reticulation system at Lynedoch is presented in Figure 3. The Biolytix system treats the sewage water from the Sustainability Institute, the school and the guesthouse. Septic tanks in turn treat the sewage water from the houses and the local shop, the Olive Leaf. From there, the effluent from both the Biolytix system and the septic tanks flows into the artificially constructed wetland. The reclaimed water drained from the wetland is then pumped to storage tanks and distributed to the required locations. The households consume the bulk of the reclaimed or grey water.

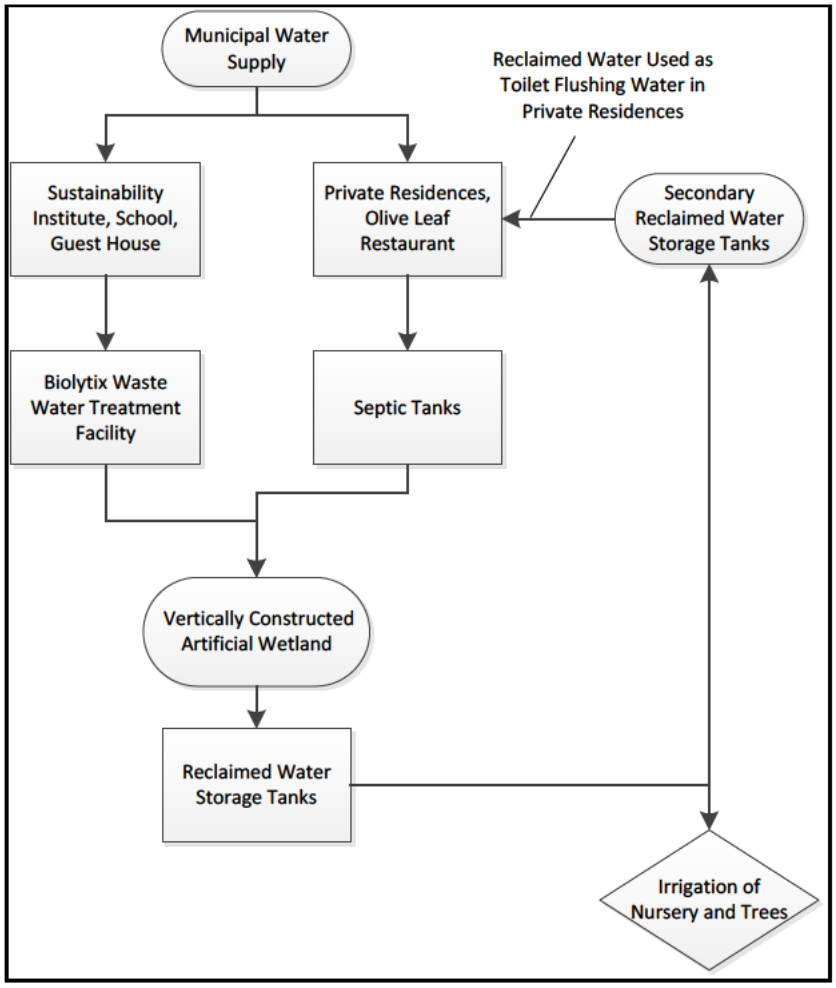

Figure 3: Lynedoch Water Reticulation System

2.3 Water Demand at Lynedoch

With the water processes at Lynedoch examined, the next step was to investigate the volumes of water usage. The water system at Lynedoch is monitored through an extensive system of water meters installed to monitor usage and provide accurate data on different zones of demand. Water flows are measured at strategic points such as entries to grey water storage tanks, treatment processes as well as the usage points of clean and grey water. The purpose of such an extensive monitoring system is to enable the operators thereof to improve and learn from the system.

Data obtained showed measurements from the start of 2011. Water demand data were available, including data for grey water volumes available after irrigation

and toilet flushing. Grey water volumes available and clean water demand are presented in Figure 4. Initial grey water measurements as well as data for January 2011 indicated negative values and were subsequently ignored due to the measurements understandably being errors. Interviews with the groundskeepers also suggested that extra grey water was always available. Looking at the actual volumes, the author concluded that extra grey water volumes existed and could be utilised for the current grey water reclamation proposal of the study.

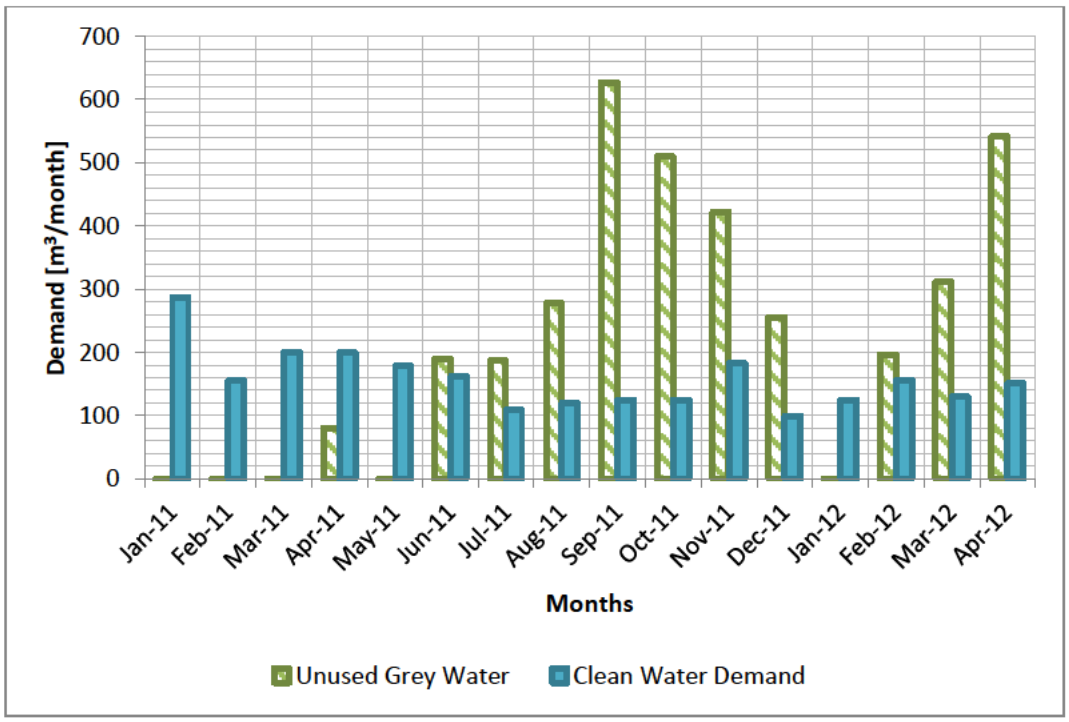

Figure 4: Available Grey Water versus Clean Water Demand

Another important factor to investigate was the clean water volumes consumed by households. This would give an indication of the demand that was required from a treatment system. Figure 5 reveals the average daily household consumption for the households at Lynedoch calculated from the monthly values. Expected seasonal changes in demand are visible although the difference is very small. More evident is the recent drop in average consumption. For the year from May 2011 to April 2012, the average dropped to 240 L per day from an overall average of 310 L per day.

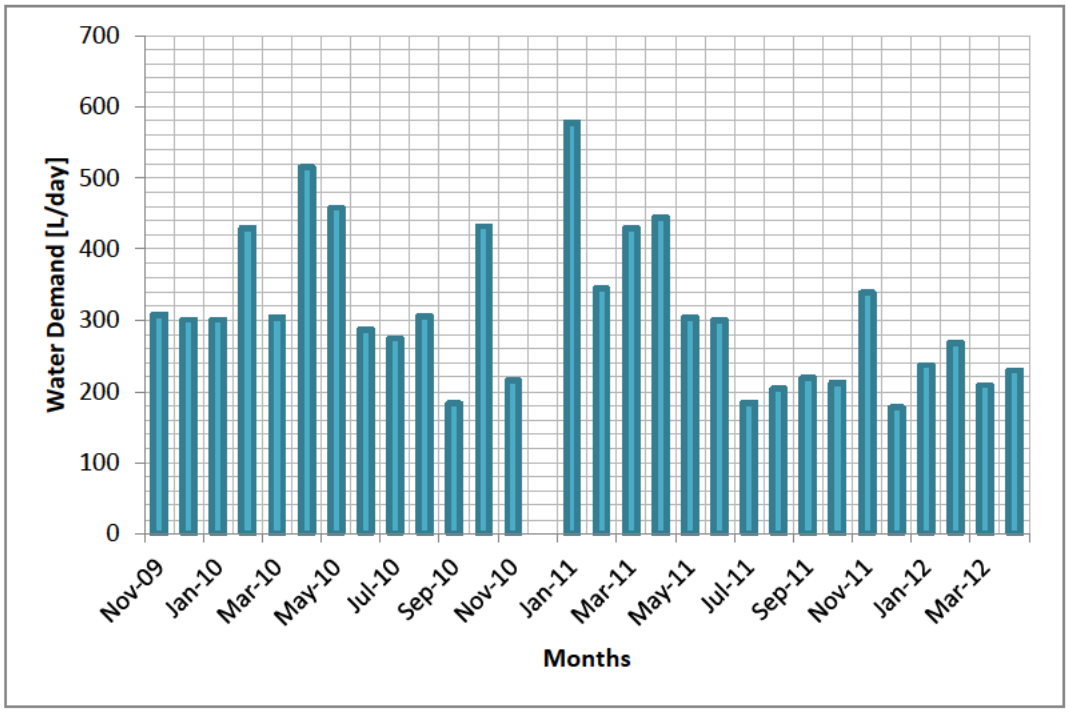

Figure 5: Average Daily Household Clean Water Demand

With these water demands available, an average household consumption amount could be proposed. This amount could then be used as a target in developing a suitably scaled system capable of meeting the clean water demand of an average Lynedoch household. Reviewing the recent average usage, it was decided to set the clean water demand at 240 L a day. Potentially, the target could be lowered even more since this would force users to be even more conservative with water use in the households. However, the greatest demand for clean water from a treatment system would be in summer when demand is slightly higher than the average; therefore, the target was kept at 240 L a day to support summer demands.

2.4 Water Quality at Lynedoch

Another aspect concerning the viability of grey water reclamation is water quality. Water quality evaluation at Lynedoch is performed by testing for various contaminants in the water. These include microbiological, chemical and inorganic contaminants. Examples of contaminants that are tested for include faecal coliforms, E. coli, pH, total suspended solids (TSS), nitrogen, phosphorus, fluoride and conductivity. All of these parameters give an indication of the level of contamination. Table 1 provides testing results from Dowling (2007) for the treated effluent from the wetland at Lynedoch. The acceptable quality levels

required are taken from the national drinking water standard, namely the South African National Standard (SANS) 241 (DWA, 2005).

Table 1: Water Quality at Lynedoch

	Faecal coliforms	E. coli	pH	TSS	Ammonia	Fluoride	Nitrate	Conductivity
Units	count/ 100 ml	count/ 100 ml		mg/L	mg/L	mg/L	mg/L	mS/m
SANS 241	10	0	5.0 - 9.5	< 1 200	< 1.5	< 1.5	< 11	< 150
Wetland sample	416	10	7.6	7	< 0.1	0.4	88	125
Remediation required	Yes	Yes	No	No	No	No	Yes	No

Source: Dowling (2007)

Also indicated are the areas in which a reduction in contamination would be required. It can be seen that improvements are needed in the faecal coliform, E. coli and nitrate areas. Faecal coliforms and E. coli are classified as microbiological contaminants, and nitrates fall into the chemical category. Based on this, it would appear that desalination processes should be able to decontaminate the treated water. The high operating temperatures of desalination systems should kill most of the microbiological contaminants, with the distillation process removing most of the chemical contaminants.

3. GREY WATER TREATMENT OPTIONS

Distillation processes are not the only manner in which grey water reclamation can be achieved, and hence other options should also be looked at. Investigation into these other treatment options will also ascertain the applicability of distillation systems in decontaminating grey water.

Conventional treatment of wastewater effluent consists of physical, chemical and biological processes, as described by Li, Otterpohl and Wichmann (2009). Physical processes include membrane filtration, distillation and sand filtration systems. Chemical processes entail using chemicals to treat the contaminants in

the water. Examples of biological processes include membrane bioreactors, up-flow anaerobic sludge blankets and artificial wetlands. Normally, a combination of processes is required for successful treatment.

Conversion of grey water into drinking water is unfortunately uncommon since grey water is mostly used for irrigation and flushing purposes. The only real effort being made to treat grey water to a drinkable water quality level takes place when water is a scarce resource. The most notable situation is found in the Namibian capital of Windhoek, and the facility is the oldest wastewater treatment facility to produce water for direct potable reuse (Van der Bruggen, 2010).

The wastewater treatment facility at Windhoek is run by NAMwater, the Namibian water corporation. Sewage water is sent through two wastewater treatment facilities before being pushed through an ultra-filtration system and a final oxidisation treatment. Windhoek tap water contains up to a maximum of one third of reclaimed water to keep salt buildup down at containable levels (NAMwater, 2006). These processes are, however, complex and need constant monitoring and maintenance.

According to Van der Bruggen (2010), the challenges facing water reuse are monitoring, pre-treatment requirements and contaminant removal. It is suggested that complementary processes are needed to overcome these challenges. In addition, the energy and capital costs associated with these processes need to be reduced. Furthermore, the public perception on water reuse needs to improve.

A solar-assisted distillation process is well suited to attaining the challenges described above since it has the potential to be low cost, requires no pre-treatment and requires minimal maintenance. Compared to the NAMwater process, it also would not result in a build-up of salt levels in the produced water.

Investigation of literature sources describing solar-powered grey water distillation revealed little. However, Hanson (2004) investigated the potential of using solar stills in treating contaminated water. Among the contaminants were nitrates and faecal coliforms. Both the nitrates and faecal coliforms were adequately removed although accidental cross-contamination did occur in some of the faecal coliform removal experiments. Velmurugan, Deenadayalan, Vinod and Srithar (2008) presented another distillation system that successfully recycled industrial effluent water. The results indicated a considerable reduction in chemical contaminants with the only biological indicator being the biological oxygen demand. Although this level dropped to zero, no further reference was made to the specific biological contaminants present.

After taking into account the findings of the literature sources described in the previous paragraphs, the author decided that solar-assisted distillation remained the most plausible solution to be used in conjunction with the processes already in place at Lynedoch. This decision was taken in light of the following: Using

membrane filtration would require technical knowledge in operation and high maintenance in keeping the membranes clean, as seen with the NAMWater system. Using grey water would increase the required maintenance due to the large amount of biological, physical and chemical contaminants present in the grey water. Similarly, chemical decontamination would not fit in with the ecological and sustainable living vision of Lynedoch.

4. CONCEPT DESIGN

With solar-assisted distillation chosen as the preferred decontamination process, a concept system was envisioned. This system would be a modular system capable of operating within the limitations of a normal household. The system had to be scalable to allow a cluster of systems to produce 240 L a day of clean potable water, meeting the requirements for an average Lynedoch household. Solar energy would be utilised with no external electrical requirements. The design had to be rugged to withstand outdoor use, and minimal supervision and maintenance were vital.

The next step was to characterise the whole system with a mathematical correlation, allowing the system to be simulated for different meteorological conditions. Various configurations could also be simulated and analysed, after which a suitable configuration could be chosen and dimensions could be derived. A prototype based on the proposed design could then be built.

However, initial investigations into the mathematical characterisation of solar-assisted distillation systems revealed that the mathematical correlations were dependent on the geometry of the distillation setup. This included needing the characteristic length of such a system, knowing the size and shape of the distillation enclosure used and knowing whether natural or forced convection was implemented. It was therefore decided to first investigate potential solar-assisted distillation configurations. From a specified configuration, a suitable mathematical correlation could then be developed.

4.1 Small-Scale Solar-Assisted Distillation Technologies and Processes

Current literature reviews on solar assisted distillation systems indicate a multitude of available designs (El-Ghonemy, 2012; Eltawil, Zhengming and Yuan, 2009). Although some of the designs are found in industry, the concept of solar-assisted distillation is still mainly found in research applications and prototype systems.

With a multitude of systems and configurations available, it was decided to firstly look at the most common type of solar desalination. This is a simple still composed of a water basin covered by a transparent material. The water heats up due to solar radiation, evaporates and then condenses on the transparent material, and the condensate is collected as distilled water.

Systems that are more complex utilise the latent heat of condensation, the heat given off when a vapour condenses into a liquid, to heat up another body of water, thereby recovering otherwise wasted heat. Such systems have more than one stage, with the number of stages, referring to the number of times that the latent heat is recovered. Some systems have direct solar energy collection abilities included in the design, and some employ indirect solar energy collection by using commercial solar water heating panels for heating the water. Specialised systems have incorporated vacuum systems to lower the ambient pressure inside the evaporation chamber, thereby allowing evaporation at lower temperatures.

For the proposed system, a simple design was envisioned, thereby hopefully reducing maintenance and operation requirements. To increase efficiency, a multiple-effect configuration was also favoured for the design. To realise this, a two-stage indirect solar energy collection system operating without vacuum was envisioned. This falls into the category of a multiple effect humidification dehumidification (MEHDH) system. A host of MEHDH configurations exists, and thus investigation was required into which configuration was the most suitable for the task at hand.

The first system that was considered was a system used by Bouchekima, Gros, Ouahes and Diboun (1998). The system is shown in Figure 6. The first tilted surface facing the sun, with the number 5 as identifier, is a transparent cover. The second surface, numbered 3, is the absorber plate. Beneath the absorber plate is a capillary fabric that transports brackish water across the back of the absorber. The absorber plate heats up the brackish water, allowing it to evaporate. The next plate acts as a condensing surface for the evaporated water. The latent heat of vaporisation released upon condensation in turn heats up the brackish water in the capillary fabric on the opposite side of the condensation plate. Evaporation and condensation occur in the same way as in the first instance, with this evaporation and condensation cycle referred to as the second stage or effect of the system.

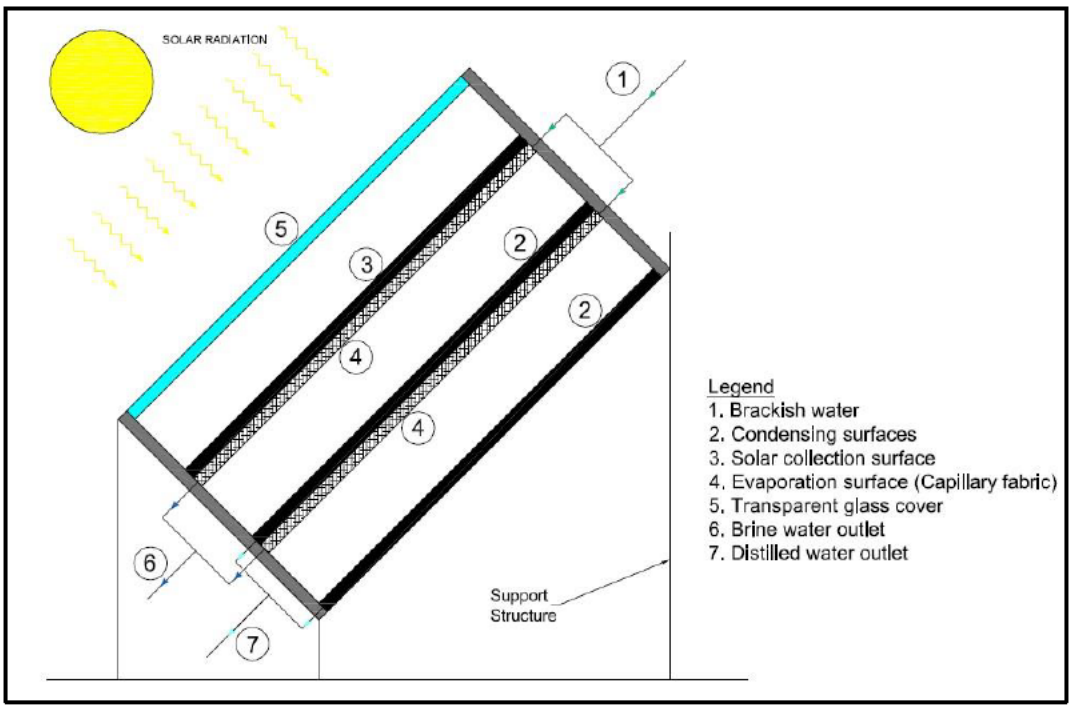

Figure 6: Capillary Film Distiller

(Bouchekima et al. 1998)

This system is a very simple one and can easily be constructed from materials typically found in a local hardware store. These include metal and glass sheets, cloth and plumbing pipes. Operation and maintenance requirements should also be minimal. The system does, however, not make use of a dedicated solar collector. This places limitations on the design. For example, the tilt of the system will be dictated by the optimum solar tilt angle. However, this could negatively affect the optimum angle for heat transfer and feed water flow rates required in the humidification process.

Baumgartner, Jung and Sizmann (1991) presented the second system that was considered. This system is a common configuration for a humidifier-dehumidifier system driven by natural convection. An enclosure is separated into three chambers by using dividing plates. Air circulation between the chambers is possible through open sections in the dividing plates. The central chamber houses a humidifier composed of suspended jute or hessian cloth. The other two chambers have clusters of pipes in them. With cooling fluid flowing inside the pipes, they act as condensing surfaces and hence the dehumidification area of the system.

This system is unfortunately not as simple in construction and maintenance

compared with the system of Bouchekima et al. (1998). The use of pipes also increases the cost of the system as compared to systems using flat plates as condensing surfaces. This system, however, does provide large surface areas in both the evaporating and condensing areas, resulting in potential higher yields.

Ahmed, Hrairi and Ismail (2009) provided a simpler multi-effect system coupled with a conventional solar still. The solar collector is separate from the humidification-dehumidification process and is referred to as an indirect solar still. Three effects are utilised as can be seen in Figure 7. The system does, however, use a vacuum pump to create a lower ambient pressure allowing evaporation to take place at a lower temperature. Although simple in theory, the vacuum system is a complex addition and will substantially increase the overall cost of the system. This higher cost had to be evaluated against the increased yield of the system induced by the vacuum system.

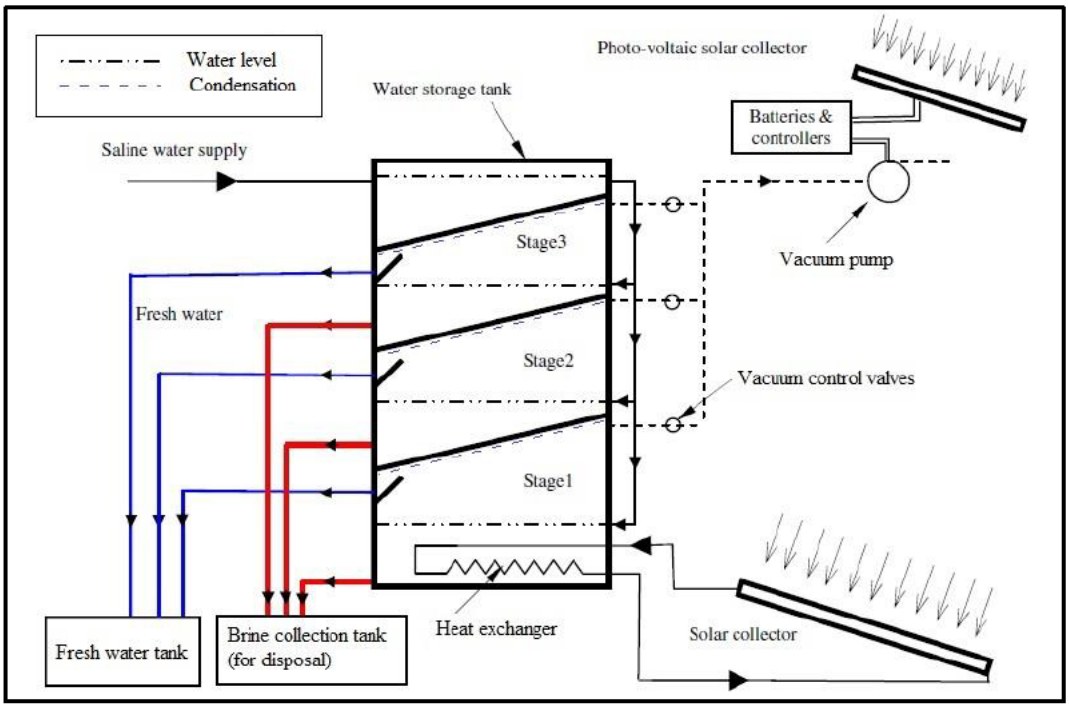

Figure 7: Diagram of an Evacuated Multistage Solar Still

(Ahmed et al. 2009)

Without the vacuum addition, the system presents a simple design with indirect solar collection. The system can also potentially operate with a gravity-driven water-feeding system.

Garg, Adhikari and Kumar (2002) provided a system similar to that of Baumgartner et al. (1991) in that the humidification-dehumidification process is of the same configuration. The system also employs indirect solar energy collection that feeds a storage tank with a heat exchanger inside, as seen in Figure 8. The heat exchanger is part of the humidification-dehumidification loop. The humidification-dehumidification chamber is again, as is the case with Baumgartner et al. (1991), a more complex configuration.

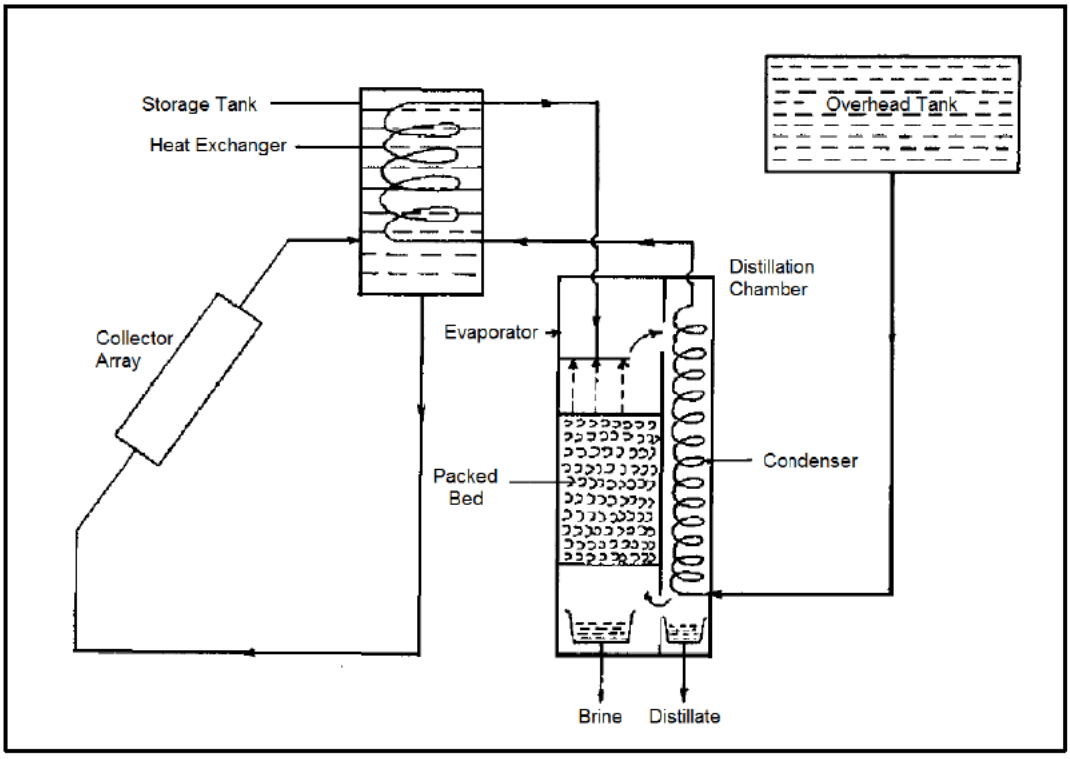

Figure 8: Multi-effect Solar Distillation System

(Garg et al. 2002)

Badran, Al-Hallaq, Eyal Salman and Odat et al. (2005) provided the system configuration seen in Figure 9. This system does not use multiple effects. It uses a conventional solar still for the humidification-dehumidification cycle with the solar collector providing additional energy to the system. The feed and constant head tanks provide a potential solution to storage of water and maintain a constant feed rate to the still.

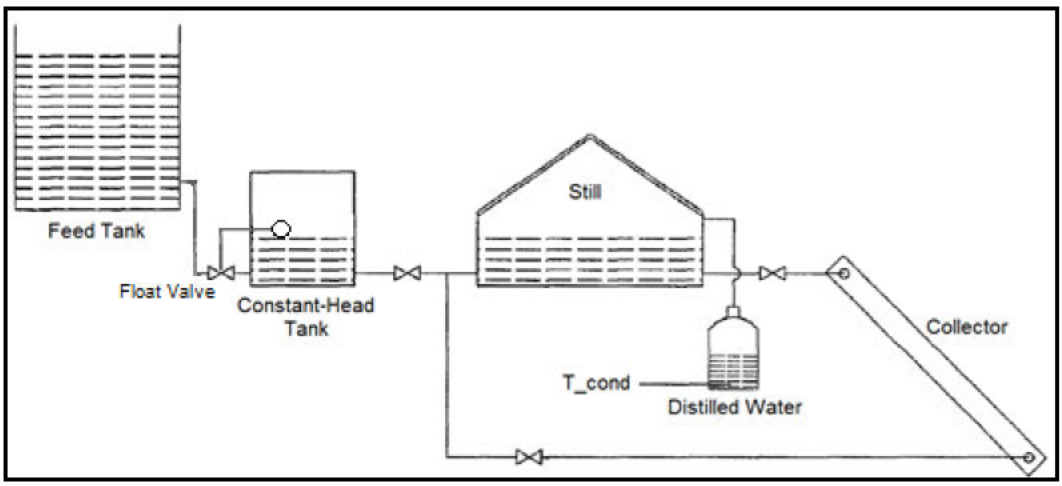

Figure 9: Solar Still Coupled with Collector

(Badran et al. 2005)

4.2 Proposed Design

All of the systems described above provided inputs and configurations that were suitable for the specific requirements of the project. The proposed design was therefore a combination of various elements found in these systems.

The design started with placing the evaporation and condensation area configuration similarly to that found in the systems of Bouchekima et al. (1998) and Ahmed et al. (2009), but in a vertical rather than horizontal position. This created an enclosure known as a distillation cell. Such distillation cells were thoroughly investigated by Ben Jabrallah, Belghith, Cherif and Corriou (2005) and their results showed positive results in terms of produced distillate flow.

Next, a circular configuration was proposed by taking the distillation cell and rotating it in a full circular configuration. This reduced areas of possible losses and increased the condensing surface area compared to the coinciding evaporator area. A suitable central storage tank was also created. The evaporator would, however, be fitted with jute cloth to increase the evaporation surface area and allow a water film to form on the outside of the evaporator plate. Two such distillation cells were proposed to create a two-stage solar-assisted distillation system with the stages referred to as Stage 1 and Stage 2. The overall system layout would be similar to the system of Badran et al. (2005) in that an indirect solar collection method was preferred.

Figure 10 shows a sectional view from the centreline of the circular configuration, seen by the dashed line on the left, to the outer tank wall of the proposed circular

design. As can be seen, the hessian cloth would be folded over the top of the water tank walls to be in contact with the treated wastewater. This would initiate the capillary action of the cloth, ensuring that the cloth stayed wet to allow continued evaporation. Te1 and Te2 refer to the temperature of the two cloths, which are also the evaporation temperatures for the two distillation cells. Tc1 and Tc2 again refer to the condensation temperatures of the respective distillation cells.

The thick arrows represent the natural convection mass and heat transfer that would take place inside the distillation cell. Since the evaporation temperatures would be higher than the condensation temperatures, a natural convection cycle would be formed. The red arrow, in the top left corner of the distillation cell, shows the warm air rising with the blue arrow, in the bottom right corner of the distillation cell, showing the colder air moving downwards. The brine wastewater and clean water at the bottom of the enclosures would flow out of holes in the bottom plate. A more detailed representation with a view of the circular configuration is seen in Appendix D.

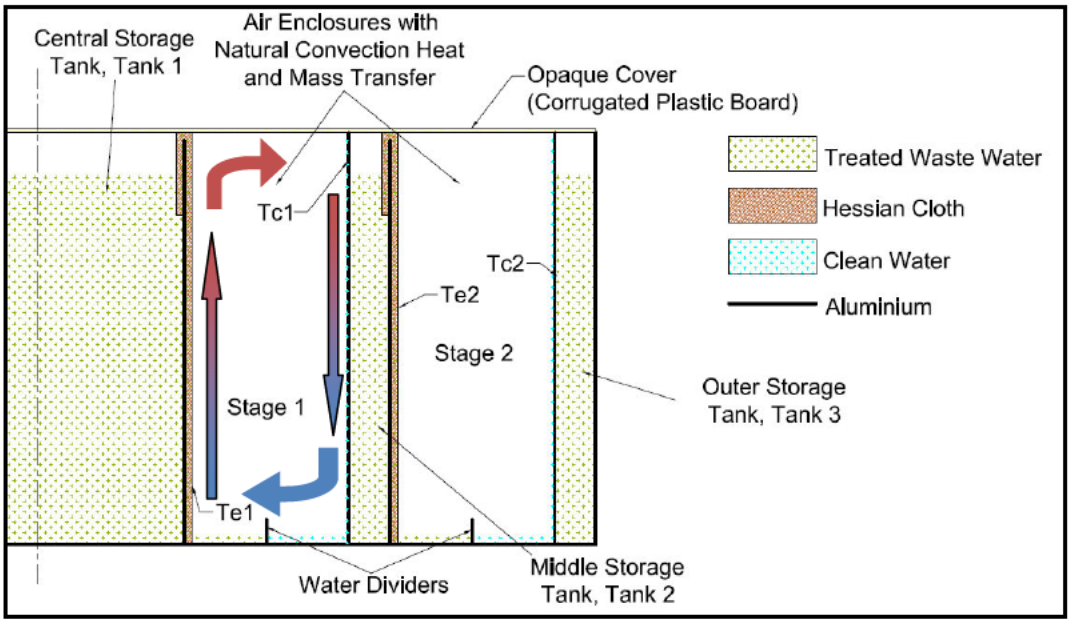

Figure 10: Section View of Proposed Circular Design

The proposed configuration had not been found in the literature and therefore represented a new configuration for solar-assisted distillation systems. The design could also be constructed using low-cost elements such as metal sheets, cloth and plumbing pipes. The heat source driving the distillation system would be in the form of commercial solar water heating panels connected to the circular

distillation system at the central water storage tank. A photovoltaic (PV)-powered water pump would drive circulation between the central water storage tank and the solar panels. Feed water would be delivered from a constant head tank.

5. MATHEMATICAL CORRELATIONS OF THE DISTILLATION PROCESS

In order for simulation of the entire proposed system to be carried out, including the solar water heating panels and proposed two-stage distillation system, each component of the system needed to be characterised by a specific mathematical correlation. All the models could then be structured together to form a model of the entire system capable of simulating the performance of the system under varying meteorological conditions.

The first step was to develop a mathematical correlation for the proposed two-stage distillation system. Although a distillation process is elementary in operation, building a mathematical correlation was more complex. It was therefore important to ensure that the mathematical correlation provided an accurate representation of an actual two-stage distillation system. With the proposed shape and configuration of the distillation system already established, the mathematical correlation could be developed.

5.1 Fundamental Equations

Although the proposed design was a solar-assisted distillation system, the distillation process was still the same as any other distillation process and could be viewed as a convective heat and mass transfer problem. Hence, the author started by looking at the fundamental conservation equations that applied to the boundary layers found in convective heat and mass transfer.

Convective heat and mass transfer is described in Chapter 18 of Convective heat and mass transfer (Kays, Crawford and Weigand, 2005). This chapter provides a basic definition and understanding of convective heat and mass transfer, and the conditions described in the chapter are very similar to the distillation process that was being investigated. The chapter looks at heat and mass transfer from one phase to another. The boundary layer investigated is a two-dimensional boundary layer with x and y coordinates. The analysis is limited to steady flow and no body-forces, and due to the low velocities encountered, viscous energy dissipation as well as pressure gradient influences on the energy equation is neglected.

With these assumptions specified, differential equations that need to be satisfied emerge. These include differential equations for the diffusion of components, diffusion of chemical elements, energy, continuity and momentum. These differential equations emanate from the differential equations developed in Chapter 4 of the same textbook, Convective heat and mass transfer (Kays et al. 2005), which in turn originate from the fundamental conservation law equations. The development of these differential equations is not shown here.

An example, similar to the distillation process encountered in this study, is used to further simplify these differential equations. The example considers a binary mixture with no chemical reactions and constant fluid properties similar to the distillation process in the study, which is a binary mixture of water and air, has no chemical reactions and the fluid properties are also assumed constant. A new set of differential equations is produced for the example case and presented on pages 402 and 403 in Chapter 18 of Convective heat and mass transfer (Kays et al. 2005).

In a study by Ben Jabrallah et al. (2005) on convective heat and mass transfer in an enclosure, the same differential equations, as per the example case above, were developed with the difference being that the equations were applicable to the y direction as well. These equations were split between the liquid phase representing the falling film of water and the gas phase representing the air and water vapour mixture found in the distillation cell. The control volume used to formulate these equations was a rectangular enclosure with the liquid falling film on the one side from where evaporation occurred. This enclosure could also be found in the proposed design and hence formed the basis for solving the applicable differential equations.

Figure 11 shows the enclosure with the applicable variables. The xy coordinate structure is used with x being the horizontal variable and y being the vertical variable. The enclosure has a width of b and a height of h. At the top of the enclosure, fluid flows in at a rate of m_in and at a temperature T_in. At the bottom, a brine flow stream and a clean water flow stream exit the enclosure. The sum of the brine flow and clean water flow rates is equal to m_in. The heat transfer rate to the liquid film is qf, with dy representing the width of the fluid film. The condensation plate is at temperature T_c.

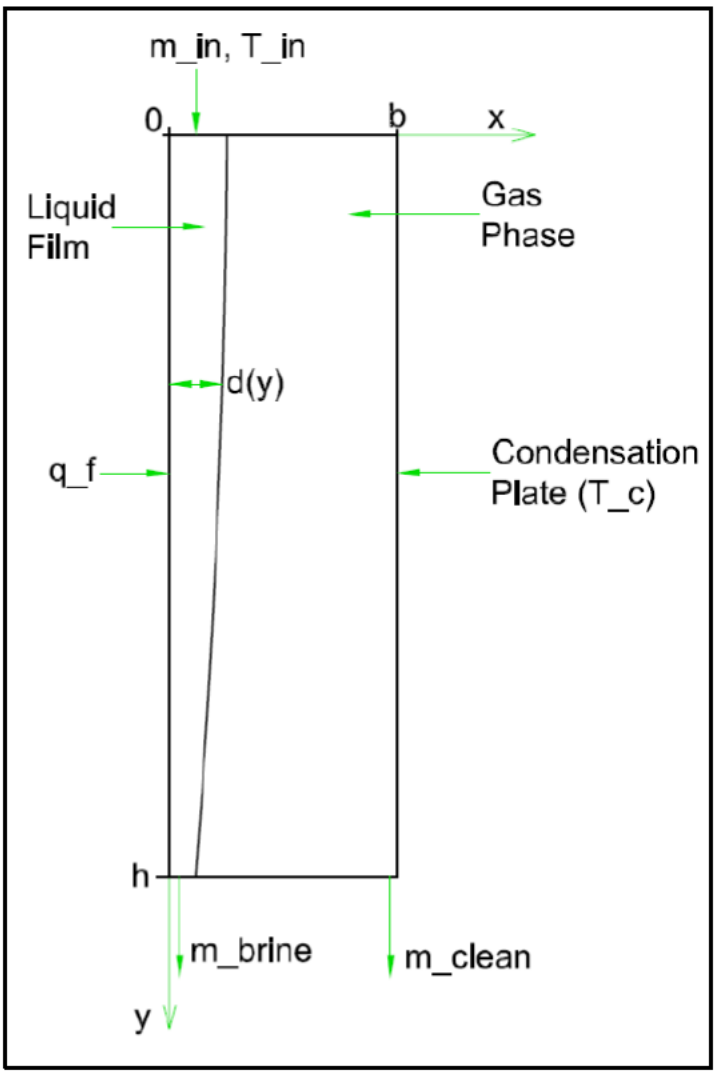

Figure 11: Scheme for Distillation Cell

(Ben Jabrallah et al. 2005)

The differential equations developed by Ben Jabrallah et al. (2005) for this enclosure are presented in the equations below. Equations 5.1 and 5.2 represent the momentum and energy equations respectively for the liquid phase. Equation 5.3 represents the continuity equation, equations 5.4 and 5.5 the u and v momentum equations respectively, Equation 5.6 the energy equation and Equation 5.7 the mass diffusion equation, all relating to the air and water vapour gas phase.

Liquid phase

$$\frac{\partial}{\partial x}\left(\mu\frac{\partial v}{\partial x}\right)+\rho g=0 \tag{5.1}$$

$$\rho c_p u\frac{\partial T}{\partial y}=\frac{\partial}{\partial x}\left(k\frac{\partial T}{\partial x}\right) \tag{5.2}$$

Gas Phase

$$\frac{\partial u}{\partial x}+\frac{\partial v}{\partial y}=0 \tag{5.3}$$

$$\rho u\frac{\partial u}{\partial x}+\rho v\frac{\partial u}{\partial y}=-\frac{\partial P}{\partial x}+\mu\left(\frac{\partial^2 u}{\partial x^2}+\frac{\partial^2 u}{\partial y^2}\right) \tag{5.4}$$

$$\rho u\frac{\partial v}{\partial x}+\rho v\frac{\partial v}{\partial y}=-\frac{\partial P}{\partial y}+\rho g+\mu\left(\frac{\partial^2 v}{\partial x^2}+\frac{\partial^2 v}{\partial y^2}\right) \tag{5.5}$$

$$\rho c_p\left(u\frac{\partial T}{\partial x}+v\frac{\partial T}{\partial y}\right)=k\left(\frac{\partial^2 T}{\partial x^2}+\frac{\partial^2 T}{\partial y^2}\right)+\rho D\left(c_{pv}-c_{pa}\right)\frac{\partial T}{\partial x}\frac{\partial m}{\partial x} \tag{5.6}$$

$$u\frac{\partial m}{\partial x}+v\frac{\partial m}{\partial y}=D\left(\frac{\partial^2 m}{\partial x^2}+\frac{\partial^2 m}{\partial y^2}\right) \tag{5.7}$$

Solving the above differential equations requires a set of boundary conditions. The boundary conditions used by Ben Jabrallah et al. (2005) were found to be applicable to the conditions found in the distillation cell of the proposed design. However, the distillation cell of Ben Jabrallah et al. (2005) utilises a constant heat flux at the liquid falling film and a constant condensation temperature at the condensation wall. The heat flux encountered in the proposed distillation cell was not a constant since the heat flux was a function of the solar energy collected by the solar water heating panels. Similarly, the condensation temperature of the condensation wall was also a function of the heat and mass transfer taking place in the distillation cell.

Discretising these differential equations and then solving them would therefore be a time-consuming task. Further mathematical models of the other components of

the proposed solar-assisted distillation system, such as the solar water heating panels and water storage tanks, would also need to be incorporated to reflect the entire solar-assisted distillation system.

It was thus the opinion of the author that although solving the governing differential equations would provide highly credible results, it did not fall within the objectives set out for the study. A simplified mathematical correlation providing an accurate estimation of the performance of the distillation cell would be more suitable. The next section describes the steps taken to find a suitable simplified mathematical correlation and the implementation thereof.

5.2 Simplified Mathematical Correlation Options

The goal of the simplified mathematical correlations was to predict the distillate flow rate of the distillation cell of the solar-assisted distillation system. In the literature, various models exist, all stemming from either a convective heat transfer viewpoint or a convective mass transfer viewpoint. These two distinct approaches are presented by equations 5.8 and 5.9 respectively (Kays et al. 2005). In evaporation terms, Equation 5.8 is seen as a heat flux-controlled evaporation process and Equation 5.9 as a mass flux-controlled evaporation process. Both also have a conductance term, in this case the heat and mass transfer coefficients, and a potential differential given by the temperature and density differences.

$$\dot{q} = h_{heat} (T_1 - T_2) \tag{5.8}$$

$$\dot{m} = h_{mass} (\rho_1 - \rho_2) \tag{5.9}$$

In order to find the mass flow rate, for Equation 5.8 the main addition is Equation 5.10. Equation 5.10 relates the mass flow rate in terms of the heat transfer rate divided by the latent heat of vaporisation for water. This only leaves the heat transfer coefficient left as an unknown, which is exactly the focus of the different researchers and the resultant different models.

$$\dot{q} = \dot{m} h_{fg}$$
$$\dot{m} = \frac{\dot{q}}{h_{fg}} \tag{5.10}$$

To calculate Equation 5.9, researchers use the so-called analogy between heat and mass transfer. The most widely used analogy is the Chilton-Colburn analogy suggested by Chilton and Colburn in 1934 (Cengel, 2006). The Chilton-Colburn analogy is presented in Equation 5.11. Transformation occurs from Equation 5.12, using the definitions for the Stanton, Schmidt and Prandtl numbers. Equation 5.15 relates the mass transfer coefficient in terms of the heat transfer coefficient, density, specific heat capacity and the Lewis number. The Lewis number is the ratio between the thermal and mass diffusivities.

$$St_{heat} \, \mathrm{Pr}^{2/3} = St_{mass} Sc^{2/3} \tag{5.11}$$

$$\frac{St_{heat}}{St_{mass}} = \left(\frac{Sc}{\mathrm{Pr}} \right)^{2/3} \tag{5.12}$$

$$\frac{h_{heat}}{h_{mass}} = \left(\frac{Sc}{\mathrm{Pr}} \right)^{2/3} \tag{5.13}$$

$$= \rho c_p \left(\frac{\alpha}{D_{AB}} \right)^{2/3} \tag{5.14}$$

$$h_{mass} = \frac{1}{h_{heat}} \rho c_p \left(Le \right)^{2/3} \tag{5.15}$$

Equation 5.15 therefore allows solving Equation 5.9 without requiring the mass transfer coefficient. This is helpful since heat transfer coefficients are more widely used and easier to obtain from literature compared to mass transfer coefficients. In solar-assisted distillation systems, finding the heat transfer coefficient is the most investigated aspect. Most researchers propose a relation to calculate the heat transfer coefficient and in turn calculate the mass flow rate of the distillation system by using either Equation 5.9 or Equation 5.10.

The first researcher to provide a mathematical correlation for predicting solar still production was Dunkle (1961) and this relation still holds true today for temperatures below 100 °C. Dunkle proposed the following:

$$q_{ew} = 0.0163 h_{heat} \frac{P_e - P_a}{T_e - T_a} \tag{5.16}$$

$$h_{heat} = 0.884 \left[\Delta T ' \right]^{\frac{1}{3}} \tag{5.17}$$

$$\Delta T ' = \left[(T_e - T_c) + \frac{(P_e - P_c)(T_e + 273.15)}{268.9 \cdot 10^3 - P_e} \right] \tag{5.18}$$

Kumar and Tiwari (1996) proposed the following correlation for the convective heat transfer coefficient. Seen in Equation 5.19, also known as the Nusselt-Rayleigh correlation, the Rayleigh number is the product of the Grasshof and Prandtl numbers. Together with the definitions of the Grasshof and Prandtl numbers and the constants *C* and *n*, a suitable convective heat transfer coefficient is calculated. The calculated convective heat transfer coefficient is then utilised in finding the mass flow rate as per Dunkle (1961), using Equation 5.16 and then Equation 5.10.

$$Nu = C(Ra)^n = C(Gr.\,\mathrm{Pr})^n \tag{5.19}$$

$$Nu = \frac{h_{heat} l}{k} = C(Gr.\,\mathrm{Pr})^n \tag{5.20}$$

$$h_{heat} = \left(\frac{k}{l} \right) C(Gr.\,\mathrm{Pr})^n \tag{5.21}$$

$$Gr = \frac{\beta g l^3 \rho^2 \Delta T}{\mu^2} \tag{5.22}$$

$$\Pr = \frac{\mu c_p}{k} \tag{5.23}$$

Chen, Bar, Ge, Miao and Sun (1984) proposed the following model for calculating the convective heat transfer coefficient:

$$h_{heat} = 0.2Ra^{0\,26}\left(\frac{k}{l}\right) \tag{5.24}$$

Adhikari, Kumar and Kumar (1990) gave the following direct correlation for calculating the mass flow rate. The constant a, is related to specific temperatures differences provided in a table not shown here.

$$\dot{m} = a(\Delta T')^n(P_e - P_c) \tag{5.25}$$

Zheng, Zhang, Zhang and Wu (2002) followed a similar method to that of Kumar and Tiwari (1996) in using the Nusselt-Rayleigh relation, Equation 5.19, to calculate the convective heat transfer coefficient. However, Zheng et al. proposed a modified Rayleigh number since their Rayleigh number depended on a different temperature differential. The temperature differential seen in Equation 5.28 is an expansion of the temperature differential used by Dunkle, Equation 5.18, since it includes the molecular weights of the moist air and vapour. The correlation of Zheng et al. calculates the convective heat transfer using Equation 5.26 together with equations 5.27 and 5.28.

$$h_{heat} = 0.2(Ra')^{0\,26}\left(\frac{k}{l}\right) \tag{5.26}$$

$$Ra' = \frac{l^3\rho g\beta}{\mu\alpha}\Delta T'' \tag{5.27}$$

$$\Delta T'' = \left[(T_e - T_c) + \frac{(P_e - P_c)(T_e + 273.15)}{\frac{M_a P_t}{M_a - M_w} - P_e}\right] \tag{5.28}$$

With different still designs, researchers tend to define their own correlations specific to their own still geometry and configuration. It was therefore difficult to evaluate which model was the best suited to the still geometry and configuration of the study. However, some researchers also use the correlations presented above rather than developing their own. Kalogirou (2004) uses the model proposed by Kumar and Tiwari (1996). Tsilingiris (2010) has done extensive work on the analysis of heat and mass transfer in solar stills and yet uses the model proposed by Zheng et al. (2002), although using different constants for the Nusselt-Rayleigh relation, Equation 5.19.

5.3 Selected Mathematical Correlation

In order to find a suitable correlation for the geometry of the proposed design, the correlations of each researcher presented above were evaluated. The Nusselt-Rayleigh relation used in some of the mathematical correlation was, however, not to be included as a parameter because the constants in the Nusselt-Rayleigh relation (Equation 5.19) are derived from experimental results based on the specific geometry of the design in question. The Nusselt-Rayleigh relation described in Section 5.4 was incorporated into the selected convective heat transfer correlation.

The correlations presented in Section 5.2 were compared against the geometry and specific configuration of the proposed circular distillation system. Evaluation was done by way of drawing up a comparison table of the selected correlations seen in Table 2. Various parameters unique to the proposed circular distillation system were used as a benchmark to find the best-suited relation. These included parameters such as the specific operating temperature range, the use of multiple effects as well as the solar energy-collecting method used.

From Table 2 it is evident that the correlation of Zheng et al. (2002) was found to be the most favoured correlation. This is due to the suitable range for temperature and Rayleigh numbers being within the proposed circular distillation operating range. Zheng et al. also incorporate a characteristic length, multiple effects and independent solar collection, and the distillation cell is not exposed to solar insolation. The only negative is that the correlation does not evaluate the humid-air component separately. However, overall the correlation of Zheng et al. still contains the most suitable elements and was therefore assumed to be the most appropriate correlation to use for the proposed circular distillation system. The correlation is presented below for clarity.

$$\dot{m} = \frac{h_{heat}}{\rho_f c_{pf} Le^{(1-n)}} \frac{M_w}{R} \left(\frac{P_e}{T_e} - \frac{P_c}{T_c} \right) \tag{5.29}$$

$$h_{heat} = C(Ra')^n \left(\frac{k}{l} \right) \tag{5.30}$$

$$Ra' = \frac{l^3 \rho g \beta}{\mu \alpha} \Delta T'' \tag{5.31}$$

$$\Delta T'' = \left[(T_e - T_c) + \frac{(P_e - P_c)(T_e + 273.15)}{\frac{M_a P_t}{M_a - M_w} - P_e} \right] \tag{5.32}$$

Table 2: Mathematical Correlation Comparison Table

		Mathematical correlations						
		Tsilingiris	Zheng	Chen	Dunkle	Adhikari	Kumar Tiwari	Ahsan
Criteria	Correlation temperature range	92	86		58	80	59.7	61
		19	33.5		42	40	36.6	25
	Incorporates characteristic length	No	Yes	Yes	No	No	No	Yes
	Maximum Rayleigh number range	7.50E +06	7.50E +06	2.00E +06	2.00E +06	2.00E +06	2.00E +06	NA
	Still or stacked	Still	Stacked	Still	Still	Still	Still	Tubular still
	Independent solar collector	No	Yes	No	No	No	No	No
	Multiple effects	No	Yes	No	No	No	No	No
	Humid-air treatment	No	No	No	No	No	No	Yes
	Air exposed to solar insolation	No	No	Yes	Yes	Yes	Yes	Yes

5.4 Nusselt-Rayleigh Relation

As mentioned in Chapter 5.3, an applicable Nusselt-Rayleigh relation, given by Equation 5.19, was investigated separately. The reason was that the geometric characteristics and subsequently the flow characteristics of the proposed circular distillation system were only reflected partially in the mathematical correlations. Using a more specific Nusselt-Rayleigh relation would result in a more accurate correlation of the proposed circular distillation system. This section looks at the available Nusselt-Rayleigh relations in the literature and suggests a suitable Nusselt-Rayleigh relation that could be used in conjunction with the mathematical correlation of Zheng et al. (2002).

The proposed circular distillation system can be described as a natural convection vertical annular enclosure. Investigations into natural convection vertical annular enclosures are limited and even fewer Nusselt-Rayleigh relations are available as compared to the more common vertical rectangular enclosures. However, Kumar and Kalam (1991), Prasad (1986), Thomas and De Vahl Davis (1970), Vekata Reddy and Narasimham (2008), and Weng and Chu (1996) do provide vertical annular enclosure correlations. Unfortunately, the correlations from Prasad are provided for very low Rayleigh numbers and the correlation of Weng and Chu does not take into account the Rayleigh number. Both these correlations were therefore not investigated further in the study.

With only three applicable correlations, more comparisons were needed. Comparing the vertical circular correlations with vertical rectangular enclosures was done since vertical rectangular enclosures are investigated more often and in more detail in the literature and share similarities with vertical circular enclosure. This is due to rectangular enclosures and circular enclosures having the same two-dimensional plane of investigation. The plane of investigation for a rectangular enclosure has insulated top and bottom walls with a temperature differential between the other two opposing walls. This is the same for circular enclosures, and the only difference occurs when investigations are conducted in the third dimension, which are not common. Similarities should therefore exist, allowing comparisons to be drawn between the vertical circular and rectangular enclosures.

The general Nusselt-Rayleigh relation provides a relationship between the Rayleigh number and the Nusselt number for given constants. When applied to rectangular and circular enclosures, another term is added to the relation. This term relates to the aspect ratio of the geometry and has an exponential constant. When the Nusselt-Rayleigh relation is applied to circular cavities, another term is introduced to incorporate the radius ratio of the geometry as well. This term also has an exponential term, which includes the radius ratio itself.

Equation 5.33 below shows the Nusselt-Rayleigh relation as used in vertical circular enclosures with the different relation constants. For vertical rectangular enclosures, the radius ratio term falls away. Table 3 shows the constants used by the different researchers. The vertical rectangular enclosures correlations are provided by Berkovsky (cited in Kays et al. 2005), Inaba (1984), Jakob (1964), Yin, Chen and Wung (1978). All of the correlations are plotted in Figure 12 for the specific Rayleigh numbers. These Rayleigh numbers are not calculated from definition but are the minimum and maximum Rayleigh number region where all the correlations apply. The thick lines represent the vertical circular enclosure correlations, and the thin lines represent the vertical rectangular enclosure correlations.

$$Nu = C(Ra)^n \left(\frac{H}{W}\right)^b \kappa^{\left(d+\frac{e}{\kappa}\right)} \tag{5.33}$$

Table 3: Constants for Nusselt Rayleigh Relation

	Constants				
	C	*n*	*b*	*d*	*e*
Researchers					
Inaba	0.271	0.25	-0.21	0	0
Jakob	0.065	0.333	-0.111	0	0
Yin	0.21	0.269	-0.131	0	0
Berkovsky	0.22	0.28	-0.25	0	0
Kumar & Kalam	0.18	0.278	-0.122	0.34	0.329
Venkata Reddy & Narasimham	0.5248	0.2001	-0.136	-0.1139	-0.6193
Thomas & De Vahl Davis	0.286	0.258	-0.238	0.442	0

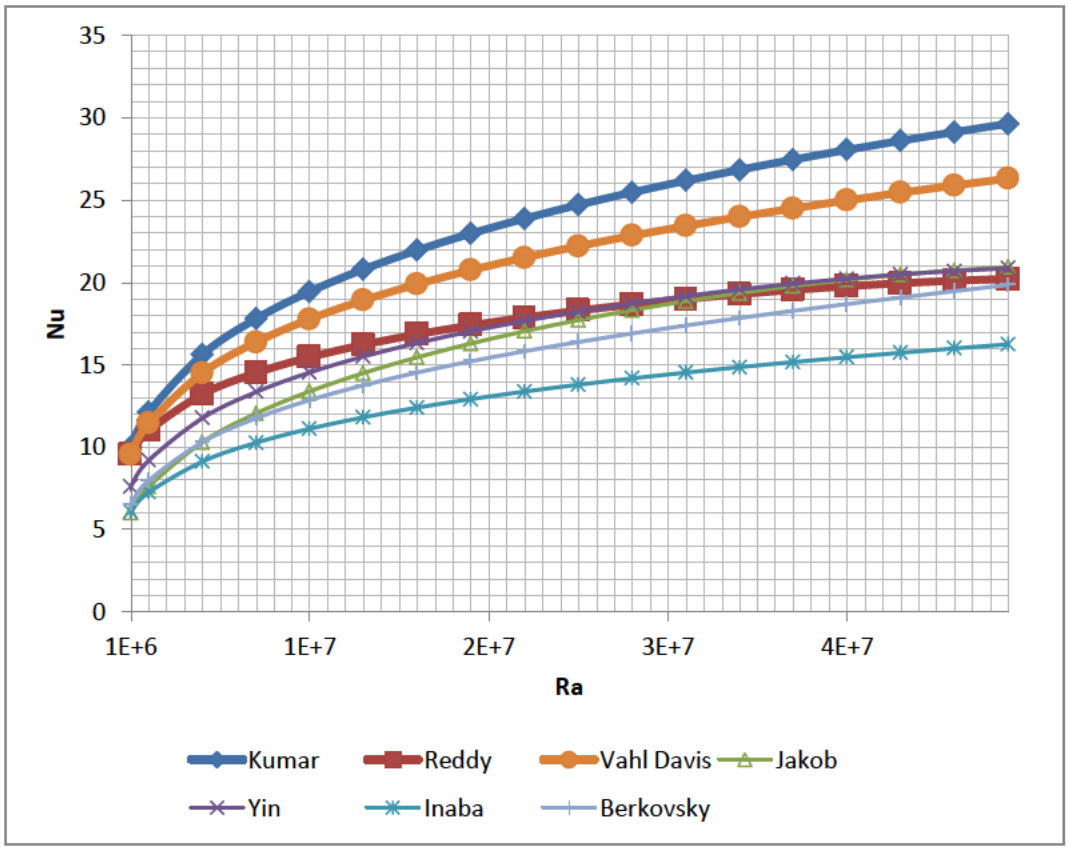

Figure 12: Nusselt-Rayleigh Relation for H/W = 5, K = 2

The Grasshof number represents the ratio of the buoyancy versus viscous forces in the fluid, in this case moist air. This is an indication of the natural convection effects present in the fluid with higher numbers relating to higher natural convection fluid velocities. The Prandtl number in turn represents the momentum versus thermal diffusivities of the fluid with higher Prandtl numbers therefore relating to more rapid velocity profile development.

Higher Rayleigh numbers, the product of the Grasshof and Prandtl numbers, should therefore translate into higher heat transfer rates since the potential for convective heat transfer is higher. This is exactly what the Nusselt-Rayleigh relation indicates. However, in this case the geometric influences are also incorporated into the aspect and radius ratios. Figure 12 thus represents the heat transfer capabilities of the fluid for the given fluid conditions and dimensional parameters at hand, according to each researcher's findings.

From Figure 12 one can see that the correlations for vertical circular enclosures predict the Nusselt number slightly higher compared to the vertical rectangular enclosure correlations. The circular correlation by Venkata Reddy and

Narasimham is the lowest of the vertical circular correlations, predicting the Nusselt number more in line with the vertical rectangular enclosure correlations. However, the correlation of Venkata Reddy and Narasimham is defined not only for the enclosure but also for the initial stage of the enclosed annular system that they investigated. This initial stage is a solid metal core. The applicability of Venkata Reddy and Narasimham's correlation to vertical circular enclosures is therefore less credible as compared against the other vertical circular and rectangular enclosures, which only apply to fluid-filled enclosures, as is the case for the proposed vertical circular distillation system. In addition, an investigation by Sankar and Venkatachalappa (2007) showed that circular enclosures did produce larger Nusselt numbers as compared to rectangular enclosures under similar conditions. The correlation of Venkata Reddy and Narasimham was consequently not investigated further.

The only options left were the correlations of Kumar and Kalam (1991) and Thomas and De Vahl Davis (1970). The applicable range of Rayleigh number usage for both correlations was found to be just below the operating conditions of the proposed circular vertical enclosure distillation system at Rayleigh numbers of 5×10^6 to 1.5×10^7. The correlation of Kumar and Kalam is, however, a more recent investigation and takes into account the results of Thomas and De Vahl Davis. Kumar and Kalam also take into account the impact of the radius ratio on the outcome. Consequently, the correlation of Kumar and Kalam was selected as the most suited correlation in determining the Nusselt-Rayleigh relation for the proposed vertical circular design.

The correlation of Kumar and Kalam (1991) was to replace the general Nusselt-Rayleigh relation used in the mathematical correlation of Zheng et al (2002). The heat transfer coefficient was then calculated using the modified Rayleigh number as per the original Zheng et al. correlation. The resultant equation is shown in Equation 5.34.

$$h_{heat} = C(Ra')^n \left(\frac{k}{l}\right)\left(\frac{H}{W}\right)^b \kappa^{\left(d+\frac{e}{\kappa}\right)} \tag{5.34}$$

5.5 Algebraic Correlation for Humid Air Properties

Although the chosen mathematical correlation provides a tool to solve for the specific distillate flow of a solar-assisted distillation cell, the results are dependent on the properties of the fluid, in this case a mixture of air and water vapour also referred to as moist air. The properties of moist air differ from those of dry air,

especially with an increase in temperature. It is thus crucial to use accurate moist air properties at the temperatures investigated to ensure accurate results.

Calculating accurate parameters of moist air is possible if the temperature of the moist air and the humidity are known. For the given application of evaporation and condensation in an enclosure, the moist air is assumed to be close to saturation levels. Therefore, the relative humidity of the air is assumed to be close to 100%. Tsilingiris (2008) also made this assumption for calculating solar still production. Furthermore, results from investigations by Ben Jabrallah, Belghith and Corriou (2006) into distillation cells showed that the humidity ratio of the moist air inside the distillation cell was close to saturation levels, again pointing towards a relative humidity of close to 100%.

Ahsan and Fukuhara (2010) did extensive research on tubular-designed solar stills. The main theme of their research was inclusion of a moist air model in the modelling of solar stills. Results from their investigations showed that the humidity inside the glass tube enclosure was below saturation levels. However, in their system, the air was exposed to solar radiation, thereby absorbing energy directly from the sun. This increased the temperature of the air above what would be expected if the air was only heated by the water, as was the case for the proposed circular distillation system in the current study. The assumption that the moist air inside the cavity was close to saturation was therefore maintained and the modelling was conducted accordingly.

As mentioned in Section 5.2, Tsilingiris did extensive work on solar stills and specifically research into the influence of variable moist air properties on distillate production. In his research, Tsilingiris (2008) presented fitted expressions for use specifically in computer simulations. Tsilingiris methodically compared his results from the correlations against literature sources, confirming their accuracy. Esterhuyse (2004) also used correlations to calculate the properties of moist air. Different humidity ratio values can be calculated using the methods used by Esterhuyse although more parameters than just the air temperature are required.

However, the correlations provided by Tsilingiris (2008) were the correlations of choice. This was due to the extensive research done by Tsilingiris on the subject of humid-air properties as well as the various validations conducted. Furthermore, the correlations of Tsilingiris are specific to the temperature region of 0-100 °C, which is in line with the current investigated temperature range. The methods of Esterhuyse (2004) are applicable to a wider temperature range extending above 100 °C. The constants of the correlations of Tsilingiris are presented in Appendix C.

With the implementation of the correlations of Tsilingiris (2008), the mathematical correlation of Zheng et al. (2002) becomes dependent on only two temperatures, namely the evaporation and condensation temperatures. Although this might

reduce the accuracy, the usefulness of the correlation increases considerably by requiring only the evaporation and condensation temperatures of a system.

6. PROPOSED PROTOTYPE MODEL PARAMETERS

The availability of a mathematical correlation to describe and predict the distillation process was a valuable tool in the design of a prototype for the proposed vertical circular distillation system. The mathematical correlation of Zheng et al. (2002) could be used to find the optimum prototype dimensions since the configuration of the vertical circular enclosure had already been finalised.

This chapter then describes how the mathematical correlation of Zheng et al. (2002) was used to help find optimum dimensions for the proposed prototype. The simulations described in this chapter show the impact of different dimensions on the distillate production rate as calculated by the mathematical correlation of Zheng et al. The dimensions include the height of the distiller system, the width of the water storage rings as well as the width of the vertical circular enclosed distillation cell.

6.1 Storage Tank Dimensions

The first step was to select the design operating temperatures, taking into account the size of the storage tank and solar collector area. Utilising the TRNSYS simulation software, described in Appendix A, a simplified average domestic solar collection model was run. This model used a 100 L water storage tank and a 2-m^2 solar collector area, similar to what was envisioned for the proposed solar-assisted vertical circular distillation system. A mean tank temperature of 70 °C emerged as a suitable operating temperature since 70 °C could consistently be reached on simulated operating days and should provide good evaporation rates.

With a fixed average tank operating temperature of 70 °C, the volume of the tank was again investigated to establish whether the initial assumption of a 100 L tank was still a valid optimum volume. Since the tank temperature is a function of the tank volume and solar collector area, simulations were conducted for a 1- and 2-m^2 solar collector area against different tank volumes.

The TRNSYS software allowed the running of extended periods of simulating a storage tank being heated by an evacuated tube collector. For this study simulations were run for solar insolation data from September until April of the next year due to the focus on the high-water-demand summer season only. Solar

insolation data were obtained from the built-in TRNSYS weather component which uses data from Meteonorm. Included in the simulation was the assumption that 20 °C feed water would flow into the storage tank at the same rate as the produced distilled water. The mathematical correlation was used to calculate the distilled water flow rate, assuming a 1-m^2 evaporator area operating at 70 °C. Since the goal for the proposed prototype design was for it to be a modular system capable of household operation, no large-volume storage tanks were investigated.

Figure 13 shows the average temperature and useful energy gain of the two different solar collector areas. From the figure, it is evident that the 2-m^2 area collector area is capable of keeping the average temperature at 70 °C for tank volumes of up to nearly 150 L. Useful energy gain per square meter of collector area, an indication of the efficiency of the collection system, also increases with an increase in tank volume although the increases are less substantial above 100 L for both the 1- and 2-m^2 solar collector areas.

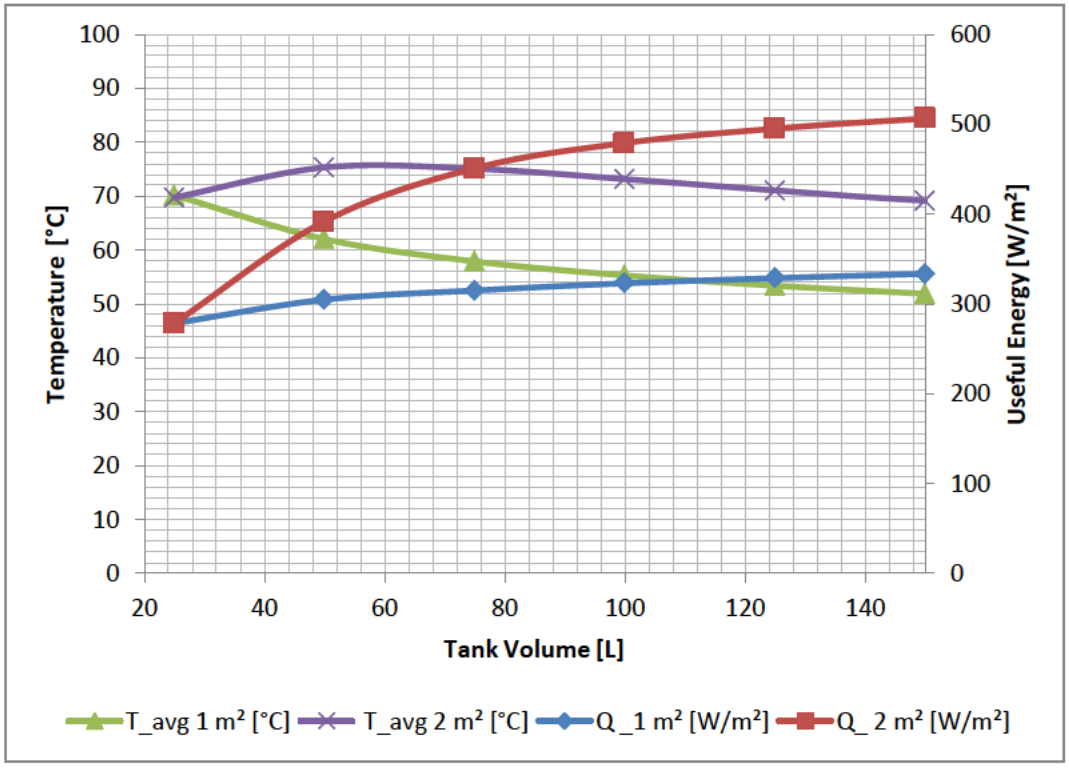

Figure 13: Average Temperature and Useful Energy versus Tank Volume

Since a mean operating temperature of 70 °C was achievable at the larger storage volumes, the initial assumption of using a tank storage volume of 100 L was still valid and was thus maintained. The 100 L storage tank was then coupled to a 2-m^2 solar collector. This tied in with the goal of keeping the size of the system suitable for household operations. With the volume fixed, the next step was to find the dimensions for the storage tank. Since the storage tank was circular, the only two parameters investigated were the diameter and the height of the storage tank.

By varying the height and diameter, optimum values could be found, which maximised the evaporation area. A larger evaporation area equated to higher distilled water production rates. Figure 14 shows the influence of different tank heights on the evaporation area, the outside tank surface and the tank diameter for a fixed volume of 100 L. This indicates that the height of the tank had to be maximised to ensure high production rates.

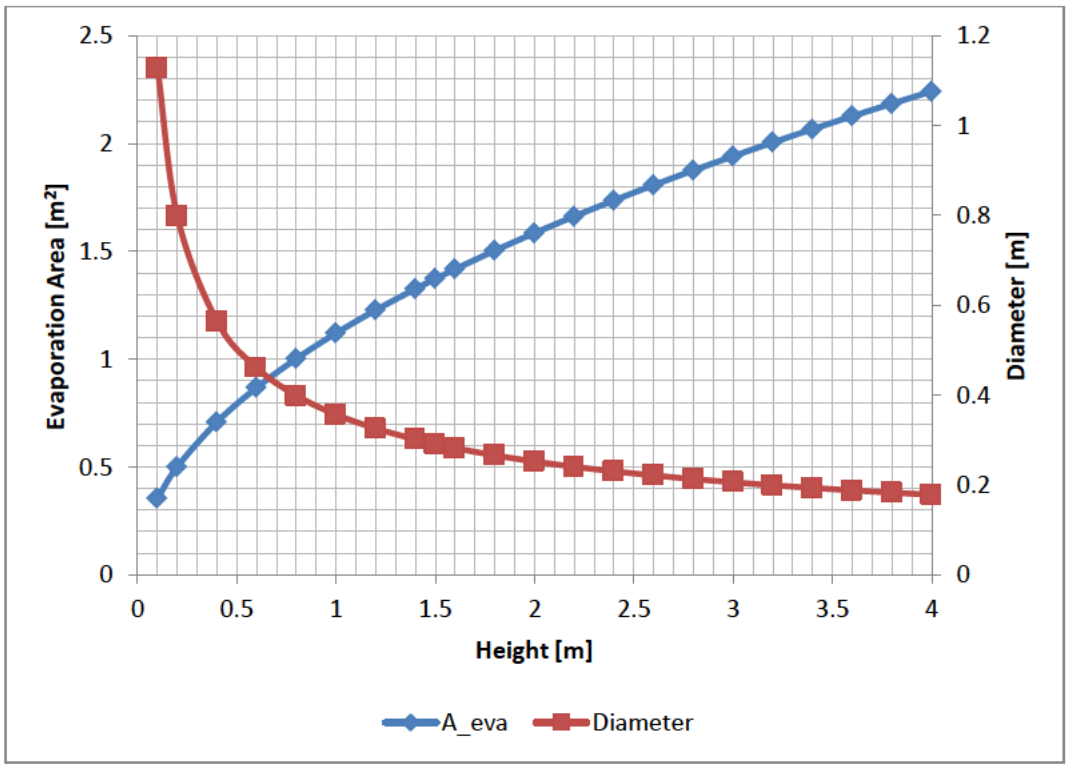

Figure 14: Evaporation Area for a Fixed Volume

6.2 Nusselt Number Influence

From Equation 5.33 in Chapter 5 it is clear that the Nusselt number and in turn the distilled water production rate, are influenced by the aspect ratio. The aspect ratio is the ratio of the height of the vertical circular annular enclosure to the width of the annular enclosure. By looking at the role of the aspect ratio in the correlation, one sees that maximising the height does not guarantee higher production rates since the constant *b* in the correlation of Kumar and Kalam is -0.122 (see Table 3). A larger height value creates a higher aspect ratio, which, when powered to the -0.122 value of the constant, creates a lower value, reducing the Nusselt number and in turn the production rate.

Fixing the Rayleigh number at 2×10^7, corresponding to a 70 °C evaporation temperature, an assumed 50 °C condensing temperature and a 0.1 m characteristic length, allows calculation of the Nusselt number for varying values of H, the height of the system. The results are presented in Figure 15 for different W values, representing the width of the system. As can be seen, minimising H is favourable although significant influence is only realised below H = 0.5. More important is the effect of an increase in W in increasing the Nusselt number.

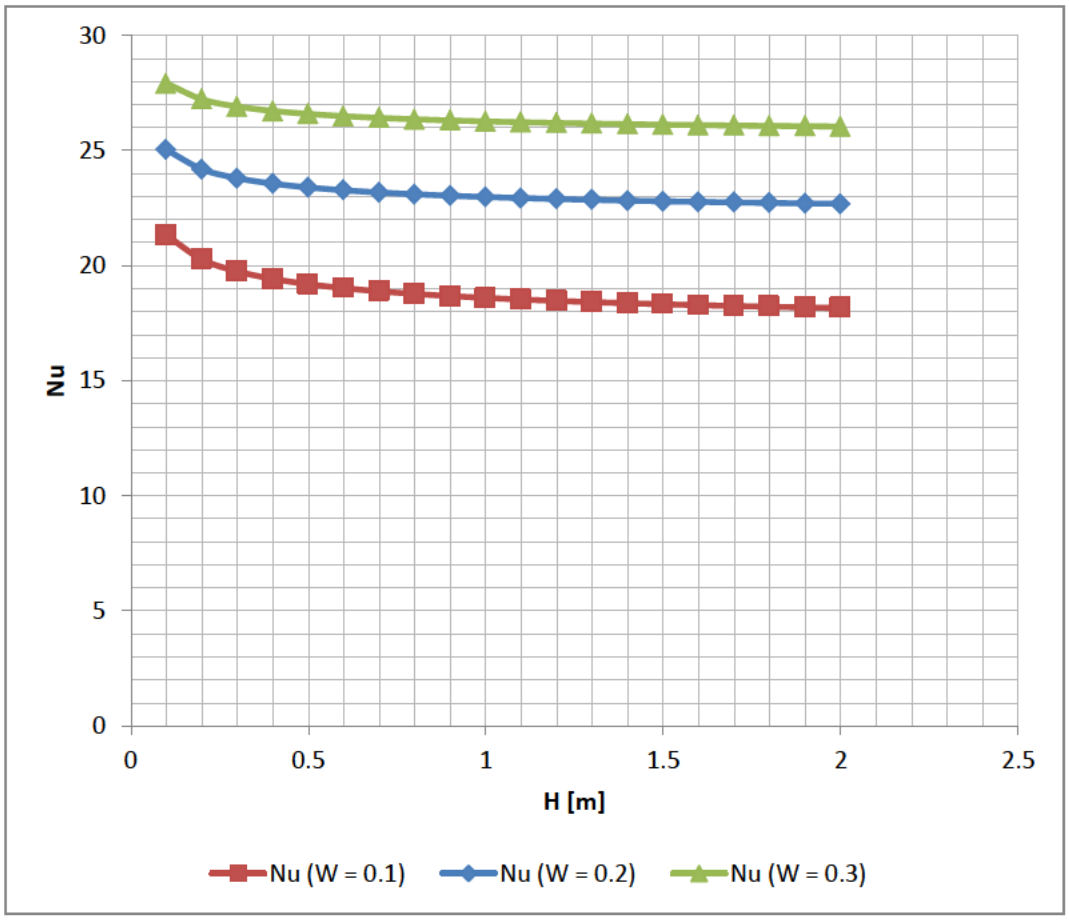

Figure 15: Nusselt Number for Varying H

Increasing the value of W also results in a decrease in the aspect ratio. Again, looking at the effect on the Nusselt number, one sees that a decreasing aspect ratio is good since it increases the Nusselt number. Maximising W, the width, is therefore a great contributor to increasing the Nusselt number and hence the production rate. This is seen in Figure 16 with dramatic increases in the Nusselt number for aspect ratios below five.

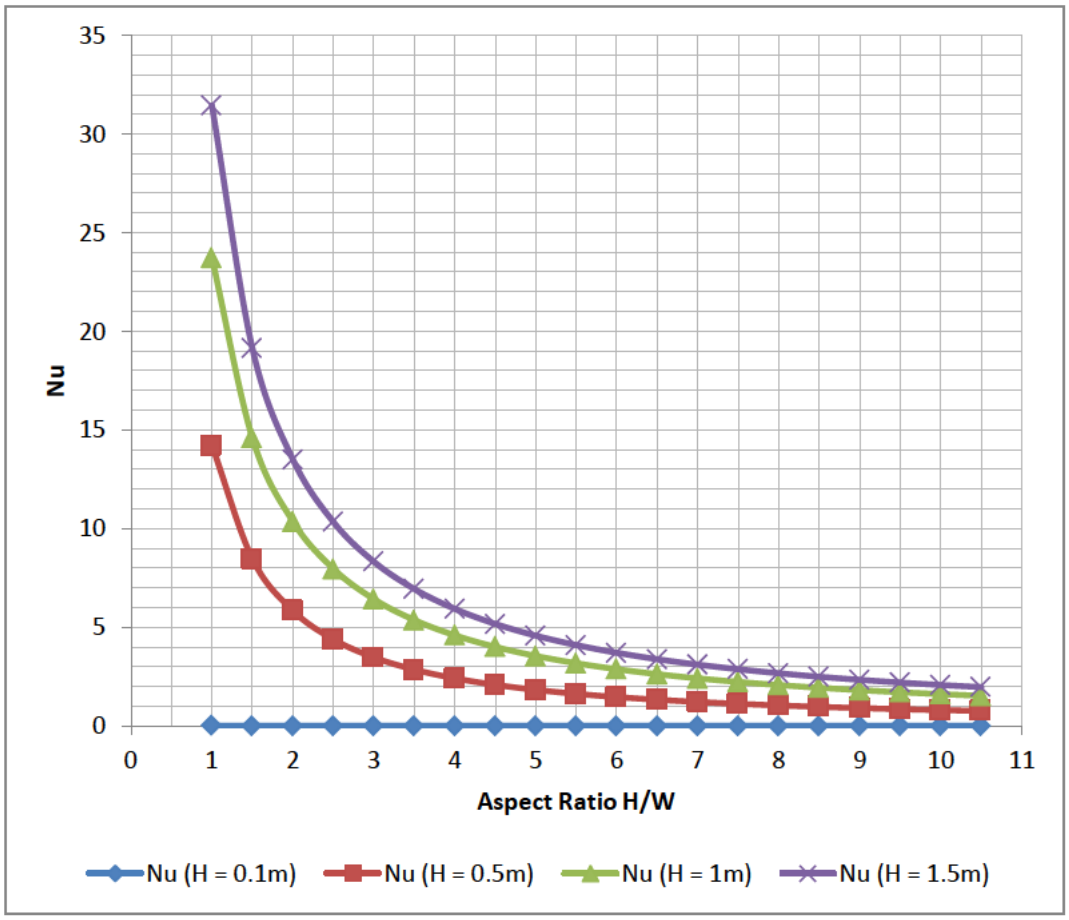

Figure 16: Nusselt Number versus Aspect Ratio for Varying H

However, it must be taken into account that H, the height, needs to be maximised for a maximum evaporation area. Therefore, in order to obtain the low aspect ratios seen in Figure 16 and still keep a large H value, a very large W value would be needed. This unfortunately increased the actual size of the proposed prototype. The initial goal was to keep the size small enough for household operation. The dimensionless value of the radius ratio *K* times the height H was thus a good indicator of the size of the system. Figure 17 shows this dimensionless number versus the aspect ratio for different heights.

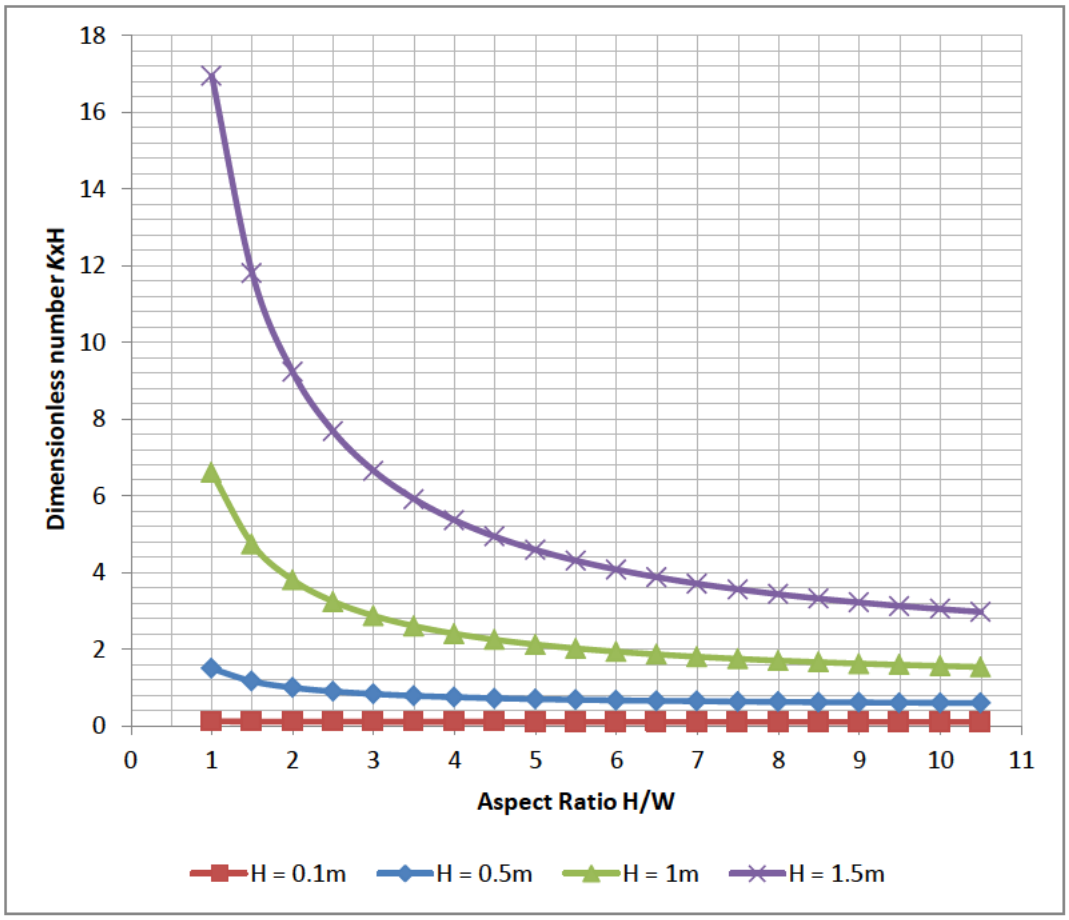

Figure 17: Dimensionless Number *K* times H versus Aspect Ratio H/W for Varying H

6.3 Chosen Prototype Dimensions

Evidently, reducing the aspect ratio (H/W) to increase the Nusselt number and production rate comes at a substantial size cost. A delicate balance between an increase in production rate against an increase in size and hence also cost, is required. Taking into consideration the data presented in Figure 14, Figure 16 and Figure 17, the author decided to fix the proposed prototype model at a height of 1 m with an aspect ratio of five, resulting in a width of 0.2 m. These were seen as optimum values that provided a high production rate whilst keeping within the size limits that a domestic household could accommodate.

Unfortunately, after initial construction of the prototype and subsequent initial testing, problems arose in terms of water leaks. It was possible to solve the problem with repairs only for a brief period since another leak would arise. This reduced the long-term operating capabilities of the prototype and reduced the stability of the system, required for accurate measurements.

Solving this problem was made possible by reducing the height of the system and subsequently the bottom water pressure. After consulting the data presented in the above figures again, the author decided to reduce the height of the system from 1 m to 0.5 m. This reduced the central storage tank volume and subsequently the evaporation area by half. However, this also resulted in an increase in the Nusselt number due to the aspect ratio now being 2.5 and in an overall reduction in size. The decision therefore reduced the production rate of the proposed system through the reduction in evaporation area but increased the production rate efficiency through the increase in the Nusselt number.

6.4 Backup System

The major drawback with using renewable energy is that it has an operational factor relating to downtime in terms of energy supply. For this reason, most renewable energy systems need some form of backup energy generation capabilities. For the proposed prototype, a similar backup system was incorporated in the design to allow for operation on cloudy days when solar insolation could be nearly zero and potentially at night as well.

This was in conflict with the original objectives of requiring no electrical requirement; however, the system was still capable of operating without the backup system if desired. No functionality was therefore lost. Moreover, the potential existed that a small PV system with battery storage could potentially act as an energy source, overcoming this limitation, albeit at a high cost.

The chosen backup system was a conventional hot water geyser element system with built-in thermostat. The thermostat had a set temperature of 70 °C, in line with the operating temperature used in the design stage. The power rating of the element was chosen as 2 kW.

The high cost associated with the PV system can be limited to only the solar panels if connection to the electricity grid is possible. Eskom makes this possible through the recently introduced Net metering option for domestic users. Net metering allows domestic users to use the Eskom electricity grid as a storage system for electricity. Surplus electricity is transferred to the Eskom grid during the daily solar energy collection period and at night electricity is received from the grid. In essence then, the Eskom grid can act as a battery storage system.

This allows constant production of distilled water. With a large enough PV system, the proposed prototype could thus run on thermal solar energy during the day with the PV system feeding electricity to the Eskom grid. At night electricity was to be drawn from the Eskom grid, providing 24 hours of operation per day. Simulation of such a backup system is possible through making use of simulation programs.

7. SYSTEM SIMULATION

Initial planning proposed that simulations of the solar-assisted distillation system should run by using components of the TRNSYS software package. This proposal did not prove to be successful, and other options were considered. The final successful simulation model used TRNSYS to simulate the interaction between the components of the solar-assisted distillation system and the collection of solar energy. The mathematical correlation of Zheng et al. (2002) was also implemented to simulate the vertical annular enclosed distillation cell through using a Microsoft Office Excel plug-in in the TRNSYS simulation software package. The correlation was programmed into an Excel file, which TRNSYS referenced at each time step. This section describes the initial proposal and the subsequent building of the final simulation model in TRNSYS. Simulations were carried out for different time periods, and with the results are presented.

The initial proposal started with identifying a suitable simulation software package. The ideal software would focus on energy flows and be able to simulate solar water collectors, water storage tanks, water flows, and evaporation and condensation processes as well as interpreting weather data. It was important to be able to incorporate weather data since this would allow the simulation to be carried out for different geographical locations.

Investigations into simulation software packages that cater for the renewable energy industry and in particular the solar industry led to the simulation program known as TRNSYS (Thermal Energy System Specialists, 2012). TRNSYS is a software package written in the FORTRAN programming language and was developed by the University of Wisconsin-Madison. TRNSYS evolved from being a research tool to becoming a commercial software package. It has been in commercial operation for 35 years and is used as the simulation software for a variety of research and commercial solar energy plants. Today TRNSYS is used in various disciplines, ranging from energy generation to thermal building analysis.

TRNSYS works on the principle of combining different components of a system rather than building the whole system at once. Different components such as solar collectors, heaters, condensers, weather data and storage tanks are all linked together to create the required system. Each component is known as a type, and a combination of these types results in a specific system or simulation model. For example, an evacuated tube collector is given the designation Type 538.

By using the linking method, building a simulation model becomes incremental and very flexible. This reduces errors and allows early simulation tests to be run, allowing analyses of the initial data to improve the system. Most renewable and conventional energy systems can be constructed using the different components

or types mentioned before. General types are also available, such as a type to carry out mathematical operations or a type providing integration and averaging. These general types enhance the analysis capabilities for the desired system. Results are presented in graphs and can be analysed over extensive time periods.

TRNSYS was therefore found to be the ideal software package for the requirements of the current study. Not only can it accurately model the various components and processes, but it also incorporates weather data. Weather data files from renowned data supplier Meteonorm are used for weather data. Data are available for numerous locations, and custom data can easily be integrated into the program. The graphical user interface also provides a good overview of the whole system, providing clarity on how the simulation process is carried out for the specific system.

7.1 Excel Modelling

Initial TRNSYS modelling involved only types found in the TRNSYS component library. However, building an accurate model from the types available proved unsuccessful. This prompted the inclusion of the mathematical correlation of Zheng et al. (2002) in the simulation model. This allowed the TRNSYS simulation model to be much more specific to the proposed solar-assisted distillation system.

TRNSYS is able to call external software programs to enhance the simulation capabilities. Programs such as MATLAB, EES and Excel can be referenced from a TRNSYS simulation. Excel was chosen as the preferred program to run the mathematical correlation. Excel is a simple yet reasonably powerful numerical tool, and it is widely available. It might be less powerful than MATLAB, but running the required mathematical correlation did not require complex calculations. Using Excel would also allow the model to be more accessible for future use.

The moist air property models described in Chapter 5.5 and provided by Tsilingiris (2007) were implemented alongside the mathematical correlation. The property models were incorporated into the Excel workbook as custom macro functions.

As mentioned in Chapter 5, the mathematical correlation can be modelled using only the evaporation and condensation temperatures. There were thus only two inputs from TRNSYS into Excel. The TRNSYS simulation process started as usual and then provided Excel with the two temperatures. Excel used these temperatures and calculated the distillate flow rate produced as indicated by the mathematical correlation of Zheng et al. (2002). The distillate output was then given back to TRNSYS. TRNSYS was now able to use the distillate flow in its

own simulation environment and provide estimates of distillate production for extended time periods.

7.2 TRNSYS Simulation Model

Building a model in TRNSYS requires a basic framework of energy and mass flows. Using the framework as a guide, the author built a TRNSYS simulation model with the various types found in the TRNSYS component library. The main focus of the model was providing accurate evaporation and condensation temperatures to the Excel mathematical model. This was crucial since the production rates were directly calculated from these temperatures.

As found in the proposed solar-assisted distillation system, the simulation model had three water storage tanks. A control volume was drawn around each tank with the subsequent inflows and outflows identified. These inflows and outflows were then connected to different TRNSYS types simulating the mass and energy flows from the water storage tanks. The average temperature of these storage tanks provided the evaporation and condensation temperatures needed for the mathematical correlation to calculate the distillate flow rate.

Figure 19 shows the three control volumes, Cv1, Cv2 and Cv3, with their respective heat transfer flows across them. Temperatures are also given with Tt the respective tank temperatures, Te the evaporating temperatures, Tc the condensing temperatures and Ta the air temperatures. The numbers refer to the respective stages. Tamb indicates the ambient temperature. Similarly, Figure 19 shows the mass flows rates with m_b referring to the brine flow rates, m_f the feed water flow rates, m_eva the evaporation rates and m_coll the flow rates from and to the solar collector. Once again, the numbers refers to the respective stages.

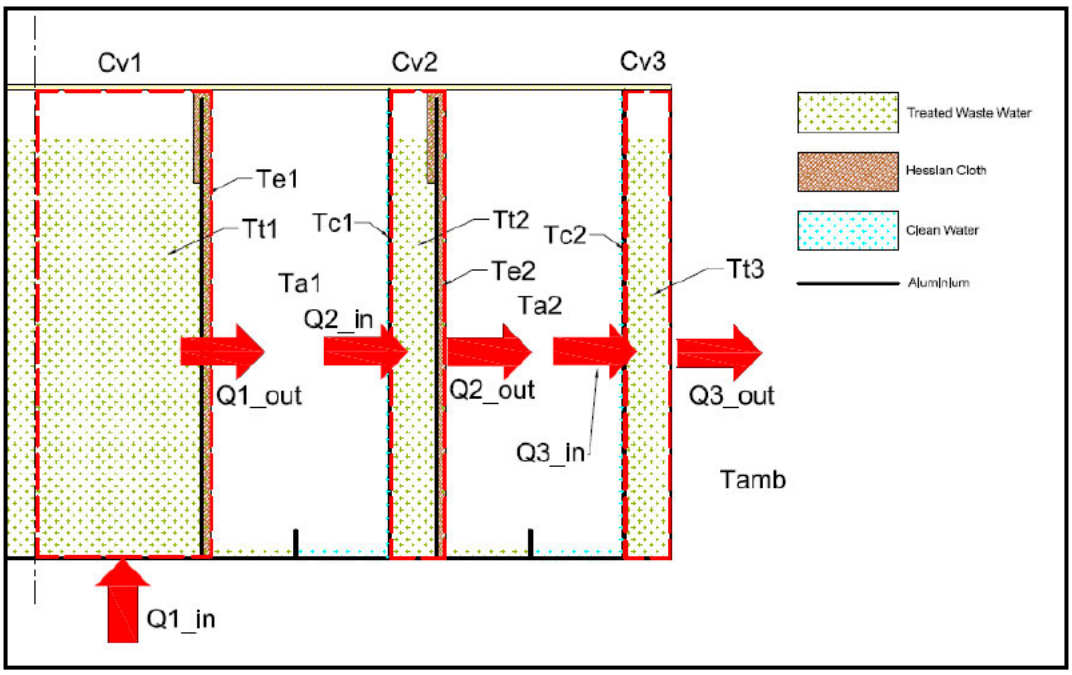

Figure 18: Energy Flows across Control Volumes with Applicable Temperatures

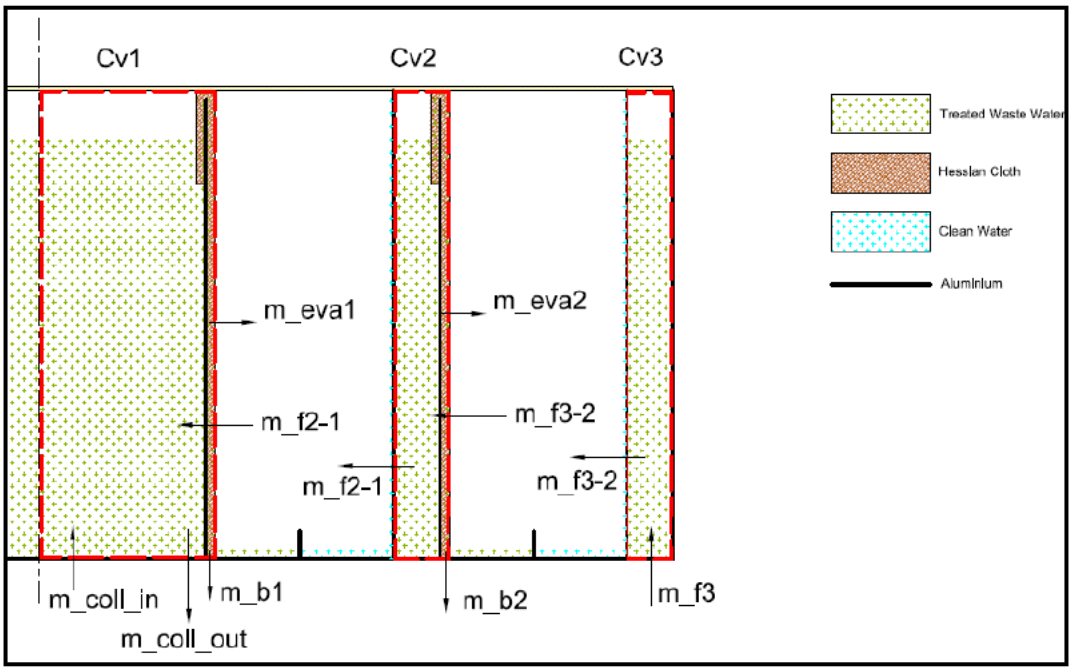

Figure 19: Mass Flows across Control Volumes

The distillation cell was simulated as an ideal system to firstly gain some insight into the functioning of the whole system. Various assumptions were made to simplify the simulation model, including assuming that the brine water flow rate was zero. This assumption was made since the capillary flow rate absorbing the water for the hessian cloth was assumed to be equal to the rate of evaporation from the hessian cloth. This assumption would be verified by the experimental model.

It was also assumed that the evaporation and condensation temperatures were equal to the respective average storage tank temperatures. This suggested that the temperature of the evaporation area, the hessian cloth, was at the same temperature as the average temperature of the storage tank that it surrounded. Moreover, the condensation area, the aluminium surface, was equal in temperature to the average temperature of the storage tank behind it. The produced distillate was also deemed to be at this temperature. These assumptions would be verified by the experimental model.

Heat losses from the top and bottom areas of the simulated prototype are also assumed negligible. This assumption is based on that the top area of the prototype was insulated with corrugated plastic sheets and heat losses from the bottom area of the prototype were deemed minimal. Only the outer tank was deemed to have suffered heat losses to the environment.

Using the control volumes in Figure 18 and Figure 19, the author built a representative model in TRNSYS. Certain assumptions were made to incorporate all of the elements into the TRNSYS model. This included modelling the sensible and latent heat transfer from tanks 1 and 2. These heat transfer elements were not available as separate types and were therefore calculated as an amount of energy, which was then removed from the tank. The energy was removed by using an auxiliary cooling device that removed energy from a fluid stream. This fluid stream is then attached to an input and output on the tank, thereby simulating the removal of energy from the tank.

7.3 Simulation of Prototype Driven by Solar Energy

With the simulation model constructed, the actual simulations could begin. The first phase was to run a simulation of the proposed prototype without any auxiliary heating present. The simulations reflected an ideal system incorporating the assumptions made earlier. Only after analysing the experimental results, to prove or disprove the assumptions made earlier, would simulations that were more accurate, be run.

The system was coupled to a 2-m^2 evacuated tube collector with the auxiliary heating switched off. Figure 20 to Figure 22 show the output of the collector-

coupled system. In Figure 20, the temperatures of each tank are visible together with the output fluid temperature of the solar collector. The collector output temperature accurately tracks the solar insolation, visible in Figure 21. Figure 21 also shows the heat transfer rates for the useful energy supplied by the solar collector to the storage tanks as well as the heat transfer rates for each stage.

From Figure 21 the efficiency of the different systems can easily be seen. The specific solar collector is able to provide around half of the energy that it receives from the sun. This is as expected since normal solar collector efficiency rates are around 40–50%. Furthermore, the first stage of the distillation system utilises all of the energy provided by the solar collector. This is due to the assumption of no heat losses from the storage tanks. The storage tanks also show the time lag of the energy flows as seen by the position of the top of the heat transfer rate curve of the stages compared to the top of the solar collector heat transfer rate curve.

Figure 22 shows the distillate produced by the two stages. Again, these graphs follow the solar cycle closely due to their dependence on temperature differences. The amount of distillate produced by the first stage compared to the second stage varies around two to three times during solar energy absorption periods.

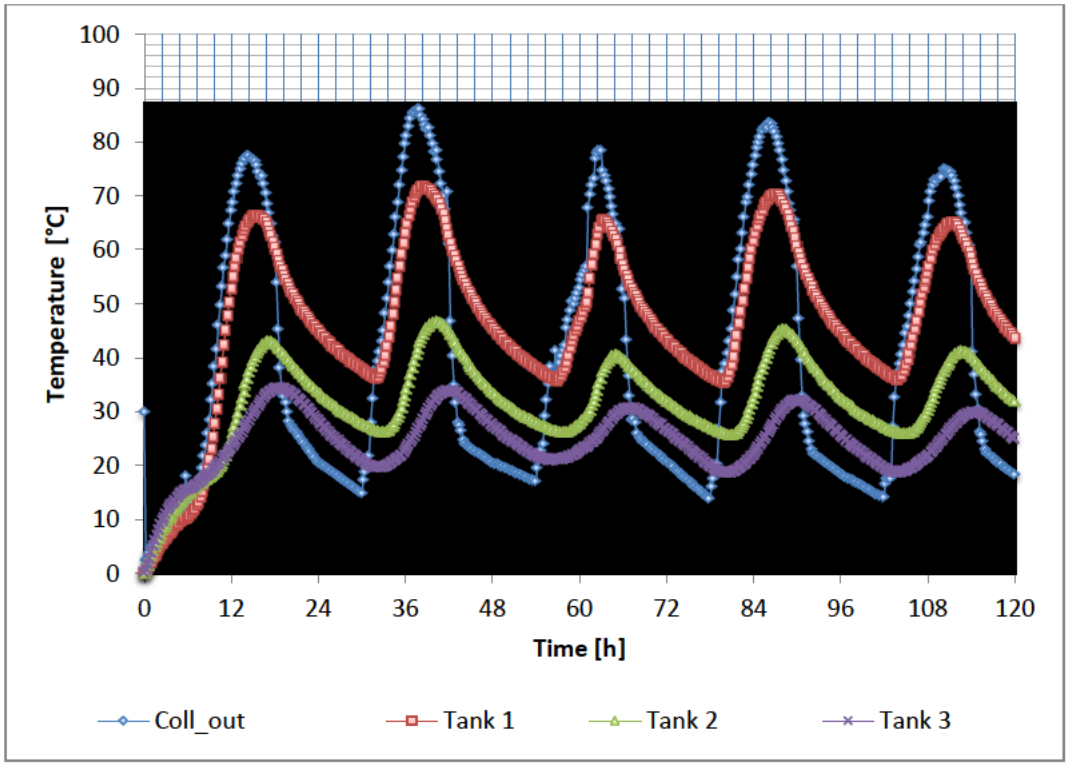

Figure 20: Tank Temperatures (Solar Collector Driven)

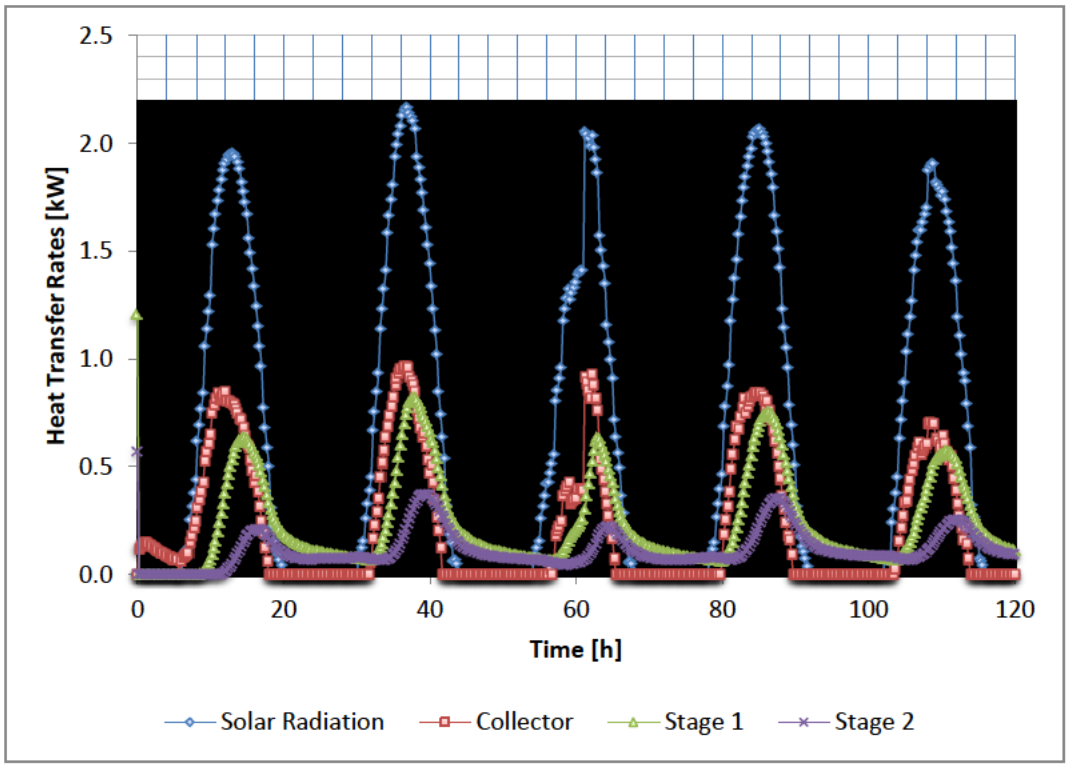

Figure 21: Heat Transfer Rates (Solar Collector Driven)

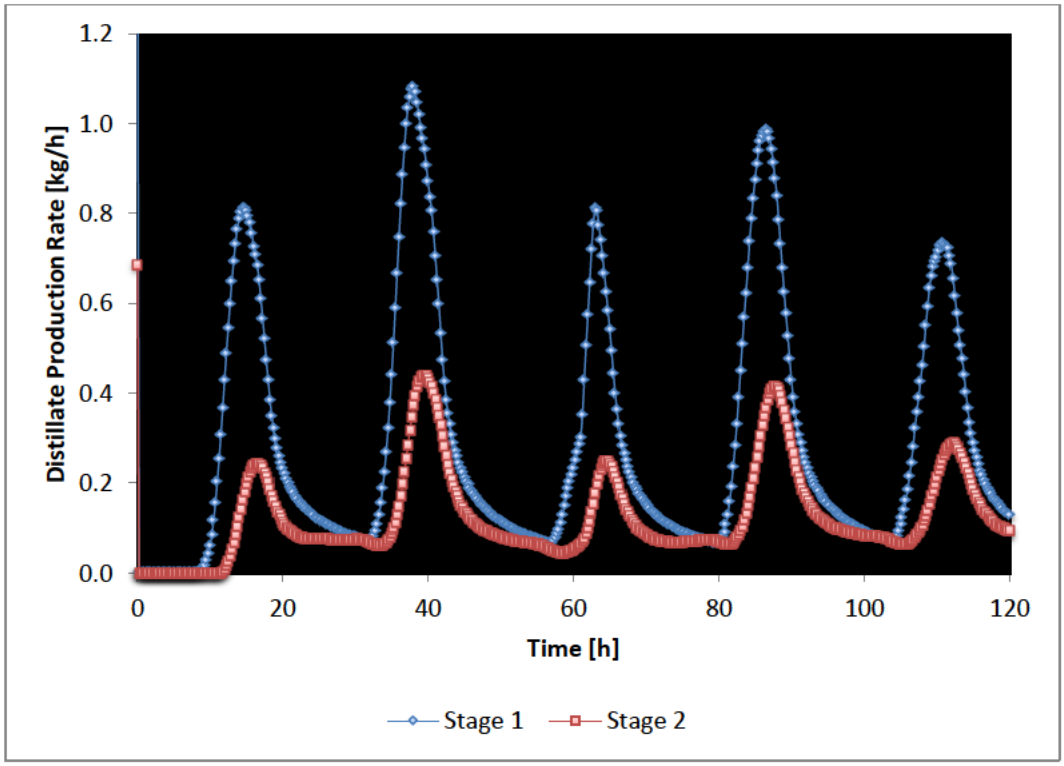

Figure 22: Distillate Production (Solar Collector Driven)

7.4 Simulation of Prototype Driven by Auxiliary Heating Element

The storage tank component in TRNSYS already has a built-in auxiliary heating element. This element was used as the backup system as per the proposed prototype design mentioned in Section 6.4. The next three figures represent the operation of the backup system together with the solar collector. The element is a 2-kW element with a 3 °C deadband.

Figure 23 indicates the average tank temperatures of the three storage tanks and the collector output temperature. The central storage tank is kept nearly constant at 70 °C except when the collector can provide higher temperatures during daytime operation. The second storage tank varies between 45 and 50 °C when steady-state operation has been achieved. The third tank fluctuates between roughly 26 and 36 °C. The larger fluctuations seen in the third tank are due to the tank being exposed to the environment. Heat losses therefore occur and are, as expected, much higher at night compared to the other tanks.

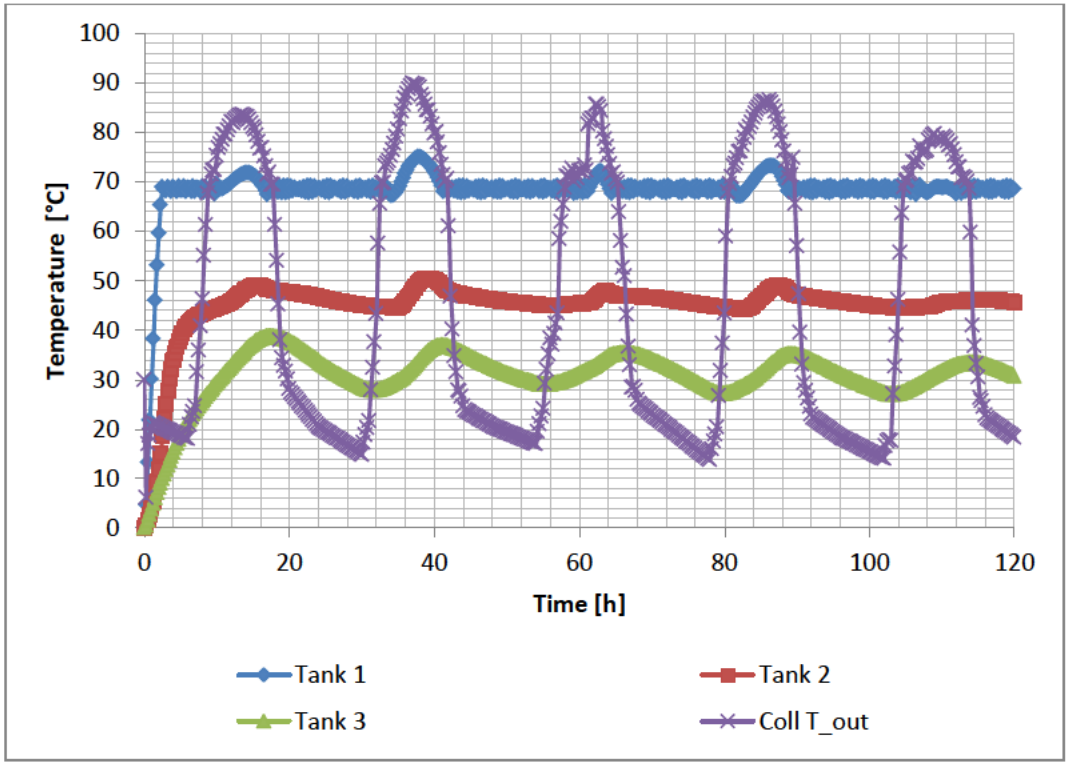

Figure 23: Tank Temperatures (Auxiliary Heating Element)

The corresponding energy flows inside the evaporation and condensation processes are presented in Figure 24. The totals represent the sum of the latent

and sensible heat transfers. From the figure, it is clear that the auxiliary backup element only draws energy when the solar collector is incapable of doing so; therefore, the day and night periods are easily identifiable when one looks at the operation of the element.

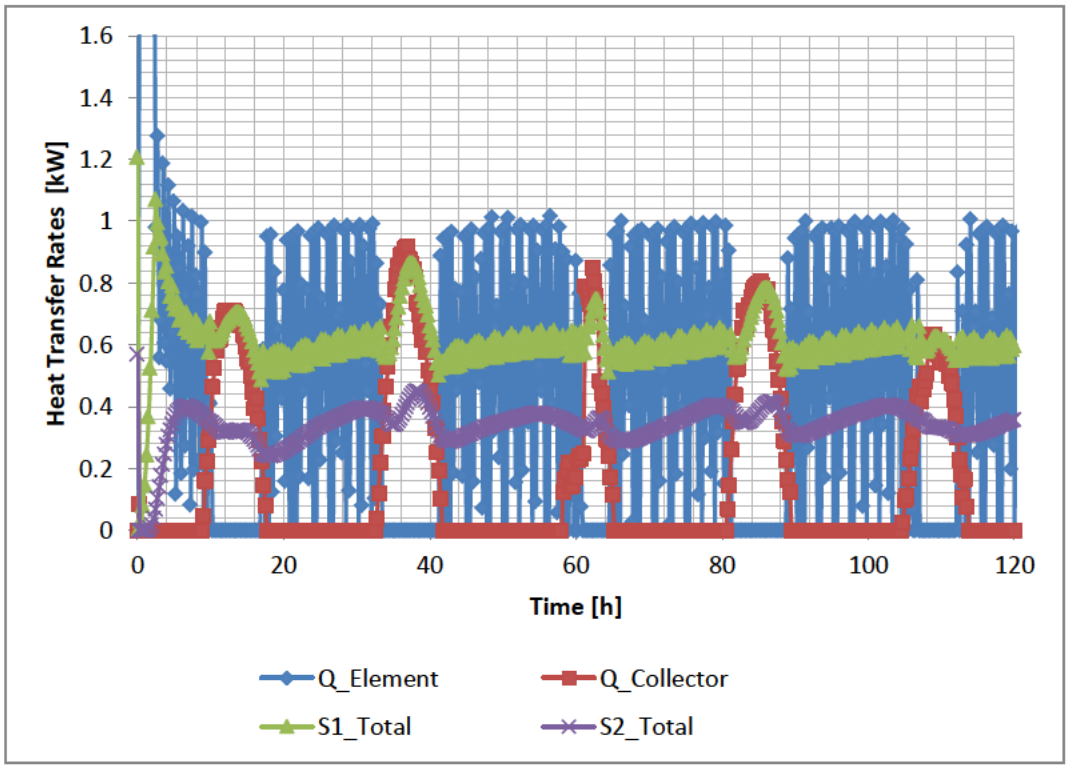

Figure 24: Heat Transfer Rates (Auxiliary Heating Element)

Figure 25 shows the rate of distillate production from the two stages. Stage one produces roughly 0.8 kg of water per hour at night with slight increases during the day. Stage two produces around 0.4 kg per hour with increases also visible during the day. Total system output is therefore between 1 and 1.4 kg of water per hour. This equates to a theoretical output of between 24 and 33.6 kg of fresh water per day.

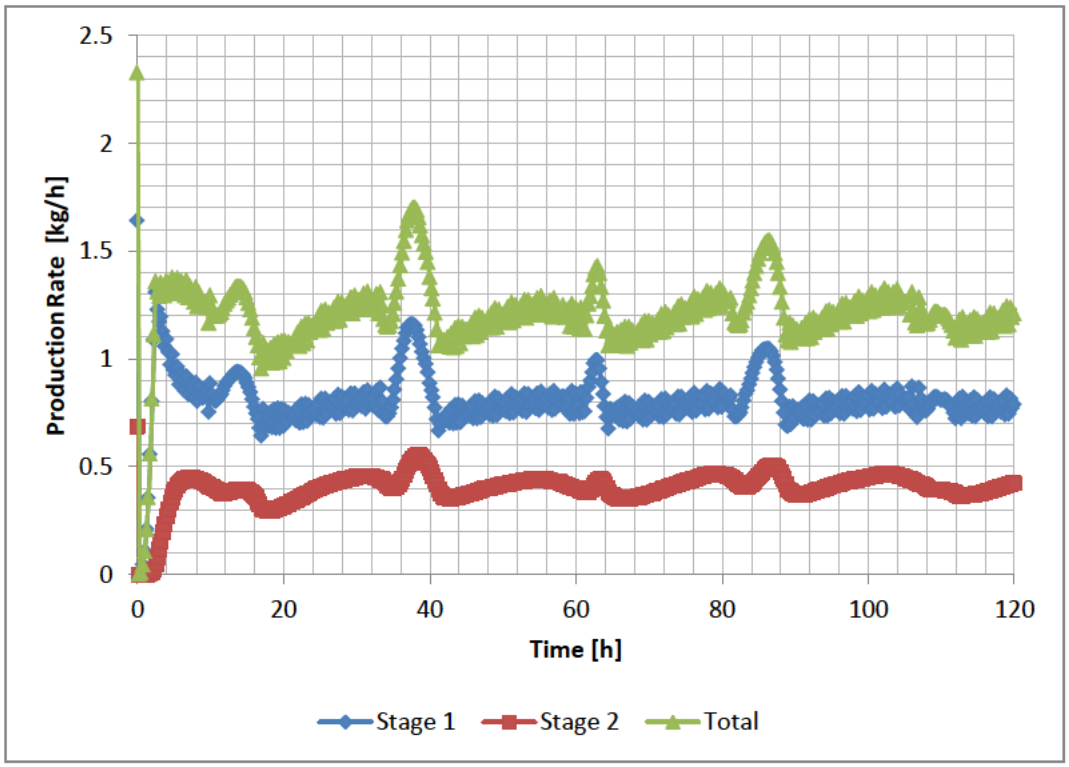

Figure 25: Production Rates (Auxiliary Heating Element)

The simulation being run over a period of one month, in this case using TRNSYS weather data corresponding to the month of September, average values could be more accurately estimated. The total average production rate was 1.3 kg/h, translating into a daily average of 31.2 kg of fresh water. Looking at the energy usage per day, one sees that the average contribution of the element was 11.86 kWh with the average solar collector contribution coming in at 2.12 kWh.

If these figures are used as a baseline, it is apparent that eight of these proposed modules could produce enough fresh water for the 250 L per day demand of an average Lynedoch household. At current electricity prices of R1.05 per kWh, the operating cost of the system would be R374.30 per month. These are only operating costs and do not include capital costs. Simplified assumptions are also made; therefore, the real cost would be higher. However, if the produced water is fed into the household geyser, savings would occur due to a reduction in electricity usage of the geyser. This provides insight into the potential of the proposed solar-assisted distillation system.

8. EXPERIMENTAL RESULTS AND ANALYSIS

After completion of the simulations of the ideal system, actual construction and experimentation of the prototype of the proposed solar-assisted distillation system began. This section does not provide detailed descriptions of the operation and capabilities of the proposed prototype as these are described in Appendix B. Only experimental results and observations are presented here. Experiments relating to the accuracy of the simulation and the mathematical correlation were conducted using normal tap water. This was due to the difficulties in obtaining large quantities of grey water for use at the experimental site. It was assumed that the use of tap water would result in the same distillate flow rates as using grey water in the distillation process. Actual grey water from Lynedoch was used in conducting the water quality experiments.

8.1 Experiment Goals

The goals of the experiments were to determine the accuracy of the simulations and the mathematical correlation and also, most importantly, to determine the quality of the water produced by the distillation of grey water. In order to accomplish this, different parameters were investigated and compared against the experimental data gathered from the prototype. Three crucial areas of investigation were Focus 1, the production rate predictions, Focus 2, the water quality, and Focus 3, the overall simulation accuracy. These focus points are discussed in the next paragraphs.

The Focus 1 area of investigation was the prediction accuracy of the mathematical correlation of Zheng et al. (2002), given two temperature inputs, namely the evaporation and condensation temperatures. This prediction accuracy was determined by using the experimental temperature data as inputs to the mathematical correlation. The production rate output of the mathematical correlation was then compared to the experimental production rate data gathered at the same time as the temperature data. This provided an accurate idea of whether the mathematical correlation could accurately predict the distilled water production rate based on only two temperatures, given the parameters of the prototype.

Focus 2 was the ability of the humidification-dehumidification process to distil the grey water into water of a drinking grade. This required taking water samples and testing them against the national drinking water standard, the SANS 241 standard. Samples of the input cold grey water, the grey water after being exposed to the high temperatures reached in the storage tank and the distilled water were taken and analysed. The reason for sampling the high-temperature exposed grey water was to see what impact the high temperature water had on the biological elements present in the grey water.

Finally, Focus 3 was the ability of the TRNSYS simulation to accurately predict the operation of the constructed prototype. The focus here was on the accuracy of the TRNSYS data to predict the different tank temperatures over a period of a five of days. These temperatures were the driving force of the whole concept and reflected the operational ability of the solar-assisted distillation prototype. Agreement in this instance would validate the TRNSYS types used, the heat and mass transfer configurations as well as all of the various assumptions made in constructing the simulation model.

Agreement on all of the above criteria would provide a simulation model capable of accurately predicting water production for a solar-assisted distillation system using only solar radiation data. Analysis could then be carried out for various locations, based solely on solar radiation data.

8.2 Focus 1: Mass Flow Results

Since the mathematical correlation of Zheng et al. (2002) relies on temperatures only, the solar collector component was not included in the conducted experiments. The main storage tank was heated with the auxiliary heating element. The thermostat of the element was set at 70 °C creating similar temperature levels to what would be experienced with normal solar collector operation. This is as indicated by the Trnsys simulation although, as seen from the measurements, the element thermostat was not very accurate. The auxiliary heating element also had a large dead band temperature, around 7 °C. Temperature variation of the central tank was therefore considerable. However, this variation was accepted as it would provide insight into the response time of the prototype.

The tests were also conducted over a five days to gather enough data. The tests were placed in the context of operating at the beginning of the day. This involved the system being at a low temperature with the central storage tank being slowly heated by the solar collector as the solar insolation increased. It was therefore anticipated that the experimental data would indicate some sort of inertia due to the system's heating up.

8.2.1 Measuring Positions

In order to validate the mass flow calculation results, the evaporation and condensation temperatures needed to be measured. These temperatures measurements needed to be accurate to reflect the corresponding distillation process. This resulted in an investigation into what the best position to measure the evaporation and condensation temperatures inside a natural convection enclosure would be. In the case of the distillation cell, the evaporation temperature would be the water suspended in the hessian fabric. Temperature

probes were therefore placed on the surface of the hessian fabric layers. Images of these placements are available in Appendix B.

Since the prototype was circular in design, it was assumed that variations in temperature along the circular dimension were negligible. In other words, temperature variation was only looked at in the vertical plane of the evaporation area or film. Temperature readings were consequently taken at three different levels of the evaporation film, namely at the bottom, middle and top of the film. Similar measurements of the condensing surface temperature were conducted by attaching the temperature probes to the condensing surface with tape.

Another indicator of having accurate temperature data was found by looking at the mathematical correlation of Zheng et al. (2002) itself. Most of the parameters used in the correlation were the properties of the humid air and were all evaluated at the mean temperature between the evaporating and condensing temperatures. Therefore, a good benchmark of using the correct evaporation and condensation temperatures was to compare the mean of the evaporation and condensation temperatures to that of the actual air temperature.

This required that the air temperature also be measured. Again, the question of where to place the probe in the air cavity became important. This prompted more investigations. Looking at isotherms found in the literature (Wee, Keey and Cunningham, 1989) offered an indication of how the air temperature profile inside an air cavity behaved. Figure 26 shows isotherms for an air cavity similar to the distillation cell found in the prototype of the solar-assisted distillation system.

The condensation film was found at $y = 0$, with the evaporation film at $y = 1$. As expected, the high-temperature air was found in the top region of the cavity, indicated by the 0.8-isotherm identifier seen in the top right corner. The 0.5-isotherm, the line above the 0.4-isotherm in the figure, would represent a good mean value for the air temperature. In this case the 0.5 isotherm was located very close to the middle of the cavity. This deduction was similar for other isotherms of similar air cavities found in the literature. Measuring the air temperature at exactly the middle of the cavity would therefore provide an accurate representation of the mean air temperature.

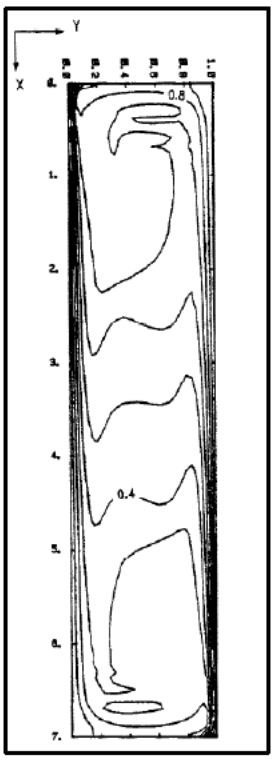

Figure 26: Air Cavity Isotherm

(Wee et al. 1989)

The following graph, Figure 27, shows the temperature profiles for different points of operation for one experiment. This includes three measurement points of the evaporation temperatures. T_eva top refers to the evaporating temperature measured by the probes interwoven into the hessian fabric. Tank_1 is the temperature of the central storage tank with T_cond the second storage tank. Both Tank_1 and T_cond were measured in the middle of their respective water cavities. Detailed information on the placement can be found in Appendix A. T_air represents the air temperature measured in the middle of the cavity as outlined above.

As can be seen in Figure 27, the large dead-band temperature is visible through the saw-tooth pattern created by the auxiliary heating element's turning on and off. This pattern is also perpetuated through the rest of the temperature measurements although the impact is less visible. The dip in some of the temperature readings at a time of 400 minutes occurred due to a visual inspection of the process in action by removing the corrugated plastic cover. The heated air escaped the enclosure, resulting in the drop in temperature of the measuring points exposed to the air, the evaporation temperature, the

condensation temperature and the air temperature. At this point, the auxiliary heater was also switched off resulting in the steady lowering of the temperatures.

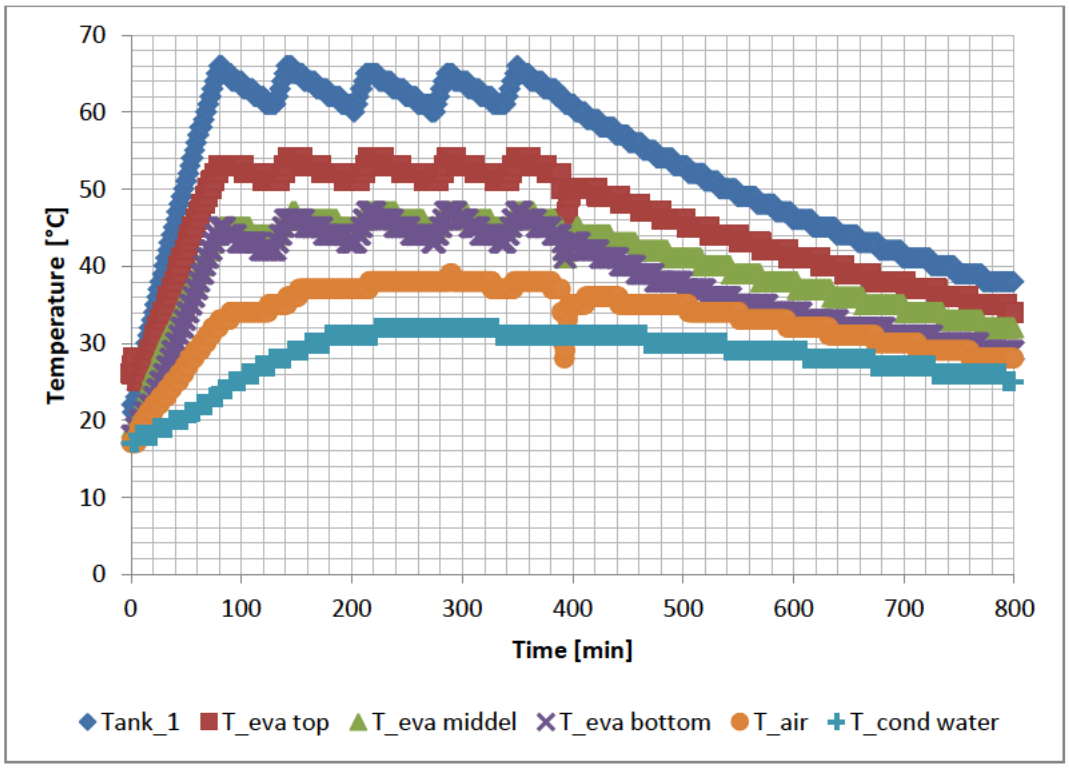

Figure 27: Daily Temperature Variations (with Auxiliary Heating on)

A suitable evaporating temperature to be used as an input to the mathematical correlation still had to be decided on. As mentioned before, the mean between the evaporating and condensing temperature measurements should compare accurately to the air temperature measured at the middle section of the enclosure. Hence, by comparison of the actual measured air temperature to the air temperature calculated from the evaporating and condensing temperatures and expression of the difference as an error percentage, an indication of which was the most accurate measurement was possible.

Three similar experiments were conducted with evaporation temperature measurements taken at three levels, namely the bottom, middle and top sections. Experiment 1 thus had Top_1, Middle_1 and Bottom_1 as measurements. Each evaporation temperature was used to calculate the air temperature together with the corresponding condensing temperature. Figure 28 shows the error percentages induced by comparison to the actual air temperature measurement.

A positive error value points to an overestimation of the air temperature and a negative error value to an underestimation. Each measurement area is grouped to look similar, differentiating between areas rather than the experiments.

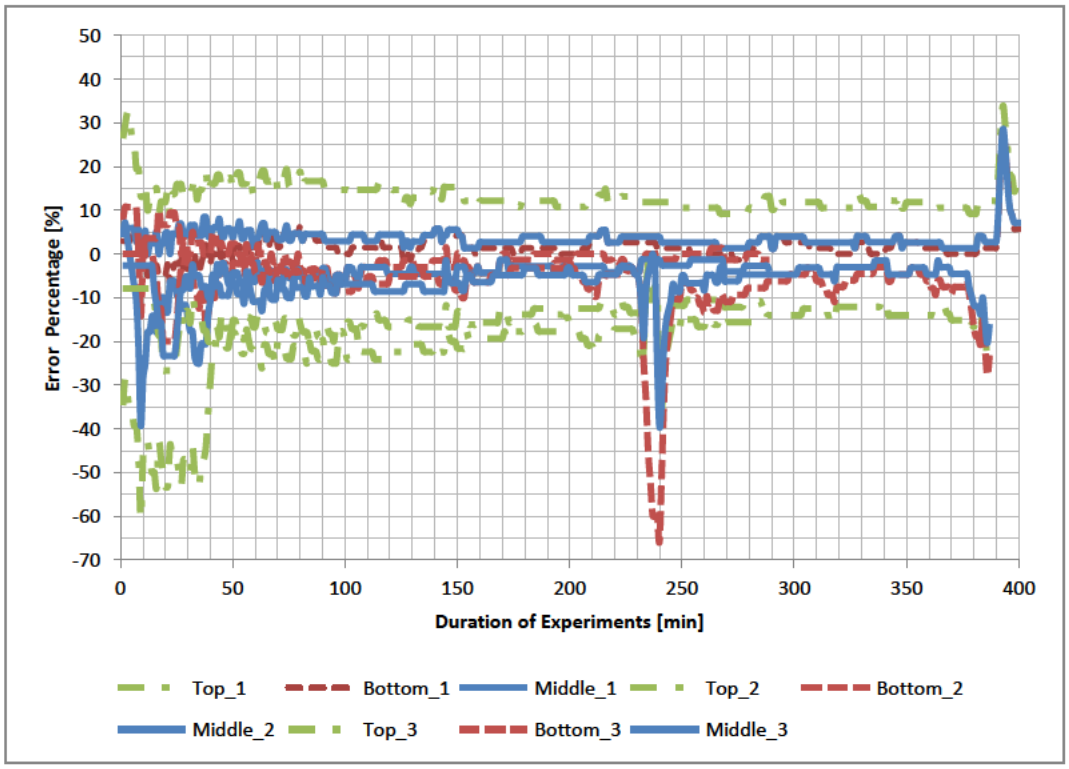

Figure 28: Error Percentage of Air Temperature Predictions

As can be seen in the graph, using the top evaporation temperature resulted in errors of more than 10%. Using the middle or bottom temperature readings resulted in errors below 10%. After the initial heating-up period of around two hours, this error decreased to around 5%. However, no decisive difference could be seen between using the middle or bottom temperatures. However, since all other readings were taken at the midpoint, the author decided to use the middle evaporation measurement point as the reference evaporation temperature. This temperature measurement would therefore be the input for the evaporating temperature of the mathematical correlation of Zheng et al. (2002) in comparing the distillate flow rates of the correlation to actual measured data.

8.2.2 Experimental Mass Flow Results

The author was now able to satisfyingly compare calculated distillate flow rates to

measured flow rates. Figure 29 shows the results from one specific experiment. It is evident that the mathematical correlation is dependent only on temperature inputs since the simulated graph resembles the temperature profiles as found in Figure 27. Also visible is the initial heating-up period when the measured flow rates are much lower than the predicted flow rates. This is as expected since the mathematical correlation does not take into account the specific heat capacity of the air or the system itself. The air and the system itself first absorb the energy received by the distillation system. Only then does the received energy drive the evaporation and condensation cycle.

However, as the system reaches steady state, the measured flow rates become more aligned to the predicted flow rates. It can also be observed that the measured results do not show any real signs of following the saw-tooth pattern, induced by the auxiliary heating element switching on and off, as is visible in the mathematical correlation results. This show the experimental flow rates were less influenced by temperature fluctuation compared to the mathematical correlation results. The model also over-predicts the flow rates.

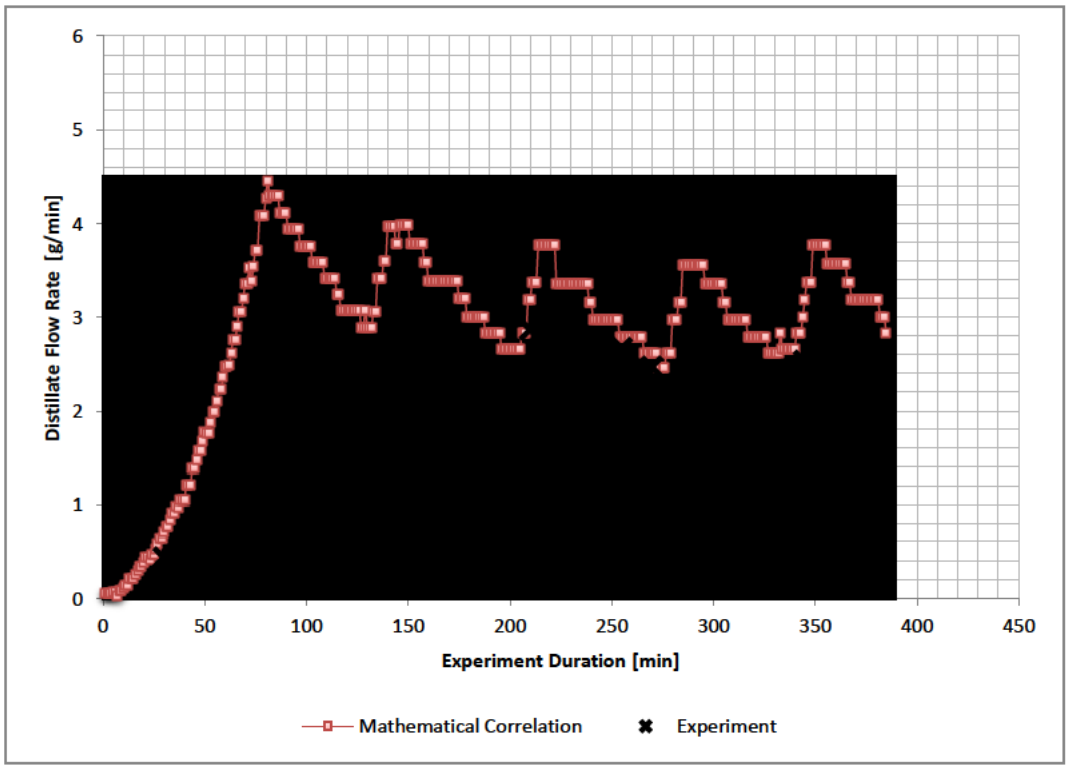

Figure 29: Experimental Distillate Flow versus Mathematical Correlation Prediction

Figure 30 shows the same results as Figure 29 but with four other experimental data-sets. Similarities between the patterns of the experimental data-sets exists, but each set is distinguishable. This shows the difficulty in repeatability of the experiments since so many uncontrollable parameters, such as the natural environmental parameters, were involved. These included the ambient temperature, the ambient air pressure as well as solar insolation received by the outside tank and the top of the prototype.

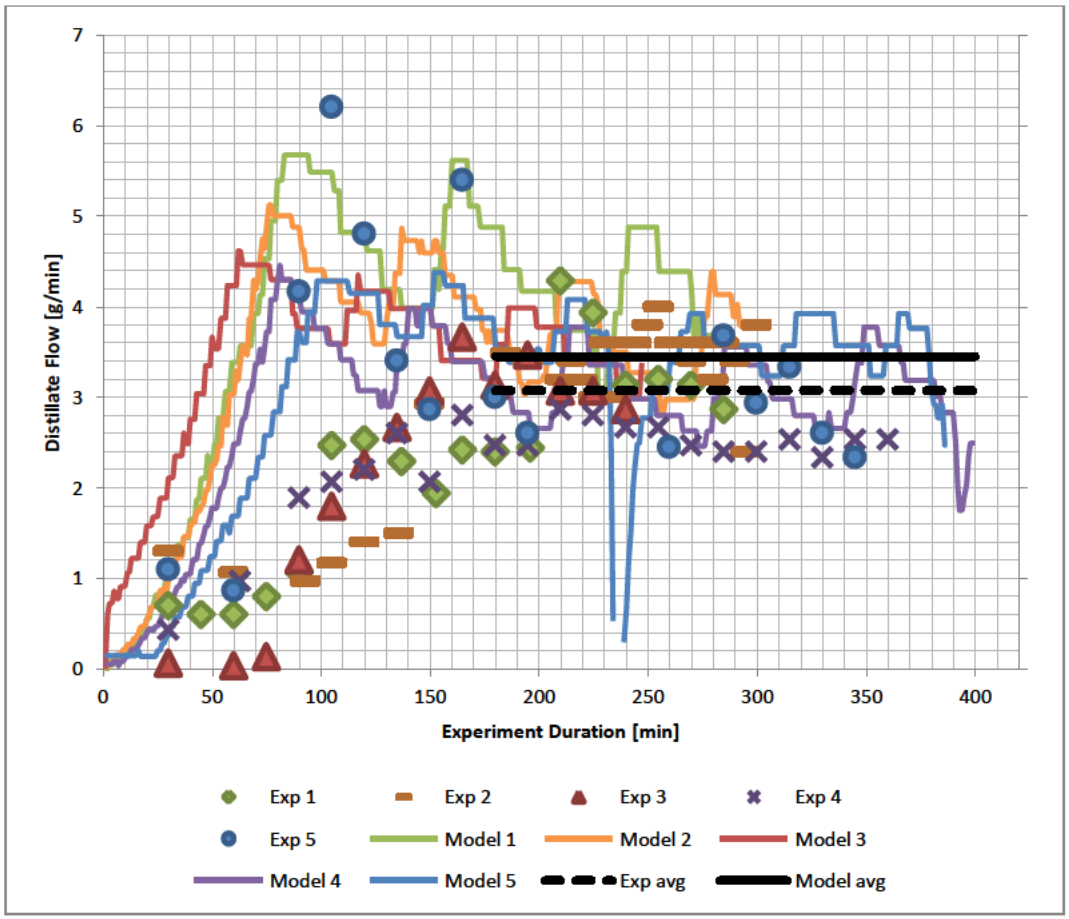

Figure 30: Experimental Versus Mathematical Correlation Flow Rates

Also visible in Figure 30 is the average flow rates of the experimental and calculated data sets after the initial heating-up period. It was assumed that steady state conditions would be reached after 180 minutes, and therefore the average rates were calculated from this point onwards. The average mathematical correlation calculated flow rate was 3.45 g per minute with the experimental data coming in at 3.07 g per minute. The mathematical correlation hence over predicted the flow rates by 12.34%.

8.2.3 Evaporation Temperature Prediction

One of the initial assumptions made for the simulation model was that the evaporation temperature was equal to the tank temperature of that particular stage. As mentioned, this assumption needed to be verified with experimental data. Plotting the ratio of the measured evaporation temperature to the measured average tank temperature over time resulted in the data shown in Figure 31. For the aforementioned assumption to be valid, the ratio should be equal to one. It is evident from the figure that the assumption is not valid since the steady state ratio values are consistently below one. This assumption should therefore be discarded in future simulations.

Another observation from Figure 31 is that the temperature ratio is very nearly constant at around 0.7. An assumption that the ratio of the evaporation temperature to the average tank temperature is 0.7 is therefore plausible. The temperature ratio is, however, only valid for operating temperatures between 50 and 70 °C since this is the temperature range from which the data that were used were gathered.

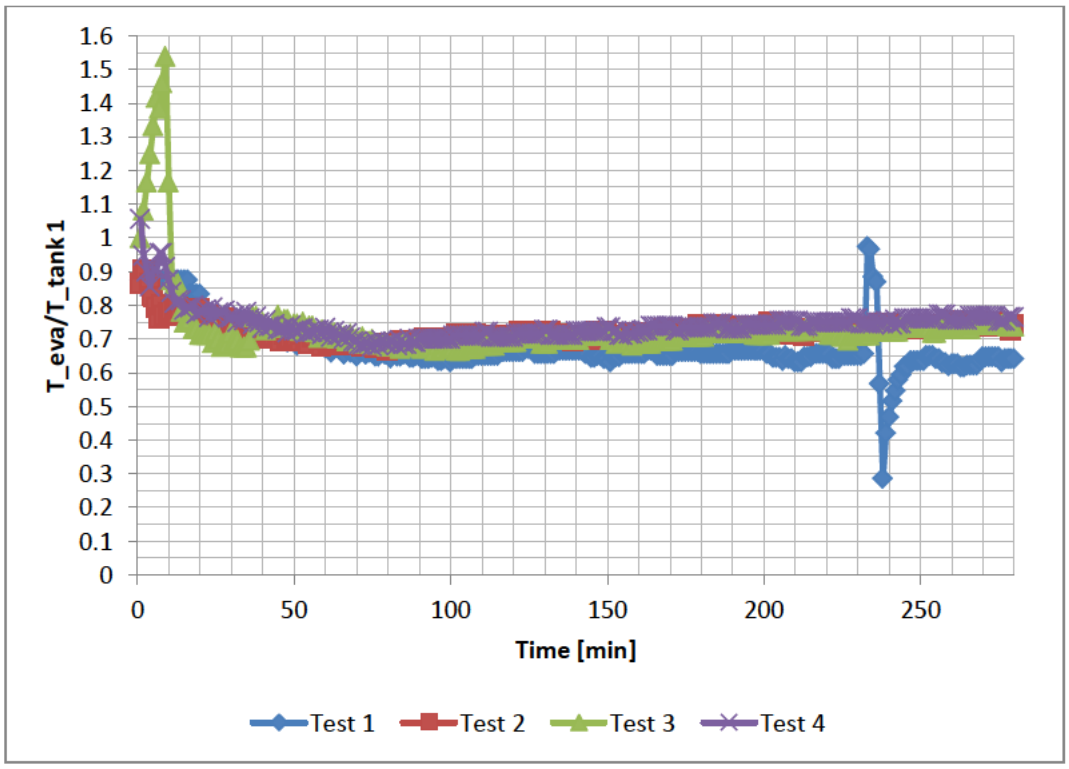

Figure 31: Ratio of Evaporation Temperature to Tank Temperature

8.3 Focus 2: Water Quality

The next experimental focus area was the quality of the produced water. The produced water was quality tested and compared to the national drinking water standard, the SANS 241. The grey water used came directly from the treated water tanks at Lynedoch. This is the raw sewage water after is has gone through the Biolytix and artificial wetland systems.

As mentioned, water samples were also taken of the grey water after it had been exposed to the high temperatures encountered in the central storage tanks. This would shed light on the impact of the high temperatures on the biological contaminants in the water.

The first sampling tests were conducted using the auxiliary heating element as a heat source. Samples were sent to Stellenbosch University's Central Analytical Facility (CAF). Although not a South African National Accreditation System (SANAS)-accredited laboratory, the purpose of testing at the CAF was to indicate the initial outcomes of the experiments. Chemical analysis was done, providing a glimpse into the state of the water and whether the distillation process was functioning properly. The CAF testing was much more cost effective than at any other facility, hence the decision to analyse the initial results at the CAF. Table E.1 in Appendix E shows the results of the initial grey water (GW 1A), the heated grey water (GW 1B) as well as the distilled product (DW 1).

The initial observation was that the grey water on its own is chemically within the limits of the SANS 241 except for the levels of nitrates. Looking at the produced distilled water, one could easily see the effect of distillation on reducing the chemical contaminant levels. This was summarised by a reduction in electrical conductivity of around 90%. High electrical conductivity is a direct result of high chemical levels present in water, specifically high salt concentrations. The results also showed that the chemical composition of the grey water was already close to acceptable levels and that the main focus would be removing all of the biological contaminants.

The second grey water experiment was again conducted with grey water from Lynedoch. For this experiment, the biological contaminants were also looked at. Bemlab was used as the testing laboratory since it is a SANAS accredited laboratory capable of testing for chemical as well as biological contaminants. The results are again found in Appendix E, Table E.1 with the cold grey water (GW 2A), the warm grey water (GW 2B) and the distilled product (DW 2) again being the samples investigated. The biological contaminant tests looked at the total bacterial count, faecal coliforms and E. coli presence.

The chemical tests revealed similar results as in the first experiment in reducing the chemical contaminants to lower values. The only element outside of the acceptable range was ammonium (NH_4) with the distillation process only capable of reducing the levels slightly. An increase in levels of iron (Fe) and Zinc (Zn) was in contrast with the anticipated effect of the distillation process. This increase could be attributed to the rusting components used on the prototype, which included nuts, bolts, washers, angle irons and the water divider, all being in contact with the distillate water at times. These components were not required in the proposed design but had to be isolated from the distillate water in the prototype. Detected levels were, however, still below maximum allowable levels.

On the biological front, the experiment revealed less conclusive results. The E. coli microbe was not detected in any sample, with total coliforms only registering in the cold grey water sample (GW 2A). The coliform level was, however, still below the acceptable level of 10 counts per 100 ml. The total bacterial level, or bacterial plate count, was unfortunately outside of acceptable limits in all samples including the distillate produced.

The third test was again conducted with grey water from the Lynedoch wetland. This time the cold-water sample was sent to the laboratory directly. Results were much more conclusive. The results are also presented in Appendix E, Table E.1. As can be seen, the grey water reveals very high levels of biological contamination as well as chemical contaminant levels above acceptable limits for electrical conductivity (EC), calcium (Ca), ammonium (NH_4), nitrates (NO_3) and total dissolved solids (TDS). The biological contaminant levels are much higher than previously, indicating the impact of residence time on the microbiological contaminants. The produced distilled water was also tested, this time against a SANS 241 test provided by Bemlab. This test was carried out according to the total testing requirements of the SANS 241 and tests against a variety of other contaminants. These results are also found in Appendix E, Table E.1.

As can be seen in Table E.1, the produced water is again not conforming to acceptable bacterial and ammonium levels. In the extensive SANS 241 tests, the only other contaminants outside acceptable levels are turbidity and lead (Pb). The lead contamination level of 11 μg/L is just outside the acceptable level of 10 μg/L with turbidity sitting at 3.29 number of transfer units (NTU) when acceptable levels are 1 NTU.

Total coliforms are on the brink of the acceptable levels at 10 with required levels at 10 or below. E. coli levels are at the acceptable level of zero. Comparison with the initial levels shows considerable reductions. Unfortunately, the total bacterial count is still far from acceptable levels.

8.4 Focus 3: Solar Collector-Driven Results

The third and final focus of the experimental results section was validation of the TRNSYS simulation. This was performed by feeding the TRNSYS simulation actual solar insolation values gathered by a pyrometer. Initially a pyrometer situated 4 m from the solar collector was to be used, but a back-up pyrometer situated 40 m meters away from the solar collector had to be used. The back-up pyrometer is operated by the Solar Thermal Energy Research Group (STERG) of Stellenbosch University's Department of Mechanical and Mechatronic Engineering (STERG, 2012). The data are freely available on the internet.

Incorporated into the TRNSYS simulation was the assumption that the evaporation temperature to average tank temperature ratio was a factor of 0.7. Figure 32 shows the experimental measurements for each of the three tanks together with the simulated temperatures according to the TRNSYS model. Although the TRNSYS results tracked the experimental results in the heating-up region, the results over-predicted the temperatures at night considerably. The same phenomenon occurred with the results for Tank 2, although the differences were not as pronounced. For Tank 3, the TRNSYS data under-predicted the experimental data slightly with one instance of over prediction. However, the overall data for Tank 3 were much closer to the TRNSYS data. This indicated that the heat transfer losses from tanks 1 and 2 were not negligible.

Tank heat transfer losses were hence incorporated for tanks 1 and 2 as well. Heat transfer losses were calculated from a tank loss coefficient parameter in TRNSYS. The coefficient values for Tank 3 were set at 50 kJ/hr.m^2.K. Values for tanks 1 and 2 are set at 25 kJ/hr.m^2.K since these tanks were not exposed to the environment as extensively as Tank 1. The results from this modification are presented in Figure 33. It can be seen that the simulated temperatures correlate much more accurately with the experimental temperatures. This is most evident for Tank 1 with Tank 2 still over- or under-predicting the temperature slightly for different times of the day. The differences in actual versus simulated data for tanks 2 and 3 can be attributed to the assumption made that the evaporation temperature to average tank temperature is a ratio of 0.7. This assumption is applicable at temperature of between 50 and 70 °C, much higher than what is encountered for tanks 2 and 3.

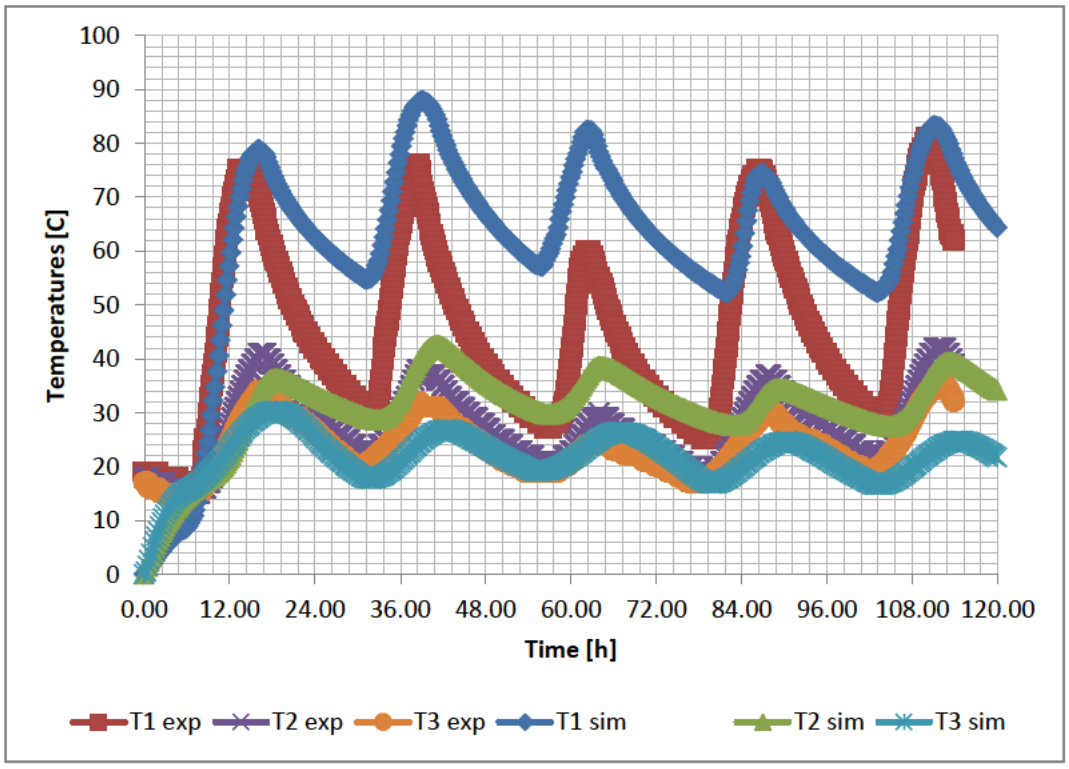

Figure 32: Simulated versus Experimental Tank Temperatures

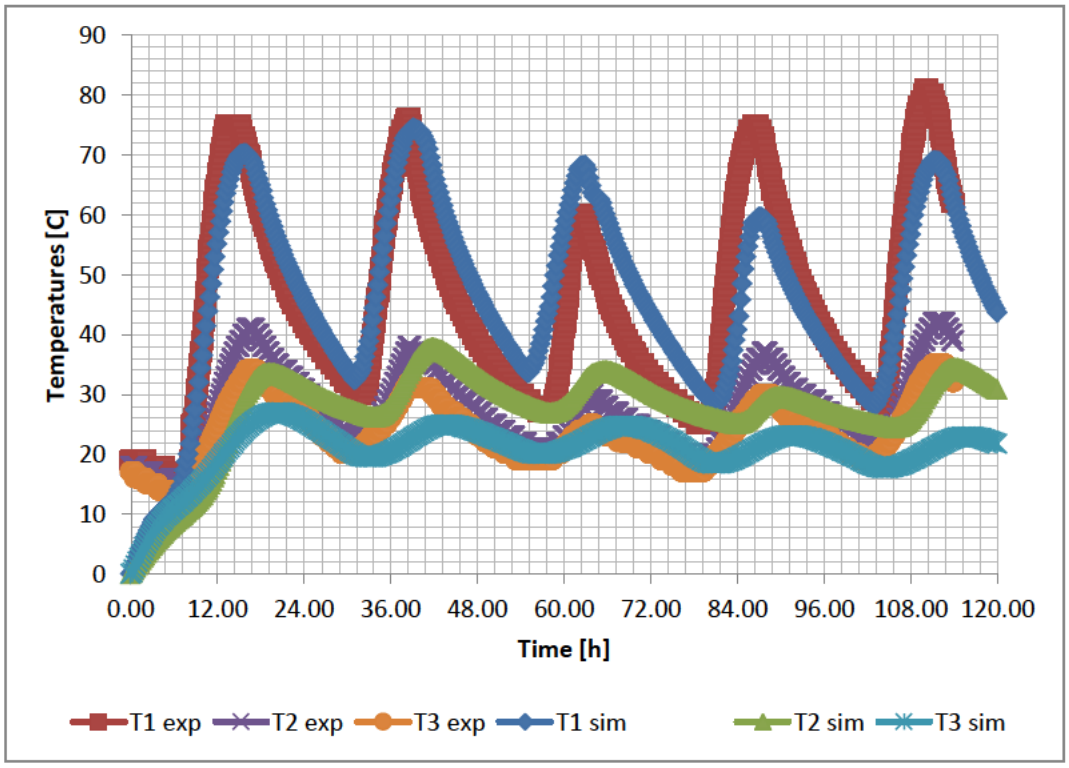

Figure 33: Simulated versus Experimental Tank Temperatures Including Heat Losses

9. CONCLUSION

Investigations into the demand for resources in South Africa in general and Stellenbosch in particular prompted a search for innovative solutions to reduce the ever-increasing demand. A potential solution that utilised solar desalination techniques to distil treated sewage effluent was proposed. The produced clean water was to be used as feed water to domestic hot water cylinders, thereby reducing water and energy demands of consumers.

A literature review explored a range of existing solar-powered desalination technologies and methods used to recycle contaminated water into water of a potable grade. Various limitations were identified and subsequently a novel indirect solar-assisted circular distiller design was proposed. The mathematical correlation of Zheng et al. (2002) was selected to characterise the proposed design, and improvements were added to the correlation. This included incorporating a Nusselt-Rayleigh relation specific to the vertical enclosed natural convection distillation cell found in the proposed design.

The mathematical correlation coupled with the concept design allowed for the design of a proposed prototype and the subsequent construction of the prototype from aluminium sheets. The prototype operated in an outdoor environment replicating the actual operating conditions for which it was designed. A standard flat-plate solar collector provided solar energy collection with a solar PV pump providing water circulation.

TRNSYS was used to build a simulation model of the proposed design. Excel was also used in conjunction with TRNSYS to aid in incorporating the mathematical correlation. This resulted in a more accurate representation of the distillation cell enclosure. Results from the simulations indicated that eight systems with auxiliary backup could produce enough water to meet the demands of an average Lynedoch household.

Experimental results from the prototype showed good correlation with the mathematical correlation in terms of predicting the production flow rate. The mathematical correlation over-predicted the results by 12.34%. The over prediction could perhaps be attributed to the mathematical correlation being based on an ideal system in terms of evaporation and condensation areas as well as distillation cell enclosure dimensions. Conversely, the prototype was subjected to an uncontrolled environment, the outdoor environment, in terms of the parameters that influenced the productivity of the prototype. A combination of these factors could be the reason for the over-prediction of the mathematical correlation; further investigation would be needed.

Initial water quality tests showed that the grey water used as a feed source was biologically not as contaminated as believed to be. However, the grey water had

been in a state of storage for a few days, and this could have contributed to the reduction in biological contaminants. Subsequent testing of the grey water at smaller time intervals validated this theory in that very high levels of contamination were found. Chemically the grey water also stood at high levels of contamination.

Results from the distilled water showed a dramatic decrease in the chemical contaminants. All levels were satisfactory except for lead, turbidity, ammonium nitrate and bacterial count. The levels for lead were at 11 μg/L with acceptable levels required to be at or below 10 μg/L. The reason for the high bacterial count is unknown although contamination or regrowth is the most likely scenario. The high turbidity levels were a result of the high bacterial count, thus only the bacterial count would need to be reduced to see a drop in turbidity.

Due to the prototype's operating in an outdoor environment, the risk of bacterial contamination was high, hence the suspicion that high bacterial levels were due to regrowth rather than an inadequate distillation process. This was confirmed by the fact that bacterial count levels were lower before the distillation process than after. The other biological indicators were total faecal coliforms and E. coli. These biological contaminants are normally associated with sewage effluent, and the high levels of initial contamination were reduced to acceptable levels by being exposed to elevated temperatures.

Pin-pointing the source of the high ammonium nitrate levels would require further investigation. This would create a better understanding of the origin of the ammonium nitrate and to what extend the distillation process is capable of removing the high levels of ammonium nitrate. However, the water quality results did show that the solar distillation process is a very effective method to remove the biological and chemical contaminants found in the treated sewage water.

Experimental verification of the TRNSYS simulation model was done by comparing experimental results of the three tank temperatures of the prototype to simulated results. Initial results showed that the simulation over-predicted the mass flow rates. The model was based on assumptions of no heat losses for the internal tanks. Subsequent incorporation of such heat losses for the internal tanks resulted in the simulation results tracking the experimental results much more closely.

Overall, the results are encouraging, and the prototype can be easily constructed and is small enough to be incorporated into a domestic household environment easily. Although eight systems were required to supply the total fresh water demand of an average Lynedoch household, even one system would reduce the fresh water demand of a household. The ability of the simulation models to predict production rates for other locations is very valuable for future application of the proposed solar-assisted distillation system. In addition, the current

problems associated with water quality levels are believed to be solvable and water of drinking quality is possible. Lessons learned from the construction of the prototype could also help in constructing a larger system in future.

This research paves the way for a system capable of reducing not only the demand for fresh water but also electricity demand through produced distilled water acting as feed water to a hot water geyser. Furthermore, reducing the demand for fresh water results in a reduction in fresh water supply infrastructure and in this case a reduction in wastewater treatment facilities as well. The potential impact of this solar-assisted distillation system in creating a sustainable society is therefore high, and continuing research into this proposed system is vital.

10. REFERENCES

Adhikari, R., Kumar, A. & Kumar, A. 1990. Estimation of mass-transfer rates in solar stills. *International Journal of Energy Research,* 14: 737–744.

Ahmed, M., Hrairi, M. & Ismail, A. 2009. On the characteristics of multistage evacuated solar distillation. *Renewable Energy,* 34: 1471–1478.

Ahsan, A. & Fukuhara, T. 2010. Mass and heat transfer model of Tubular Solar Still. *Solar Energy,* 84: 1147–1156.

Badran, A., Al-Hallaq, I., Eyal Salman, I. & Odat, M. 2005. A solar still augmented with a flat-plate collector. *Desalination,* 172: 227 – 234.

Baumgartner, T., Jung, D. & Sizmann, R. 1991. Open multiple effect desalination with low temperature process heat. *Desalination,* 81: 299–307.

Ben Jabrallah, S., Belghith, A. & Corriou, J. 2006. Convective heat and mass transfer with evaporation of a falling film in a cavity. *International Journal of Thermal Sciences,* 45: 16–28.

Ben Jabrallah, S., Belghith, A., Cherif, A., Corriou, J. & Dhifaoui, B. 2005. Experimental study of the evaporation of a falling film in a closed cavity. *Desalination,* 180: 197–206.

Biolytix. 2008. *How Biolytix works* [Online].
Available: http://www.biolytix.co.za/?page_id=4 [2012, 20 January].

BioRegional, 2012. [Online]
Available: http://www.oneplanetvision.net/ [2012, 13 January].

Bouchekima, B., Gros, B., Ouahes, R. & Diboun, M. 1998. Performance study of the capillary film solar distiller. *Desalination,* 116: 185–192.

Cengel, Y.A. 2006. *Heat and mass transfer: A practical approach.* Third ed. Singapore: McGraw Hill.

Chen, Z., Bar, L., Ge, X., Miao, Y.X. & Sun, X. 1984. Natural convection heat transfer across air layers at various angles of inclination. *Engineering Thermophysics, (Special Issue)* 211–220.

Department of Water Affairs, 2005. *A drinking water quality framework for South Africa,* [Pretoria]: Department of Water Affairs.

Department of Water Affairs, 2011a. *2011 Blue Drop Report,* [Pretoria]: Department of Water Affairs

Department of Water Affairs, 2011b. *2011 Green Drop Report,* [Pretoria]: Department of Water Affairs.

Dowling, T. 2007. *Lynedoch's water and sanitation system.* [Online] Available: http://www.sustainabilityinstitute.net/newsdocs/documents/doc_details/320-lynedochs-water-and-sanitation-system-terry-dowling [2012, 13 January].

Dunkle, R. 1961. Solar water distillation: The roof type still and a multiple effect diffusion still. *International Developments in Heat Transfer,* 5: 895.

El-Ghonemy, A. 2012. Water desalination systems powered by renewable energy sources: Review. *Renewable and Sustainable Energy Reviews,* 16: 1537–1556.

Eltawil, M.A., Zhengming, Z. & Yuan, L. 2009. A review of renewable energy technologies integrated with desalination systems. *Renewable and Sustainable Energy Reviews,* 13: 2245–2262.

Esterhuyse, B.D.W. 2004. *The effect of ionization of spray on the wetting characteristics of an adiabatically cooled heat exchanger.* Stellenbosch: Stellenbosch University.

Garg, H., Adhikari, R. & Kumar, R. 2002. Experimental design and computer simulation of multi-effect humidification (MEH)-dehumidification solar distillation. *Desalination,* 153: 81–86.

Goedgedacht farm. 2012. *Projects* [Online]. Available: http://www.goedgedacht.org.za/index.php?option=com_content&task=view&id=33&Itemid=123 [2012, 14 January].

Hanson, A. 2004. Distillate water quality of a single-basin solar still: Laboratory and field studies. *Solar Energy,* 76: 635–645.

Hartwig, G. & Sebitosi, A.B. 2010. *Design of a solar operated desalination system for use in South Africa*. Proceedings of the International Conference on Domestic Use of Energy, 29–31 March 2010, Cape Town.

Inaba, H. 1984. Experimental study of natural convection in an inclined air layer. *International Journal of Heat and Mass Transfer,* 27(8): 1127–1139.

Institute of Engineering and Technology. 2009. *Energy* [Online]. Available: http://www.theiet.org/factfiles/energy/energy-prin-page.cfm [2012, 30 October].

Jakob, M. 1964. Free heat convection through enclosed plane gas layers. *Journal of Heat Transfer,* 68: 189–193.

Kalogirou, S.A. 2004. Solar thermal collectors and applications. *Progress in Energy and Combustion Science,* 3(30): 231–295.

Kays, W.M., Crawford, M.E. & Weigand, B. 2005. *Convective Heat and Mass Transfer* [Singapore]:McGraw Hill.

Kumar, R. & Kalam, M. 1991. Laminar thermal convection between vertical coaxial isothermal cylinders. *International Journal of Heat and Mass Transfer,* 34: 513–524.

Kumar, S. & Tiwari, G. 1996. Estimation of convective mass transfer in solar distillation systems. *Solar Energy,* 57: 459–464.

Lazenby, H. 2012. *Energy intensive users prepared to reduce demand* [Online]. Available: http://www.engineeringnews.co.za/print-version/energy-intensive-users-prepared-to-reduce-electricity-demand-2012-01-10-1 [2012, 11 January].

Li, F., Otterpohl, R. & Wichmann, K. 2009. Review of the technological approaches for grey water treatment and reuses. *Science of the Total Environment,* 407: 3439–3449.

NAMwater. 2006. *Frequently asked questions* [Online]. Available: http://www.namwater.com.na/data/faq2.html [2012, 15 October].

NETGroup. 2006. *Electrical infrastucture master plan.* Stellenbosch: Stellenbosch Municipality.

One Planet Communities. 2012. *Communities* [Online]. Available: http://www.oneplanetcommunities.org/communities/ [2012, 13 January].

Prasad, V. 1986. Numerical study of natural convection in a vertical, porous annulus with constant heat flux on the inner wall. *International Journal of Heat and Mass Transfer,* 29(6): 841–853.

Sankar, M. & Venkatachalappa, M., 2007. Numerical investigation of combined buoyancy and surface tension driven convection in an axi-symmetric cylindrical annulus. *Nonlinear Analysis: Modelling and Control,* 12(4): 541–552.

Solar Thermal Energy Research Group. 2012. *Stellenbosch weather* [Online]. Available: http://weather.sun.ac.za/ [2012, 10 November].

Stellenbosch Municipality. 2012. *Third generation Integrated Development Plan 2012–2017.* Stellenbosch: Stellenbosch Municipality.

Sustainability Institute. 2012. *Sustainability Institute: Lyndoch Eco Village* [Online].
Available: http://www.sustainabilityinstitute.net/lynedoch-ecovillage/detailed-story [2012, 14 January].

Thermal Energy System Specialists. 2012. *Trnsys At a Glance* [Online].
Available: http://www.trnsys.com/ [2012, 25 July].

Thomas, R. & De Vahl Davis, G. 1970. *Natural convection in annular and rectangular cavities – a numerical study*. Proceedings of the Fourth International Heat Transfer Conference, Volume 4.

Tsilingiris, P. 2007. The influence of binary mixture thermophysical properties in the analysis of heat and mass transfer processes in solar distillation systems. *Solar Energy,* 81: 1482–1491.

Tsilingiris, P. 2008. Thermophysical and transport properties of humid air at temperatures range between 0 and 100 °C. *Energy Conversion and Management,* 49: 1098–1110.

Tsilingiris, P. 2010. Modeling heat and mass transport phenomena at higher temperatures in solar distillation systems – the Chilton-Colburn analogy. *Solar Energy,* 84: 308–317.

Van der Bruggen, B., 2010. The global water recycling situation. In I.C. Escobar & A.I. Schafer (eds). *Sustainability: Science and engineering. Volume 2* [Amsterdam]:Elsevier. 41–61.

Velmurugan, V., Deenadayalan, C., Vinod, H. & Srithar, K. 2008. Desalination of effluent using fin type solar still. *Energy,* 33: 1719–1727.

Venkata Reddy, P. & Narasimham, G. 2008. Natural convection in a vertical annulus driven by a central heat generating rod. *International Journal of Heat and Mass Transfer,* 51: 5024–5032.

Wee, H.K., Keey, R.B. & Cunningham, M.J. 1989. Heat and moisture transfer by natural convection in a rectangular cavity. *International Journal of Heat and Mass Transfer*, 32(9): 1765–1778.

Weng, L. & Chu, H. 1996. Combined natural convection and radiation in a vertical annulus. *Heat and Mass Transfer,* 31: 371–379.

Yin, S.H., Chen, K. & Wung, T.Y. 1978. Natural convection in an air layer enclosed within rectangular cavities. *International Journal of Heat and Mass Transfer,* 21: 307–315.

Zheng, H., Zhang, X., Zhang, J. & Wu, Y. 2002. A group of improved heat and mass transfer correlations in solar stills. *Energy Conversion and Management,* 43: 2469–2478.

APPENDIX A: TRNSYS SIMULATION PROGRAM

As mentioned in Section 7 TRNSYS was selected as the desired simulation software package. This section provides an overview of the TRNSYS simulation environment and the contribution it made in satisfying the objectives of the research.

The ideal software for the task at hand in the study, simulating a solar-assisted distillation system, would have a focus on energy flows and be able to simulate solar water collectors, water storage tanks, water flows, and evaporation and condensation phenomena as well as interpret weather data. It was important to be able to incorporate weather data since this would allow the simulations to be carried out for different locations.

There are many software packages available that can carry out each of the simulations set out above separately. Performing all of the simulations simultaneously, however, is not an easy task. When one looks at simulation packages catering for the renewable energy industry and in particular the solar industry, one finds that the simulation program known as TRNSYS (Thermal Energy System Specialists, 2012) is used extensively. TRNSYS is a software package written in the FORTRAN programming language and was developed by the University of Wisconsin-Madison. TRNSYS evolved from being a research tool to becoming a commercial software package. It has been in commercial operation for 35 years and was used as the simulation software for the Solar Energy Generating System plants in California. Today TRNSYS is used in various disciplines, ranging from energy generation to thermal building analysis.

TRNSYS works on the principle of combining the individual elements of a system to form the desired simulation model. Most renewable and conventional energy systems can be constructed using these elements. As mentioned in Section 7, these elements are called ‘types’. For instance, an evacuated tube collector is given the designation Type 538. Various secondary components are also available to enhance the analysis of the desired systems. Results are presented in graphs and can be analysed over extensive periods.

TRNSYS was therefore a suitable software package for the study since it could simulate the various elements found in the solar-assisted distillation system, model the distillation process as well as incorporate weather data. Weather data files from renowned data supplier Meteonorm are used as the provider of the weather data. Data are available for most majors cities around the world and custom data can easily be integrated into the program. The graphical user interface in TRNSYS allows for easy construction of systems by combining types with link lines providing an overview of the flow of information. This provides flexibility to create the most accurate model of a system without the need to devise and program custom simulation models.

TRNSYS has an extensive list of available types for solar collection, storage and utilising the flow of energy. Unfortunately, specific types modelling the evaporation and condensation cycle of the distillation system proved unsuitable for the specific conditions found in the solar-assisted distiller. Initially the solar assisted distillation system was intended to be built entirely from the different types available in TRNSYS. It was planned that the evaporation and condensation areas of the design would be modelled by a humidifier and cooling coil, respectively, with both types found in TRNSYS. The two different stages could be modelled individually with latent heat absorbed by the cooling coils acting as the heat input to the second water volume. Air would then also act as the transport mechanism, as was the case in the proposed distillation enclosure.

The humidifier component was chosen as Type 641, a simple adiabatic humidifier. Air enters the humidifier after which water is added to the air stream, increasing the humidity of the air. An energy balance then determines the state of the outlet air. Various checks are performed to ensure that the outlet air state is within the limits set by the user. Iterations occur until the outlet values fall within a specified tolerance. The air flow is a set parameter, and initial simulation is done with a low velocity to mimic natural convection air flow found in the distillation enclosure. Various other parameters can be adjusted to desired levels.

Type 508 was selected for the cooling coils. Type 508 simulates a simple cooling coil on the basis of a bypass function. The air stream is split up into two air streams with the one bypassing the cooling coils and the other flowing over the cooling coil, and thereby dehumidifying the air. The dividing factor between the two air streams is determined by a parameter specified by the user. The two air streams then mix again to form the state of the outlet air. The condensate that is formed in the cooling process of the cooling coil is the produced distillate.

The following configuration was hence used for the simulation model for the solar assisted distillation system: A standard flat-plate solar collector, Type 539, heats up the first-stage storage tank, Tank 1. Tank 1 in turn supplies hot water to the humidifier, Type 641. The humidifier uses the hot water to humidify an air stream. The humidified air stream then enters Type 508, the cooling coil. Here the air stream is dehumidified using the temperature of the second storage tank, Tank 2, as the temperature at which the condensing coils operate. Distillate is produced from the condensation on the cooling coils. The dehumidified air stream then returns to the humidifier since it is a closed air system. The liquid water inside the cooling coils absorbs the latent heat of condensation and is fed to Tank 2, simulating the flow of the latent heat in the system. Another humidifier and cooling coil combination is then run in the same manner with the temperature of Tank 2 now feeding the heated water to the humidifier.

A stable model producing representative results could unfortunately not be found. Although similar in function to the evaporation and condensation areas of the proposed design, the humidifier and cooling coil were unable to perform as required due to the low energy and mass flow rates found in the solar-assisted distillation system. The humidifier and cooling coils, types 641 and 508, are more applicable to larger scale systems where forced convection and high energy and mass flows are predominant.

The most prevalent case is the low airflow rates used. Since it is a natural convection airflow, the flow rates will be low. Assuming a constant, low airflow rate is thus not very representative of the actual conditions and, as found in the initial simulations, not suitable for the chosen types. A more specialised accurate airflow model would be needed to simulate the airflow between the humidification and condensing areas. TRNSYS can use flow modelling software such as FLUENT to tackle the problem, but a less complex approach was favoured and hence investigated.

It was found that TRNSYS allowed for the creation of custom types by creating custom-programmed simulation models. An idea came about to use the mathematical correlation of Zheng et al. (2002), developed in Section 5, to simulate the evaporation and condensation stages of the proposed solar-assisted distillation system. TRNSYS is written in the FORTRAN programming language and although an instruction manual exists on how to create a custom type, the actual process turned out to be much more difficult. Not only must the FORTRAN programming language be mastered, but FORTRAN language compilers are also needed separately from TRNSYS to compile the custom FORTRAN code.

Fortunately, TRNSYS is able to call external software programs to enhance the simulation capabilities. Programmes such as MATLAB, EES and Excel can be called from a TRNSYS simulation. It was thus decided that the easiest solution was to build the mathematical correlation of Zheng et al. (2002) in Excel. Excel is a simple yet powerful numerical tool and it is widely available, enabling more accessibility for future use of the simulations.

The following list tabulates the components used in the final simulation model. The first part details the TRNSYS description of the type, and the last part refers to how the components were used in the simulation. Although these do not always differ, some components were used differently from their intended use, hence the subsequent explanation. A snapshot of the simulation model as built in TRNSYS is shown in Figure A.1. Figure A.1 also has overlaying descriptions to show where the different elements of the solar-assisted distillation system are located in the model, showing how each aspect of the whole system is treated individually.

TRNSYS component	Differential controller
Designation	Type 2b
TRNSYS description (TESS, 2012)	The on/off differential controller generates a control function with a value of 1 or 0. This value is a function of the difference between upper and lower temperatures Th and Tl, compared with two dead-band temperature differences DTh and DTl. The new value of the control function depends on the value of the input control function at the previous time step. The controller is normally used with the input control signal connected to the output control signal, providing a hysteresis effect. However, control signals from different components may be used as the input control signal for this component if a more detailed form of hysteresis is desired.
Used in simulation as	Differential controller to calculate when the pump should be on and off

TRNSYS component	Meteonorm weather data file
Designation	Type 15-6
TRNSYS description (TESS, 2012)	This component serves the purpose of reading data at regular time intervals from an external weather data file, interpolating the data at timesteps of less than one hour and making it available to other TRNSYS components. The model also calculates several useful terms including the mains water temperature, the effective sky temperature, and the heating and cooling season forcing functions.
Used in simulation as	Weather data generator providing an input to the solar collector.

TRNSYS component	Equation editor
Designation	Not applicable
TRNSYS description (TESS, 2012)	The ‘insert new function’ allows basic mathematical operations to be implemented in TRNSYS. Logical operators are available as function.
Used in simulation as	Calculator performing basic mathematical operations and manipulating values in the simulation.

TRNSYS component	Evacuated tube collector
Designation	Type 538
TRNSYS description (TESS, 2012)	This component models the thermal performance of an evacuated tube solar collector. The thermal performance of the collector array is determined by the number of modules in series and the characteristics of each module. In this mode, the user must provide results from standard tests of collector efficiency versus a ratio of fluid inlet temperature minus ambient temperature to solar radiation.
Used in simulation as	Solar collector. Exchanged on occasion for a flat-plate collector when required by the simulation. Default values were used for collector characteristics.

TRNSYS component	Pump
Designation	Type 3b
TRNSYS description (TESS, 2012)	This pump model computes a mass flow rate using a variable control function, which must have a value between 1 and 0 and a fixed (user-specified) maximum flow capacity. In this instance of Type 3, pump power may also be calculated, either as a linear function of mass flow rate or by a user-defined relationship between mass flow rate and power consumption. A user-specified portion of the pump power is converted to fluid thermal energy.
Used in simulation as	Pump to circulate water from the storage tank through the solar collector.

TRNSYS component	Storage tank
Designation	Type 60c NoHeat
TRNSYS description (TESS, 2012)	Type 60 models a stratified liquid storage tank. This instance of Type 60 models a vertically cylindrical tank with two inlet and two outlet flows, and no internal heat exchangers. It includes calculation of losses from the tank to the flue if desired and assumes that all stratification nodes of the tank are uniform in size and that the heat transfer resistances between each node and the ambient are equal.
Used in simulation as	Storage tanks simulating the three circular storage tanks found in the proposed design.

TRNSYS component	Integrator
Designation	Type 24
TRNSYS description (TESS, 2012)	This component integrates a series of quantities over a period of time. Each quantity integrator can have up to but no more than 500 inputs. Type 24 is able to reset periodically throughout the simulation, either after a specified number of hours or after each month of the year.
Used in simulation as	Integrator to integrate values over certain time periods such as day and months to produce specific data.

TRNSYS component	Online plotter with output file
Designation	Type 65a
TRNSYS description (TESS, 2012)	The online graphics component is used to display selected system variables while the simulation is progressing. This component is highly recommended and widely used since it provides valuable variable information and allows users to immediately see when the system is not performing as desired. The selected variables are displayed in a separate plot window on the screen. In this instance of the Type 65 online plotter, data sent to the online plotter are automatically printed, once per time step, to a user-defined external file.
Used in simulation as	Plotter to graph data, allowing the user to view the data as well as print the data to an external file. This allowed the user to use the data externally, such as in Excel.

TRNSYS component	Online plotter
Designation	Type 65d
TRNSYS description (TESS, 2012)	The online graphics component is used to display selected system variables while the simulation is progressing. This component is highly recommended and widely used since it provides valuable variable information and allows users to immediately see when the system is not performing as desired. The selected variables will be displayed in a separate plot window on the screen. In this instance of the Type 65 online plotter, no output data file is generated.
Used in simulation as	Plotter to graph data, allowing the user to view the data in the program only.

TRNSYS component	Data reader
Designation	Type 9a
TRNSYS description (TESS, 2012)	This component serves the purpose of reading data at regular time intervals from a data file, converting it to a desired system of units and making it available to other TRNSYS components as time-varying forcing functions. This component is very general in nature and can read many different file types.
Used in simulation as	Device to read external solar radiation data from a text file. In this instance, the solar data from the local weather station were fed into the simulation with this device.

TRNSYS component	Auxiliary cooling device
Designation	Type 92
TRNSYS description (TESS, 2012)	An auxiliary cooling device is modelled to reduce the temperature of a flow stream, using either internal control, external control or a combination of both types of control. The cooling device is designed to remove energy from the flow stream at a user-designated rate ($Qmax$) whenever the external control input is equal to one and the cooling device outlet temperature is less than a user-specified maximum ($Tset$).
Used in simulation as	Device to model the latent heat loss incurred by the evaporating water, which then acted to cool the storage tank water. The latent heat of vaporisation was calculated from the mass flow rate produced at a specific point in time. A fixed mass flow rate was set and then used to calculate a set temperature according to $q = mcdT$ with the other temperature being the tank temperature. This calculation was performed by an equation editor. This calculated set output was then the input set temperature of this device with the same set mass flow rate as used in the calculation. The result was the removal of energy from the storage tank, as would occur due to the latent heat of vaporisation.

TRNSYS component	Excel -program caller
Designation	Type 62

TRNSYS description (TESS, 2012)	This TRNSYS type implements a link with Excel. The Fortran routine communicates with Excel through a component object model (COM) interface for fast data transfer. TRNSYS sends the component's inputs to given cells in the Excel worksheets. Those cells must be identified by defining an Excel name ('Inp1' ... 'Inp10'). In Excel, names can be defined i.e. by using the shortcut 'CTRL+F3'. In the same way outputs must get names like 'Out1' ... 'Out10'.
Used in simulation as	Component used to incorporate Excel input model. The simulation provided values to the device, and the device then returned appropriate values.

TRNSYS component	Tee-piece
Designation	Type 11h2
TRNSYS description (TESS, 2012)	The use of pipe or duct tee-pieces, mixers and diverters that are subject to external control is often necessary in thermal systems. This instance of the Type 11 model uses Mode 1 to model a tee-piece in which two inlet liquid streams are mixed together into a single liquid outlet stream.
Used in simulation as	Tee-piece to combine two fluid flows.

TRNSYS component	Auxiliary heating device
Designation	Type 6
TRNSYS description (TESS, 2012)	An auxiliary heater is modelled to elevate the temperature of a flow stream using either internal control, external control or a combination of both types of control. The heater is designed to add heat to the flow stream at a user-designated rate ($Qmax$) whenever the external control input is equal to one and the heater outlet temperature is less than a user-specified maximum ($Tset$). By specifying a constant value of the control function of one and specifying a sufficiently large value of $Qmax$, this routine will perform like a domestic hot water auxiliary with internal control to maintain an outlet temperature of $Tset$. By providing a control function of zero or one from a thermostat or controller, this routine will perform like a furnace, adding heat at a rate of $Qmax$ but not exceeding an outlet temperature of $Tset$. In this application, a constant outlet temperature is not sought and Tset may be thought of as an arbitrary safety limit.
Used in simulation	As with the auxiliary cooling device, this device

as	modelled the latent heat of condensation. A set temperature was calculated by an equation editor for a fixed mass flow rate and tank temperature by $q = mcdT$. This calculated set temperature was then the set temperature of this device, which flowed at the same mass flow rate in and out of the storage tank. This then simulated the latent heat of condensation received by the storage tank from the previous evaporation and condensation cycle.

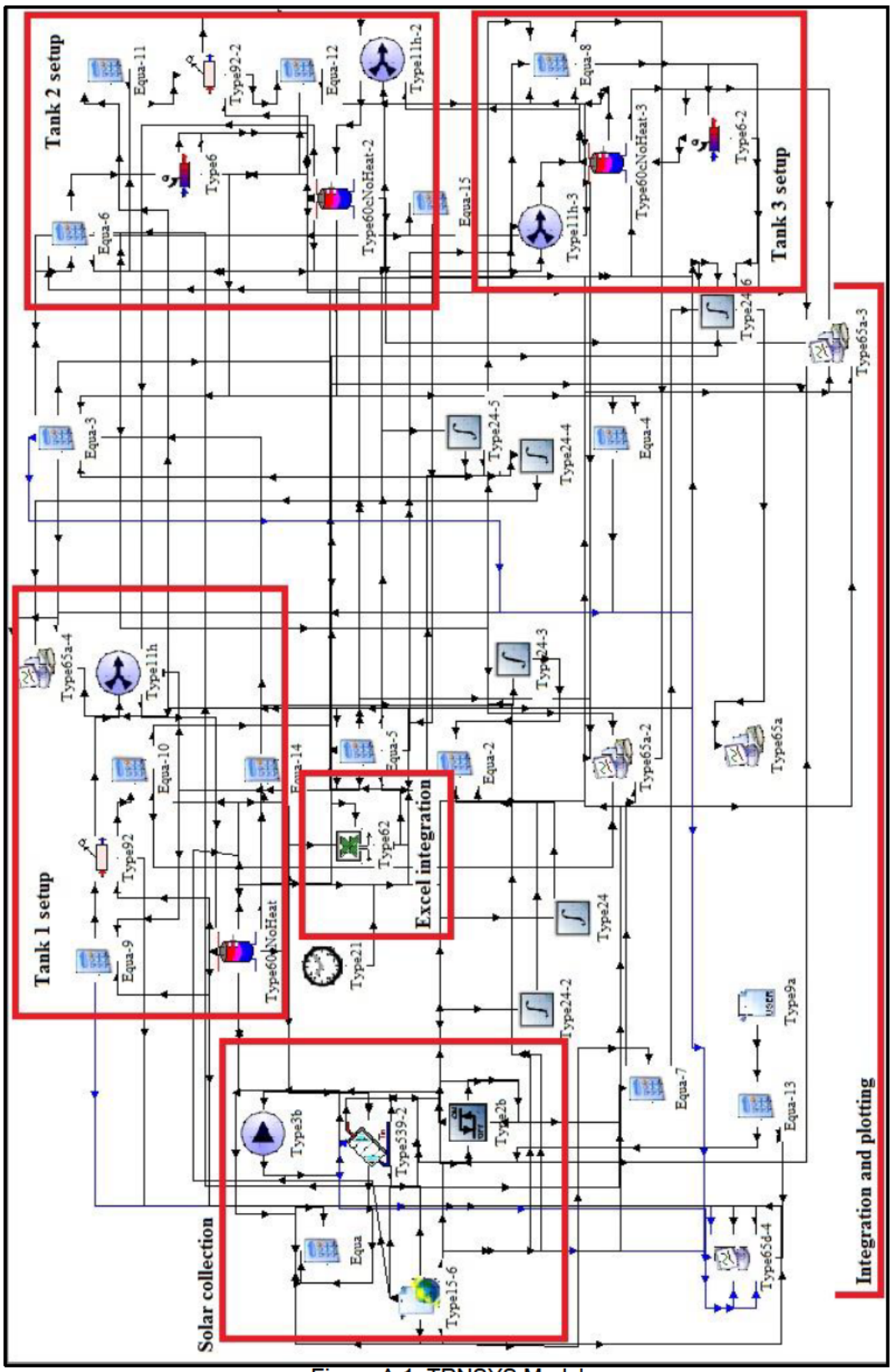

Figure A.1: TRNSYS Model

APPENDIX B: EXPERIMENTAL SETUP

This appendix provides more detail on the experimental setup. The experimental testing was set up on the solar roof of the Department of Mechanical and Mechatronic Engineering.

Solar insolation was deemed adequate although shading of the collector would occur at sunrise and sun-set. This presented a solution in controlling the PV-powered solar pump. Placement of the PV panel was strategically done to provide power to the pump only at times when solar radiation was sufficient. According to the TRNSYS simulations, the solar collection panel stops providing hot water to the prototype around 17:00. The PV panel was thus positioned so that shading of the panel occurred at around 17:00. This provided an effective way of ensuring that the pump did not run when insufficient heat was supplied.

The solar collector was set up in close proximity to the prototype distiller to minimise pipe lengths. The collector was pointed north to maximise solar collection. The PV panel was positioned next to the collector also pointing north. The angle of the PV panel was 20° to the horizontal. For the collector, the angle was set at 35° to the horizontal in line with setting the angle equal to the latitude of the location.

A constant head feed water tank was positioned next to the solar-assisted distillation system to keep a constant water level inside the storage tanks. A clear plastic bucket was used, providing visual confirmation of the water level. This bucket was attached to the distillation unit by plumbing pipe. A float valve was built into the bucket to replenish water supply once the water level dropped due to operation of the still. A storage tank was placed at an elevated height and attached to the float valve input via a pipe, ensuring that enough pressure was available to allow the float valve to operate as required. The storage tank could then be refilled at regular intervals without disrupting operation of the solar-assisted distillation system.

The circular distillation enclosure was assembled by means of rivets, support angles and a bonding agent known as Sikaflex 252. Sikaflex 252 is a heat- and chemical-resistant boding agent suitable for the high-temperature, high-humidity and water-prone environment of distillation enclosures. It is furthermore classified as suitable for use in foodstuff environments.

Placement of the PT 1000 temperature probes was, as mentioned in the Section 8.2, in the middle of the vertical plane as well as in the middle of the distillation enclosure in which the probe was placed. Therefore, the probes were set at 250 mm from the bottom and in the case of the distillation enclosure, 100 mm away from the condensing and evaporating walls.

An overall equipment connection diagram is given in Figure B.1. The feed water storage tank feeds the float valve in the constant head tank. From here the water levels in the annular water storage tanks are kept constant. If the water level drops, the constant head tank will first feed into the outer annular storage tank. This provides the outer water storage tank with low-temperature water, ensuring a temperature differential between the outer and middle water storage tanks. This is vital since the temperature differential ensures the operation of the natural convection distillation process. Water is fed from the outer water storage tank to the middle water storage tank through a pipe connection located on the opposite end of the input from the constant head tank as seen in Figure B.1. This prevents low temperature water from migrating directly to the middle and then inner water storage tanks.

Table B.1 shows detailed specification for the equipment used. Figures B.2 to B.4 are photos taken of different aspects of the prototype. Figure B.2 shows the PV panel and flat-plate solar collector at the back with the circular distillation enclosure system located in the foreground. The distillation enclosure is covered and closed off with corrugated plastic sheets that in turn are covered with a protective blue plastic sheet, seen in Figure B.2. The blue sheet is kept in place by nylon strings with logs placed on top to ensure that the corrugated plastic cover is kept in place.

Figure B.3 provides a view of the placement of one of the PT 1000 probes on the hessian fabric on the outside of the inner storage tank wall, which is the first-stage evaporation area. The top section of the heating element inside the inner storage tank can be seen at the top of the figure. This is the heating element used as a backup, and it is used to heat the water for experiments without solar energy assistance. Figure B.4 shows the interior of the circular distillation system with the corrugated plastic cover removed. The first evaporation surface, seen in the middle of the figure, is the outer wall of the inner storage tank, Tank 1. The second evaporation surface is the outer wall of the middle storage tank, Tank 2. The first condensation surface is then the inner wall of Tank 2, with the second condensation surface being the inner wall of the outer storage tank, Tank 3. The outer wall of Tank 3 is exposed to the outside environment.

Distillate was collected in a container, and the mass of the distillate was measured using the scale mentioned in Table B.1. The scale had a resolution of 1 g. Measurements were taken in time steps of 15 minutes during buildup phases, which usually took up to 150 minutes. After the buildup phase, measurements were taken in time steps of five minutes to increase data resolution, providing more insight into changes that the system might undergo.

Temperature measurements were taken with PT 1000 resistance temperature detectors, and the data were logged by a Steca TR 6202mc solar controlling device. The resolution of the logged data is at 1 °C, which was unfortunately not

very high. The PT 1000 probes are capable of providing high-resolution data, and in hindsight, a higher resolution data logger would have been a better option.

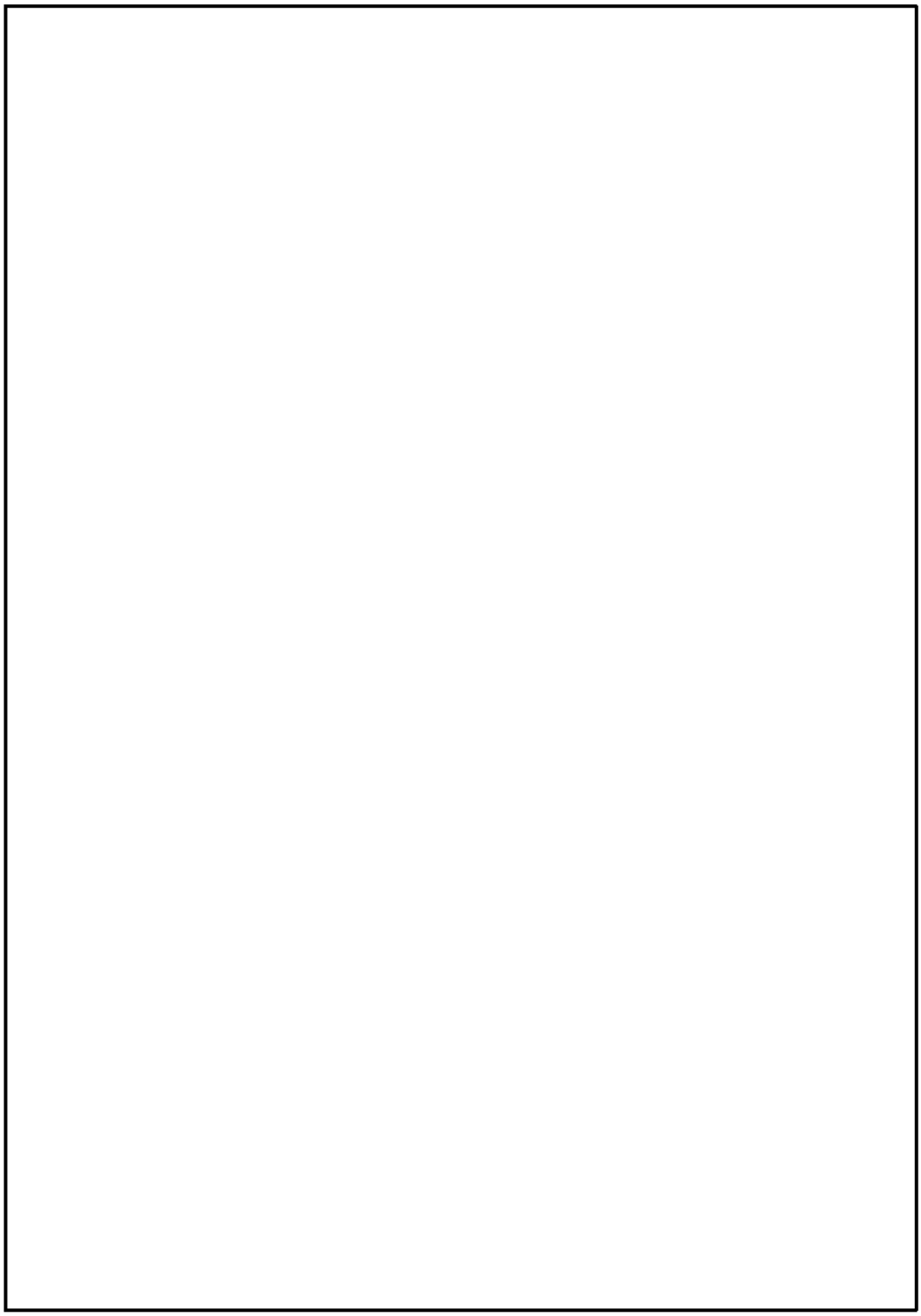

Figure B.1: Equipment Connection Drawing

Table B.1: Equipment Specifications

Experimental equipment		
Description	Type	Parameters
Solar panel	Flat-plate panel	Area: 2.4 m^2 Angle: 35° to horizontal
Data logger	Steca TR 6020mc	Six temperature inputs SD card reader for data logging
Scale		Accuracy: ± 1 g
Solar pump	Laing eco-circ vario D5-38/700B	Input voltage: 8 - 24 V Max current: 1.5 A Max pressure: 10 bar
Temperature probes	PT1000	Accuracy: ± 0.5 °C
Valves	Ball valve	Standard plumbing ball valves
PV panel		Angle: 20° to horizontal Output: 16.5 V @ 0.61 A Power rating: 10 Wp
Float valve	Vertical travel float	Standard plumbing float valve
Pipes	Copper	15 mm diameter
Pipes	Steel braided plumbing pipe	10 sections
Prototype cover	Correx corrugated plastic	1.2 x 0.6-m sheets

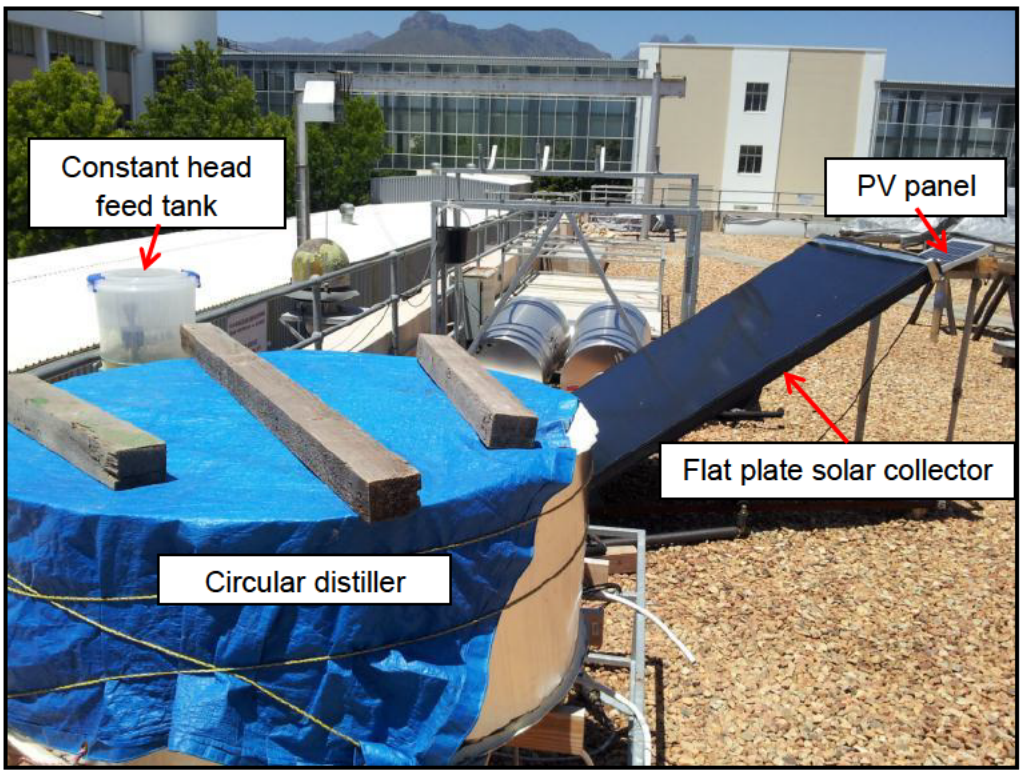

Figure B.2: Prototype Layout

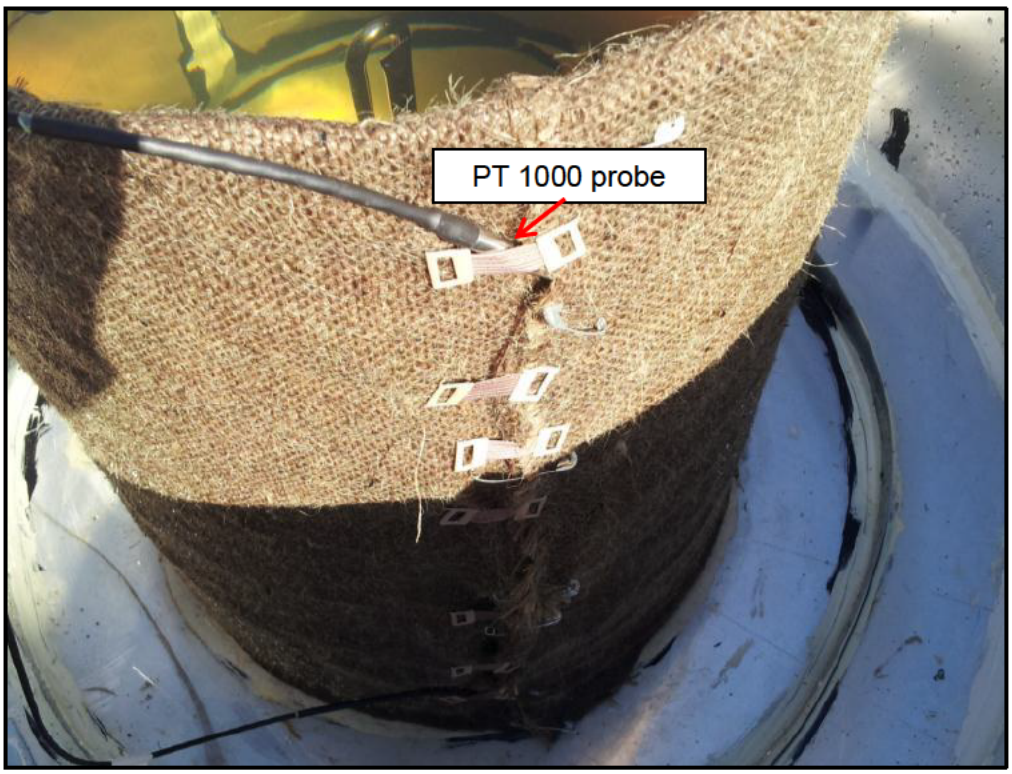

Figure B.3: PT1000 Temperature Probe Placement (for Top Evaporation Temperature Evaluation)

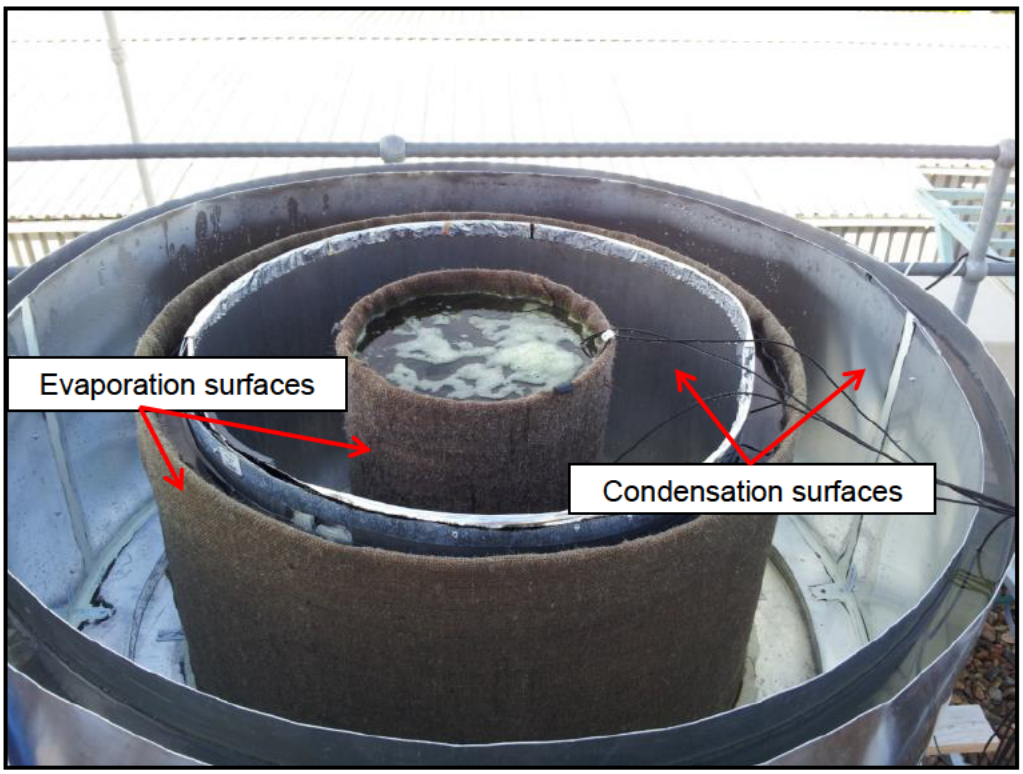

Figure B.4: Prototype without Corrugated Plastic Cover

APPENDIX C: SAMPLE CALCULATIONS

This appendix details the process of the mathematical correlation of Zheng et al. (2002) used to calculate a produced distillate from two temperatures. This process is exactly the same as the calculation done by the Excel spread-sheet. This spread-sheet is found in the TRNSYS simulation model and is used to calculate a distillate flow rate from two temperatures. These temperatures are the evaporation and condensation temperatures. Table C.1 presents the various constants used in calculating the moist air properties, as mentioned in Section 5.5. The calculations are done according to Equation C.1 where X represents the desired property, $C_0 - C_5$ represents the constants found in Table C.1 and T is the temperature of the moist air in °C. The constants and equation are from Tsilingiris (2008).

$$X = C_0 + C_1 T + C_2 T^2 + C_3 T^3 + C_4 T^4 + C_5 T^5 \qquad \text{C.1}$$

Table C.1: Constants Used in Moist-Air Correlation Calculations

Numerical constants for use in calculating moist-air properties			
Constant number	Density (CD)	Viscosity (CV)	Thermal conductivity (CK)
0	1.293393662	1.715747771E-5	2.40073953E-02
1	-5.538444326E-3	4.722702075E-8	7.278410162E-05
2	3.860201577E-5	-3.663027156E-10	-1.788037411E-07
3	-5.2536065E-7	1.873236686E-12	-1.351703529E-09
4		-8.050218737E-14	-3.322412767E-11
5			
Constant number	Specific heat capacity (CH)	Thermal diffusivity (CA)	Prandtl number (CP)
0	1.004571427	1.847185729E-5	0.7215798365
1	2.05063275E-3	1.161914598E-7	-3.703124976E-4
2	-1.631537093E-4	2.373056947E-10	2.240599044E-5
3	6.2123003E-6	-5.769352751E-12	-4.162785412E-7
4	-8.830478888E-8	-6.369279936E-14	4.969218948E-9
5	5.071307038E-10		
Constant number	Saturated vapour pressure (CB)		
0	7.073034146E-01		
1	-2.703615165E-02		
2	4.360882110E-03		
3	-4.662575642E-05		
4	1.034693708E-06		
5			

Assuming an evaporation temperature of 70 °C and a condensing temperature of 40 °C, the first step is calculating the moist air properties at saturation. The properties are all calculated at a temperature of 55 °C, the midpoint between the evaporation and condensation temperatures.

Density:

$$\rho = CD_0 + CD_1T + CD_2T^2 + CD_3T^3 \quad \text{C.2}$$

$$= 1.293393662 + (-5.538444326E\text{-}3)(55) + (3.860201577E\text{-}5)(55)^2 + (-52536065E\text{-}7)(55)^3$$

$$= 1.018\ [\text{kg/m}^3]$$

Viscosity:

$$\mu = CV_0 + CV_1T + CV_2T^2 + CV_3T^3 + CV_4T^4 \quad \text{C.3}$$

$$= 1.715747771E\text{-}5 + (4.722702075E\text{-}8)(55) + (-3.663027156E\text{-}10)(55)^2 + (1.873236686E\text{-}12)(55)^3 + (-8.050218737E\text{-}14)(55)^4$$

$$= 1.822E\text{-}05\ [\text{Ns/m}^2]$$

Thermal conductivity:

$$k = CK_0 + CK_1T + CK_2T^2 + CK_3T^3 + CK_4T^4 \quad \text{C.4}$$

$$= 2.40073953E\text{-}02 + (7.278410162E\text{-}05)(55) + (-1.788037411E\text{-}07)(55)^2 + (-1.351703529E\text{-}09)(55)^3 + (-3.322412767E\text{-}11)(55)^4$$

$$= 2.694E\text{-}02\ [\text{W/m K}]$$

Specific heat capacity:

$$c_p = CH_0 + CH_1T + CH_2T^2 + CH_3T^3 + CH_4T^4 + CH_5T^5 \quad \text{C.5}$$

$$= 1.004571427 + (2.05063275E\text{-}3)(55) + (-1.631537093E\text{-}4)(55)^2 + (6.2123003E\text{-}6)(55)^3 + (-8.830478888E\text{-}8)(55)^4 + (5.071307038E\text{-}10)(55)^5$$

$$= 1.104\ [\text{kJ/kg K}]$$

Thermal diffusivity:

$$\alpha = CA_0 + CA_1T + CA_2T^2 + CA_3T^3 + CA_4T^4 \quad \text{C.6}$$

$$= 1.847185729\text{E-}5 + (1.161914598\text{E-}7)(55) + (2.373056947\text{E-}10)(55)^2$$
$$+(-5.769352751\text{E-}12)(55)^3 + (-6.369279936\text{E-}14)(55)^4$$
$$= 2.404\text{E-}05\ [\text{m}^2/\text{s}]$$

Prandtl number:

$$\text{Pr} = CP_0 + CP_1T + CP_2T^2 + CP_3T^3 + CP_4T^4 \quad \text{C.7}$$

$$= 0.7215798365 + (-3.703124976\text{E-}4)(55) + (2.240599044\text{E-}5)(55)^2$$
$$+(-4.162785412\text{E-}7)(55)^3 + (4.969218948\text{E-}9)(55)^4$$
$$= 0.745$$

Diffusion coefficient:

$$D_{w-air} = 1.87\text{E-}10 \left(\frac{(T + 273.15)^{2.072}}{\frac{P_f}{101325}} \right) \quad \text{C.8}$$

$$= 1.87\text{E-}10 \left(\frac{(55 + 273.15)^{2.072}}{\frac{101.325}{101325}} \right)$$
$$= 3.056\text{E-}5\ [\text{m}^2/\text{s}]$$

With the diffusion coefficient known, the Lewis number can be calculated:

$$Le = \frac{\alpha}{D_{w-air}} \quad \text{C.9}$$

$$= \frac{2.404\text{E-}5}{3.056\text{E-}5}$$
$$= 0.78$$

With all of the moist air properties available, the next step is to calculate the saturated vapour pressures at the evaporation and the condensation temperatures, again with the correlation provided by Tsilingiris (2008).

Saturated vapour pressures at 40 and 70 °C:

$$P_{vc} = CB_0 + CB_1T + CB_2T^2 + CB_3T^3 + CB_4T^4 \quad \text{C.10}$$
$$= 7.073034146\text{E-}01 + (-2.703615165\text{E-}02)(40) + (4.360882110\text{E-}03)(40)^2 + (-4.662575642\text{E-}05)(40)^3 + (1.034693708\text{E-}06)(40)^4$$
$$= 6.268 \text{ [kPa]}$$

$$P_{ve} = CB_0 + CB_1T + CB_2T^2 + CB_3T^3 + CB_4T^4 \quad \text{C.11}$$
$$= 7.073034146\text{E-}01 + (-2.703615165\text{E-}02)(70) + (4.360882110\text{E-}03)(70)^2 + (-4.662575642\text{E-}05)(70)^3 + (1.034693708\text{E-}06)(70)^4$$
$$= 29.033 \text{ [kPa]}$$

$$P_{vf} = CB_0 + CB_1T + CB_2T^2 + CB_3T^3 + CB_4T^4 \quad \text{C.12}$$
$$= 7.073034146\text{E-}01 + (-2.703615165\text{E-}02)(55) + (4.360882110\text{E-}03)(55)^2 + (-4.662575642\text{E-}05)(55)^3 + (1.034693708\text{E-}06)(55)^4$$
$$= 14.122 \text{ [kPa]}$$

$$P_t = P_a + P_{vf} \quad \text{C.13}$$
$$= 101.325 + 14.122$$
$$= 115.447 \text{ [kPa]}$$

The total pressure is calculated as the air pressure of dry air plus the partial vapour pressure calculated at the midpoint temperature, 55 °C. Now one can start to calculate the modified Rayleigh number, starting with the modified

temperature difference. The molecular weight of air is 28.96 kg/kmol and of water 18.016 kg/kmol.

$$\Delta T'' = \left[(T_e - T_c) + \frac{(P_{ve} - P_{vc})(T_e + 273.15)}{\frac{M_a P_t}{M_a - M_w} - P_{ve}} \right] \quad \text{C.14}$$

$$= \left[(70 - 40) + \frac{(29033 - 6268)(70 + 273.15)}{\frac{(28.96)(115447)}{28.96 - 18.016} - 29033} \right]$$

$$= 28.26\ ^{\circ}\text{C}$$

$$Ra' = \frac{X^3 \rho g \beta}{\mu \alpha} \Delta T'' \quad \text{C.15}$$

$$= \frac{(0.2)^3 (1.018)(9.81)(1/(55 + 273.15))}{(1.822\text{E-}5)(2.404\text{E-}5)} (28.26)$$

$$= 15\ 708\ 101$$

With the modified Rayleigh number known, the next step is to calculate the Nusselt number:

$$Nu = C(Ra')^n \left(\frac{H}{W} \right)^b \kappa^{\left(d + \frac{e}{\kappa} \right)} \quad \text{C.16}$$

$$= 0.18(15708101)^{0.278} \left(\frac{0.5}{0.2} \right)^{-0.122} (2.12)^{\left(0.34 + \frac{0.329}{2.12} \right)}$$

$$= 23.38$$

Therefore, the heat transfer coefficient is

$$h_{heat} = Nu\left(\frac{k}{l}\right) \qquad \text{C.17}$$
$$= 23.38\left(\frac{0.02694}{0.2}\right)$$
$$= 3.15\ [\mathrm{W/m^2\ °C}]$$

Finally, the mass flow rate for the given temperatures can be calculated:

$$\dot{m}_d = \frac{h_{heat}}{\rho_f c_{pf} Le^{(1-n)}} \frac{M_w}{R}\left(\frac{P_e}{T_e + 273.15} - \frac{P_c}{T_c + 273.15}\right) \qquad \text{C.18}$$
$$= \frac{(3.15)}{(1.018)(1104)(0.78)^{(1-0\,278)}} \frac{(18.018/1000)}{8.31}\left(\frac{29033}{343.15} - \frac{6268}{313.15}\right)$$
$$= 4.70\text{E-}4\ [\mathrm{kg/s.m^2}]$$

The produced distillate is given per square meter of evaporation area. Over a period of one hour, the production rate is 1.692 kg/h.m^2.

APPENDIX D: DEMONSTRATION MODEL DRAWINGS

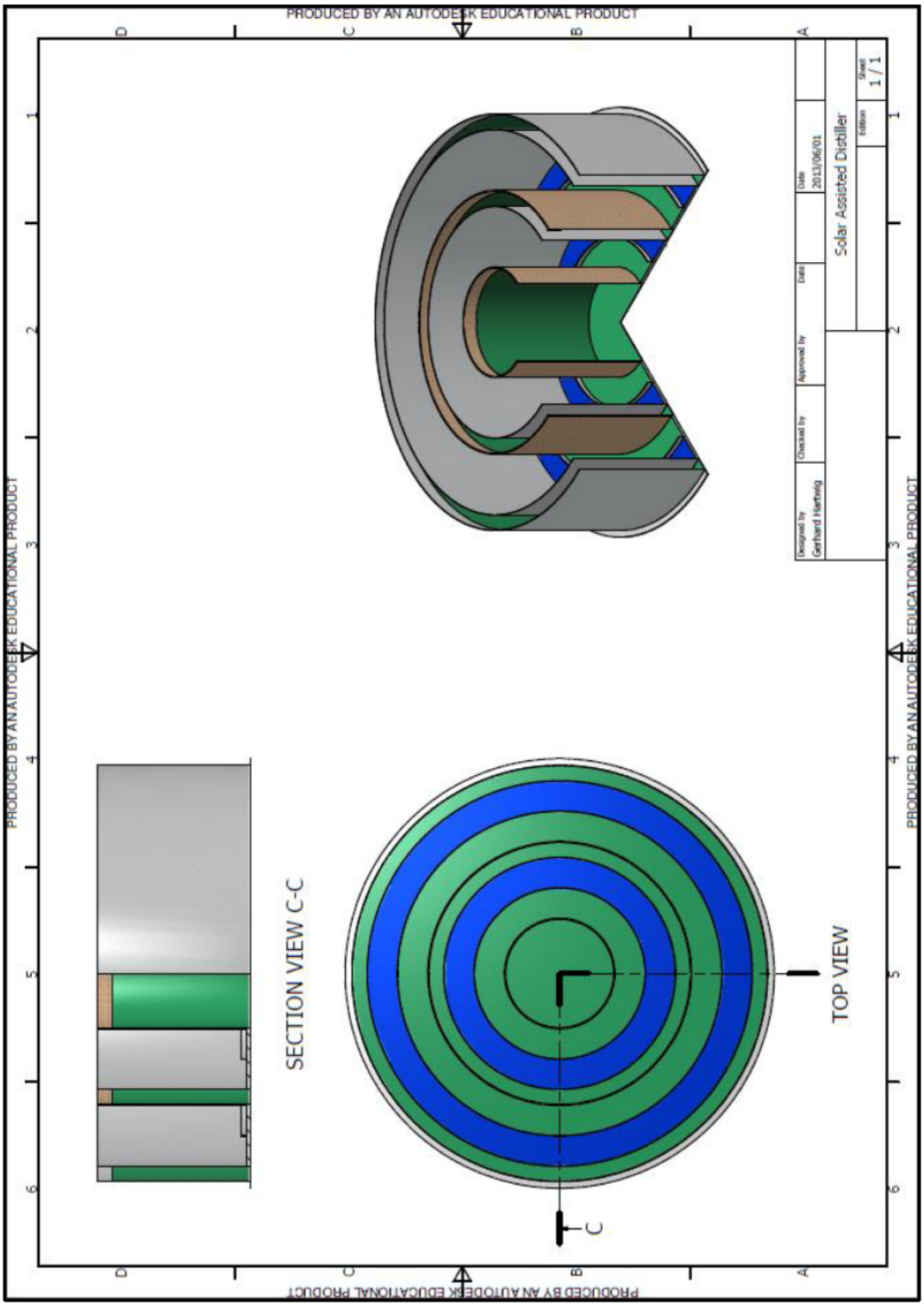

Figure D.1: Demonstration Model Design

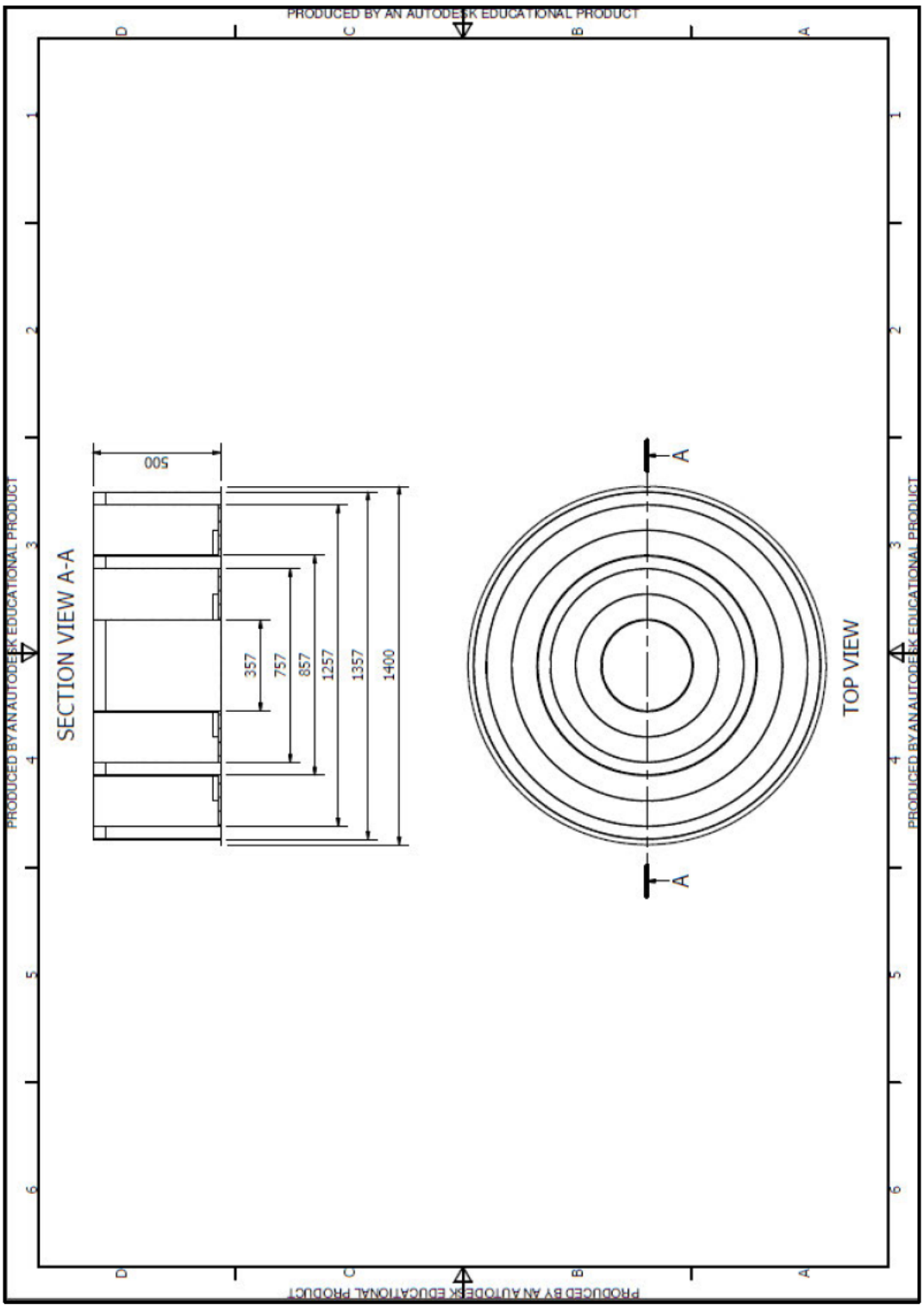

Figure D.2: Demonstration Model Design Dimensions

APPENDIX E: WATER QUALITY TESTING RESULTS

The water quality results are made up of laboratory test results. GW refers to the grey water used as the feed water to the solar-assisted distillation system. The one in GW1 would refer to the test number, A refers to the cold grey water sample, and B to the grey water sample after being exposed to the high temperature encountered in the solar-assisted distillation system. Hence, GW2 B would refer to the high temperature grey water sample of test number two. DW refers the distilled water sample that is produced by the solar-assisted distiller with the number again referring to the test number. TW3 refers to a normal tap water sample that was included in the tests to act as a benchmark for the distilled water results.

Table E.1: Water Quality Data

Source experiment		Limit		GW1 A	GW1 B	DW1		GW2 A	GW2 B	DW2		TW3	GW3 A	GW3 B	DW3		Lab method
Lab. test no.								12 873	12 874	12 872		14 413	14 296	14 412	14 414		
Colour	*mg/l Pt*	15													12.2		
EG	*mS/m*	170		113	111	11		83	79	8		9	193	169	15		3 135
TDS	*mg/l*	1 200						532	510	55		56	1 256	1 099	98		
pH		5.0 - 9.7		8.8	8.1	8.1		9.3	9.3	7		7.6	7.7	8.1	7.7		3136
Turbidity	*NTU*	1													3.29		

Total bacteria count	P	DOC	Cu	SO_4	Na	K	NO_3-N	Mg	F	Cl	Ca	NH_4-N
/1 ml	*mg/l*	*mg/l*	*µg/l*	*mg/l*	*mg/l*	*mg/l*	*mg/l*	*mg/l*	*mg/l*	*mg/l*	*mg/l*	*mg/l*
1000			2000	500	200		11		1.5	300		1.5
			0	44	80	19	21	12		95	97	
			0	48	79	19	24	12		97	99	
			0	0	1.6	0.4	0	0.3		2.6	4.8	
>30000	1.25		**0.03**	53	78.7	23.9	7.86	15.6	0.3	113.7	87.2	2.84
9300	1.65		**0.03**	62	80.8	20.4	7.83	14.4	0.4	128.7	87.3	2.85
>30000	0.12		0.06	11	4.6	2.4	0.05	0.5	0	8.3	8.1	2.25
20	0		0.01	17	7.2	2.6	1.71	1.2	0	15	13.8	1.81
>30000	3.98		0.01	101	161.2	38.8	34.75	16.8	0.3	202.7	159.4	11
<10	1.09		0.74	94	111.7	19.8	12.65	18.6	0.2	154.2	137.8	11.35
>30000	0.13	27.8	67	12.41	0.51	2.57	1.28	0.56	0	4.41	2.38	15.11
3 146	3 132				3 126	3 126	3 134	3 126		3 138	3 126	3 133

Mn	Pb	Fe	CN	Co	Cr	Cd	As	Sb	Al	Zn	E. coli	Coli-forms
µg/l	µg/l	µg/l	µg/l	µg/l	µg/l	µg/l	µg/l	µg/l	µg/l	mg/l	/100ml	/100ml
500	10	2 000	70	500	50	3	10	20	300	5	0	10
200		340								0		
200		550								0		
30		130								0		
		0.03								**0.02**	N/D	3
		0								**0**	N/D	N/D
		0.18								2.28	N/D	N/D
		0.07								0	N/D	N/D
		0.68								0.02	959	8664
		0.14								0.06	N/D	N/D
11	11	153	0	2	1	1	**0**	**0**	120	0.77	N/D	10
3 126	3 126	3 126		3 126	3 126	3 126	3 126	3 126	3 126	3 126	3 146	3 146

Hg	*µg/l*	6													0		
Ni	*µg/l*	70													5		3 126
Se	*µg/l*	10													**0**		3 126
V	*µg/l*	200													**0**		3 126